博士論文（要約）

Study on corium behavior in BWR lower plenum by the improvement of DCA module in SAMPSON

(SAMPSON の DCA モジュール改善による BWR 下部プレナムにおける炉心溶融物挙動に関する研究)

韋 宏洋

Study on corium behavior in BWR lower plenum by the improvement of DCA module in SAMPSON

SAMPSON の DCA モジュール改善による BWR 下部プレナムにおける炉心溶融物挙動に関する研究

June 2016

A dissertation submitted to
The University of Tokyo In partial fulfillment of the requirements
For the degree of Doctor of Philosophy
In
NUCLEAR ENGINEERING AND MANAGEMENT

Hongyang WEI

韋 宏洋

Abstract

This thesis presents the study on penetration tube effects on corium behavior in BWR lower plenum by the improved Debris Coolability Analysis (DCA) module in SAMPSON (2013). The thesis includes improvement of heat transfer between molten pool and RPV wall model, development of one-dimension (1-D) jet breakup model, and implementation of penetration tube melt model. The corium behavior in BWR lower plenum has been understood through improved DCA module. The effects of control rod guide tubes (CRGTs) on jet breakup process have been clarified through an original jet breakup experiment. The failure mechanism of BWR lower plenum has been investigated by implementation of penetration tube melt model.

Chapter 1 states the background, necessity, and objectives of current study. As the last in-vessel barrier in nuclear reactor, the integrity of the Reactor Pressure Vessel (RPV) is important. In a hypothetical nuclear reactor severe accident, the failure of reactor pressure vessel (RPV) lower head could cause a direct attack on the containment basement, and further containment failure could lead to fission product release to the environment. Corium behavior in reactor lower plenum has vital effects on the integrity of RPV. Thus, deep understanding of the progression of corium behavior in lower plenum is essential to enhance safety and reliability of nuclear power.

Most of severe accident experiments were used to point out the significant events and clarify the specific phenomena in detail. It is difficult to clarify different phenomena in full-range of a severe accident scenario by experiments. Integrated experiments used to simulate different severe accident conditions and using radioactive nuclides are difficulty and costly. Thus, it is necessary to have a code for the whole-plant severe accident analysis. Currently, MELCOR and MAAP are widely used in severe accident analysis. These two codes mainly use lumped parameter method, empirical correlations, and user tuning parameters. These two codes have the capability of evaluation of severe accident measurement and sensitivity analysis of PRA Level2 studies.

From the perspective of mechanistic modeling, the United States Nuclear Regulatory Commission (USNRC) has developed RELAP/SCDAP for the analysis of severe

accident events in the reactor vessel and CONTAIN for the events inside the containment. They adopted simplified models. Due to the complexity of severe accident phenomena, these mechanistic codes still could not obtain a sufficient understanding of these phenomena.

Considering the importance and necessity mentioned above, SAMPSON has been developed based on fundamental physical principles, theoretical-based equations and mechanistic models. The features of SAMPSON are very fewer user tuning parameters, high-speed simulation on the parallel processing of computers, multi-dimensional mechanistic models and consideration of various events in a hypothetical severe accident. Moreover, SAMPSON can be used to simulate a wide range of scenarios covering from the normal operation to the hypothetical severe accident events. As a result, the advantages of SAMPSON have been validated against phenomena in DCA module such as natural convection, fluid spreading and solidification.

However, the original DCA module in SAMPSON was more suitable for pressurized water reactor (PWR). Therefore, the original DCA module have never been considered jet breakup process and the penetration tubes in BWR lower plenum. Hence, this study aims to study corium behavior in BWR lower plenum from a more mechanistic and fundamental perspective by the improved DCA module.

Chapter 2 describes how heat transfer between molten pool and RPV wall model has been improved. Validation work needs to be conducted before using DCA module to analyze corium behavior in BWR lower plenum. The crust growth model has been implemented into DCA module and heat transfer between molten pool and RPV wall model has been improved. The improved and modified DCA module has been validated against LIVE-L4 test. Compared to simulation results of original DCA module, the improved DCA module could predict the LIVE-L4 test process reasonably by comparing molten pool average temperature, crust growth rate and heat flux along vessel wall, which indicated that the heat transfer model in the improved DCA module could be used to evaluate the heat transfer more accurately for the real condition in BWR lower plenum.

Chapter 3 shows how jet breakup model has been incorporated into DCA module and validation work against FARO-L8 test. Based on Kelvin-Helmholtz instability and Rayleigh-Taylor instability, a 1-D jet breakup model has been implemented into DCA module. Both 1-D jet breakup model and the Institute of Applied Energy (IAE) proposed jet breakup model have been used to simulate FARO-L8 test. By comparing the jet breakup fraction, departure droplets' diameter, vessel pressure and water swell, the implemented 1-D jet breakup model could be proved as a proper tool to simulate such phenomena. This indicated that the developed 1-D jet breakup model could be capable to simulate jet breakup process accurately and could be extrapolated to simulate jet breakup process in reactor case.

Chapter 4 presents the detailed jet breakup experiment that used to confirm whether the implemented jet breakup model is suitable for BWR. Since the implemented jet breakup model is based on PWR, the effects of CRGTs on jet breakup process need to be considered for BWR. In order to identify the effects of CRGTs on the jet breakup behavior, a molten material (U-alloy) breakup experiment considering CRGTs in a BWR lower plenum has been conducted under isothermal boundary conditions. The experiment results showed that CRGTs could prevent the jet breakup process and this prevention ability depends on pitch/diameter (P/D) ratio. Relative breakup fraction has been proposed to evaluate the jet breakup process in BWR lower plenum. The experiments also indicated that CRGTs had almost no effect on the fragmentation droplet diameter. Based on the current jet breakup experiment results, the implemented 1-D jet breakup model has been modified for BWR.

Chapter 5 presents the molten pool test simulation after the implementation of penetration tube melt model. Besides the effects of CRGTs on the jet breakup process, the CRGTs and Instrument Guide tubes (IGTs) could also act as the heat sink for molten pool in BWR lower plenum. The penetration tube melt model has been developed and incorporated into DCA module. By assuming no corium leakage from failed CRGTs or IGTs, the improved DCA module has been used to evaluate BWR lower plenum failure mechanism. The simulation results indicated that penetration tubes could fail earlier than RPV wall, which needs to be considered in the evaluation of BWR severe accident management.

Chapter 6 summarizes the whole thesis. The improved DCA module used in this study is able to simulate the corium behavior in BWR lower plenum. Furthermore, in this study, the penetration tube effects on the corium behavior have been investigated. This approach has succeeded in attaining the following achievements:

- The DCA module has been modified for BWR lower plenum analysis. The heat transfer model between molten pool and RPV wall has been improved and validated against LIVE-L4 test. The 1-D jet breakup model has been implemented into DCA module and validated with FARO-L8 test. After implementation of penetration tube melt model, molten pool simulation has been conducted to study penetration tube effects on corium behavior and BWR lower plenum failure mechanism.

- The effects of penetration tubes on corium behavior have been clarified. During corium falling process, jet breakup process could happen. How CRGTs could affect jet breakup behavior has been investigated and relative breakup fraction has been proposed to evaluate jet breakup fraction in BWR. After falling process ends and corium pool forms in the BWR lower plenum, a simulation test has been conducted. In BWR lower plenum, penetration tubes could fail earlier than RPV wall, which has to be considered in severe accident management.

Acknowledgement

I would like to express my special appreciation and sincere gratitude to my supervisor Professor Koji Okamoto for being a great mentor in my Ph.D. study and life. Without his guidance and help in my research, I would not have been able to achieve my Ph.D. study successfully. His constant encouragement even at difficult times was something which I am really thankful for.

I would also like to express my thanks to Dr. Nejdet Erkan and Dr. Masahiro Kondo for their valuable comments and suggestions on writing this thesis. My gratitude also goes to Professor Shunichi Suzuki, for his kind help and valuable advices in preparing this thesis.

My sincere thanks are also expressed to Associate Professor Mikio Sakai, Dr. Masanori Naito and Dr. Satoshi Someya, for their valuable comments and suggestions on completing this thesis.

My heartfelt thanks also goes to every previous and current members of Okamoto Laboratory during the past three years of my Ph.D. study. Without their help, my study and life in Japan would not have been so colorful and interesting.

My sincere gratitude is also expressed to Dr. Hiroaki Suzuki and Dr. Hiroyuki Suzuki in the Institute of Applied Energy (IAE), for proving me the IMPACT/SAMPSON code.

I would like to thank Dr. Xiaoyang Gaus-Liu and Dr. Alexei Miassoedov, for their kind help during my internship in KIT.

I would also like to thank both Ms. Xin Li and Ms. Jinzhu Lin from Waseda University for their kind support on my academic study and doctoral thesis. Without their help and support, I would not be able to pass my doctoral final defense and finish this thesis smoothly.

The finical support from China Scholarship Council (CSC) for my Ph.D. study also greatly appreciated.

Finally I would like to thank my family, especially my parents, for all their constant love and encouragement.

Contents

List of Figures

List of Tables

Chapter 1 Introduction

1.1 Background

During a severe accident in light water reactor (LWR), there is potential risk of radioactive release to the environment if the safety functions are not retained and ensured. For a typical nuclear power plant, in order to prevent the release of radioactive materials, there are four physical barriers: the fuel matrix, the fuel cladding, the pressure boundary of the reactor coolant system, and the containment system, as shown in Figure 1-1. In a severe accident with loss of cooling, decay heat and additional oxidation heat of the core materials could cause fuel rods to melt, leading to the failure of the first and second barriers. High temperature molten core materials could relocate into the lower plenum and threaten the third barrier. If there is still no sufficient cooling for molten core materials at this stage, Reactor Pressure Vessel (RPV) would failure, leading to the failure of the third barrier. The failure of RPV could cause high temperature corium discharge into containment. This might lead to the failure of the last barrier, and a large amount of radioactive release from nuclear power plant to the environment. Thus, how to prevent the radioactive release is very important in establishing severe accident management guidance[1].

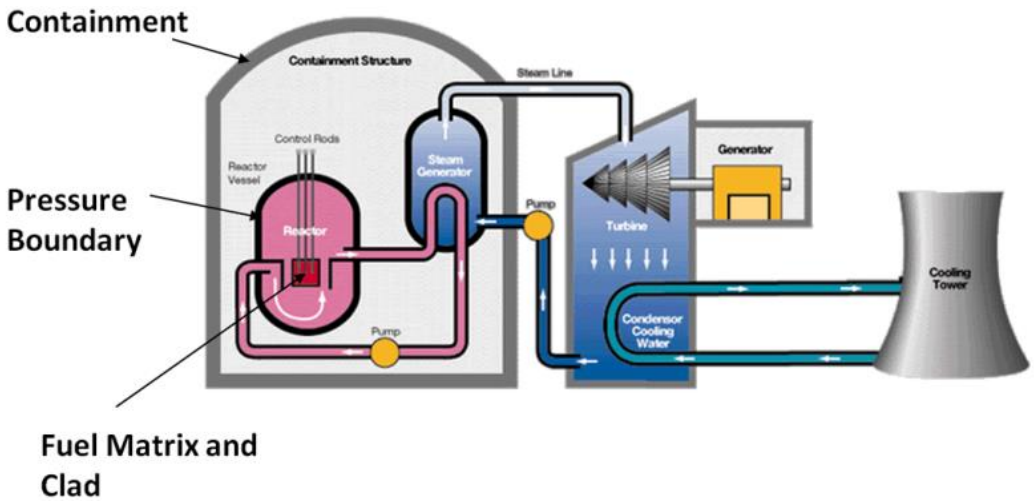

Figure 1-1 Four physical barriers in a typical nuclear power plant[2]

Since RPV is the last in-vessel barrier in nuclear reactor, how to keep its integrity is very important in order to prevent further late containment threats such as molten

corium-concrete interaction (MCCI). The high temperature molten core materials from the core region could fall into lower plenum. During the falling process, the jet breakup process could happen and cause the pressure in the lower plenum to increase and threaten the integrity of RPV. After falling process, molten pool and debris bed could form in the lower plenum. The thermal and mechanical loading from molten pool, debris bed could threaten the integrity of RPV. The RPV could failure due to creep rupture at last, as shown in Figure 1-2. If RPV fails, it could cause high temperature corium to discharge into containment and lead to MCCI, direct containment heating or steam explosion in light water reactors[3]. Consequently, the progression of corium behavior in lower plenum should be investigated intensively to understand its process and keep the integrity of RPV.

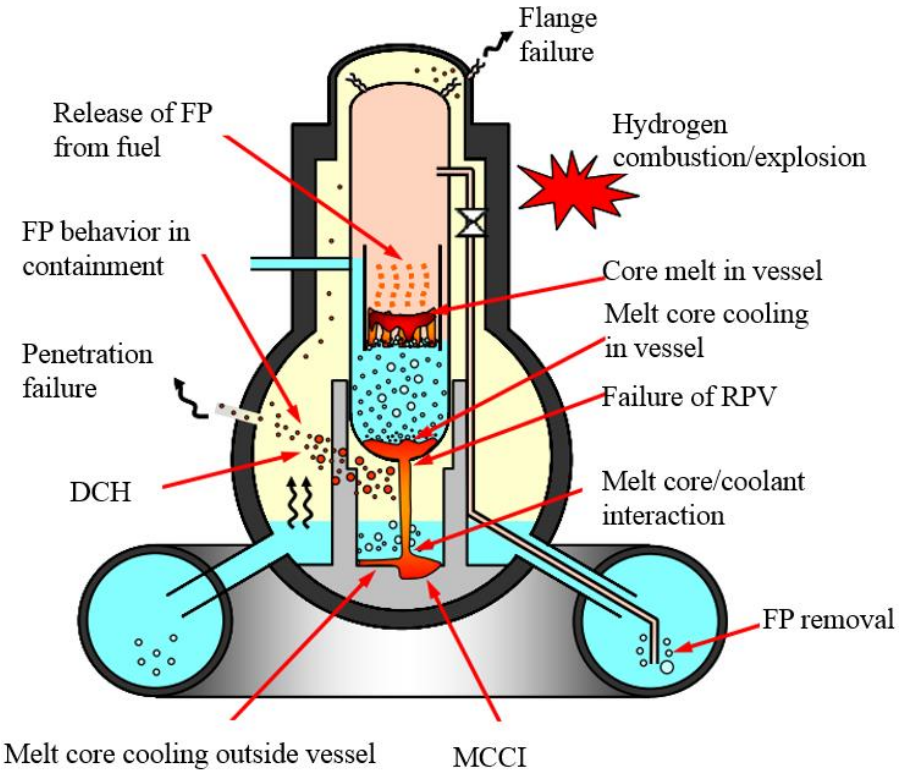

Figure 1-2 Severe accident phenomena in BWR[4]

On March 11, 2011, due to a huge tsunami triggered by the Great East Japan Earthquake, three of the six reactors (Unit 1, 2 and 3) of Fukushima Daiich Nuclear Power Plant were damaged by loss of cooling water. The reactor core was heated up and pressure rose after no cooling water was injected into the reactor. Large amount

of hydrogen was generated and hydrogen explosion occurred, causing radioactive material to release to the environment[5].

According to the analysis results [6], it is very likely that RPV failure must have occurred in Units 1-3. This is the first severe accident occurred in Boiling Water Reactor (BWR) in history. Compared to Pressurized Water Reactor (PWR), there is little research related to BWR severe accident before Fukushima accident. It is still not clear about detailed progression of core degradation and corium behavior in lower plenum. For the Fukushima post-accident management, it is also required the detail knowledge on core material conditions in lower plenum. Thus, it is necessary to carry out the intensive study on corium behavior in BWR lower plenum in order to further ensure the safety and reliability of nuclear power.

1.2 Severe accident phenomena in BWR lower plenum

Compared to PWR, corium behavior in BWR lower plenum is more complicated. This is because there are more than 200 tubes in BWR lower plenum. These tubes can be divided into control rod guide tubes (CRGTs) and instrument guide tubes (IGTs)[7]. Difference almost reflect in penetration tubes influence on jet breakup process, molten pool and debris bed formation, and failure mechanism of BWR lower head[8].

1.2.1 Core degradation

First, after lack of coolant, the decay heat and additional oxidation heat could lead to the core heating up. The core heating up could lead to the core loss original geometry. The occurrence of such phenomenon can last from a few minutes to several hours, with the range of temperature from 1500 K to 3000 K. Early at low temperature, geometrical deformation is mainly ballooning and rupture of fuel rods. In low pressure accident sequences, when core temperature ranges from 1000 K to 1200 K, zircaloy cladding could begin to balloon, and rupture could occur. In high pressure accident sequences, damage of zircaloy cladding may delay until core temperature reaches 1500 K. When core temperature ranges from 1500 K to 1700 K, chemical reactions among Fe-Zr, B_4C- Fe, Ag-Zr, and B_4C-Zr would lead to early liquefaction and relocation of core structures. In this process, most important result is control

materials separating from fuels[9]. When the core temperature is above 2000 K, zircaloy cladding will melt. In some cases, zircaloy will fall into lower core region. When fuel and oxidized cladding material reach their melting point, fuel and remaining oxidized cladding material will slump to lower core region. Depending on slumping material location and temperature gradient inside the core, ceramic fuel and oxidized cladding material could relocate to a cooler core region. Bundle experiments indicate that the collapse temperature of the fuel is about 2500-2600 K, followed by molten pool formation[3], as shown in Figure 1-3.

Core materials, initial uncovery, core heating rate and system pressure would influence core degradation time[10]. Among core materials, chemical reaction is main reason of core degradation, this can also lead to formation of low melting point alloys. Thus, in all core oxidation process, zircaloy oxidation behavior by steam could have very huge effects on core degradation and hydrogen production. Some experiments also suggest that oxidation of B_4C could play an important role in generation of hydrogen and other gases[3].

For BWR, two-phase flow before severe accident has influence on timing of dry-out and core uncovery. It is possible that radial mixing happens in PWR while there is no radial mixing among BWR core channels. Because configuration of gap and channel affect melt debris relocation path, debris in channel and debris in gap are separated before canister is melted through by ablation. Moreover, in PWR, supporting plate damage could lead to collapse of fuel and debris above it. In the other hand, in BWR core plate damage will not lead to collapse of fuel modules, but BWR core collapse depends on the integrity of CRGTs in lower plenum[3].

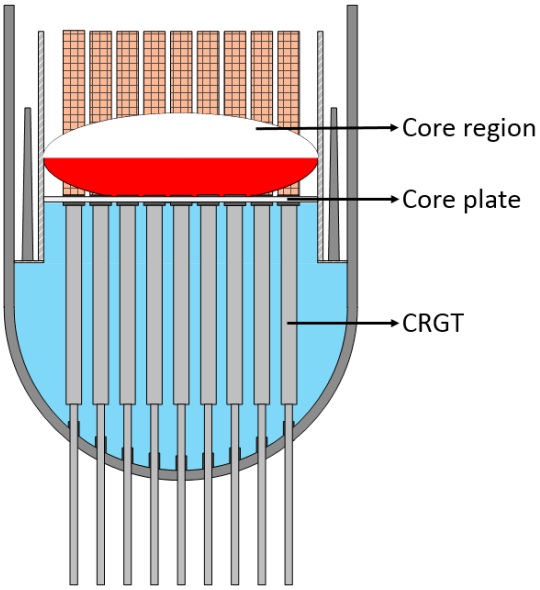

Figure 1-3 Process of molten pool in core region

1.2.2 Jet breakup process

A further rise in temperature of collapsed core materials could cause molten core materials to move to lower plenum[11]. This falling behavior of molten core materials into lower plenum depends on water condition in lower plenum. In the dry condition, molten core materials can directly contact with lower head structure and melt through structure quickly. In the other hand, in wet condition, jet breakup process could happen during molten core materials falling process. Jet breakup process is a violent fuel coolant interaction. Due to instability between molten jet and coolant, fragmentation behavior could happen. Molten droplets could departure from jet surface. The size of such molten droplets is very small, usually the order of several millimeter. The heat transfer between molten droplets and coolant is very strong, and it will cause the system pressure in the vessel to increase very quickly. The remaining molten jet could form molten pool in the lower plenum. The molten droplets could be cooled down and form debris bed in the lower plenum[12]. The fragmentation behavior of melt will provide long-term coolability of debris and vessel wall. Heating

of lower head structure will be delayed and this could reduce direct attack from melt to vessel and risk of immediately vessel damage[3].

The molten core materials falling mass and falling position would influence the jet breakup process. The falling path of core material from the original core region to the lower plenum can be divided into two kinds: one is sideward falling along the peripheral region of the core and another is downward falling through the failed core plate. Different core degradation process could cause different molten core materials falling mass. The falling position and falling mass provide the initial condition for jet breakup process, which will affect how much of jet could become molten droplets. The jet breakup behavior provides initial conditions for later molten pool and debris bed behavior in lower plenum[3].

However, for BWR, jet breakup process may be quite different. Due to large number of CRGTs and IGTs, jet breakup process could be restrained in BWR lower plenum. In detail, jet could only flow inside flow channel formed by structure in BWR lower plenum, as shown in Figure 1-4. From this viewpoint, the jet radiation expansion behavior would be limited and molten droplets falling behavior would also be limited by these CRGTs[13], [14]. The jet may contact with structure during falling process, and part of jet may solidify on structure surface. Moreover, the CRGTs could also affect the jet falling position. Unlike the condition jet falls outside CRGTs, molten core materials could also fall inside the CRGTs.

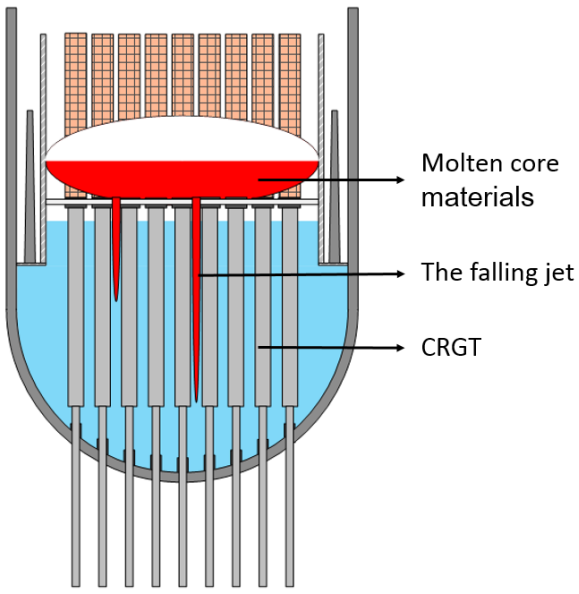

Figure 1-4 Jet breakup process in BWR lower plenum

1.2.3 Molten pool and debris bed behavior

When the molten core materials falls into lower plenum, after jet breakup process, it may form different morphologies. If the material temperature is higher than melting point, molten pool could form directly by the falling materials. Molten pool behavior is the mixture of multi-component and multi-phase phenomenon at high temperature, and could form stratified pool configuration with oxidic and metallic layers. The metallic layer could be over oxidic layer and occupy the upper part of the molten pool due to the density difference of oxidic and metallic materials. Heat transfer of molten pool is a complex phenomenon, of which may include focusing effect, upward radiation heat transfer (if lower plenum in dry condition), heat transfer between dry and wet particle bed and heat transfer between corium and coolant[3]. In the other hand, the solidified fragmentation particles could form debris bed in the lower plenum. If debris bed is surrounded by water and is not subject to critical heat flux and limitation of porosity, debris will not be heated up and will be quenched. If convection heat transfer from debris to coolant is smaller than heat generation, debris will be dry out and melt, mixture with molten pool again[3].

The falling core materials from the core region could also include metallic components. If water still exist in the lower plenum, these metallic components could breakup up and oxidized by water and change the composition of molten pool. For large molten pool, the decay heat could cause the corium pool temperature further heat up. Vaporization of metals and fuel could happen, and this could affect the fission product release. If water could keep injecting in the lower plenum during severe accident progression, it could provide better cooling for debris bed and molten pool, and also mitigate the thermal loading from molten pool and debris bed to RPV wall[3].

Compared to PWR, the molten pool and debris bed behavior is more complex due to the existing of CRGTs, as shown in Figure 1-5. After water boiling off, CRGTs will be heated and melting and provide corium metal mass. This will cause a higher fraction of metal mass inside BWR corium. Also, CRGT cooling system of BWR provides a method for in-vessel coolability and retention. It is because water flows inside BWR CRGTs under normal operation. Cooling flow inside CRGTs can be

provided by a battery driven pump, because cooling flow rate inside CRGTs is small. Coolant flow inside CRGTs can be used to remove decay heat in process of accident. This method could act as a mitigative method to reduce thermal load for lower head structure, reduce vessel failure time, reduce mass of melt discharge from lower plenum when RPV failure, and provide possibility for corium cooling and retention[15], [16].

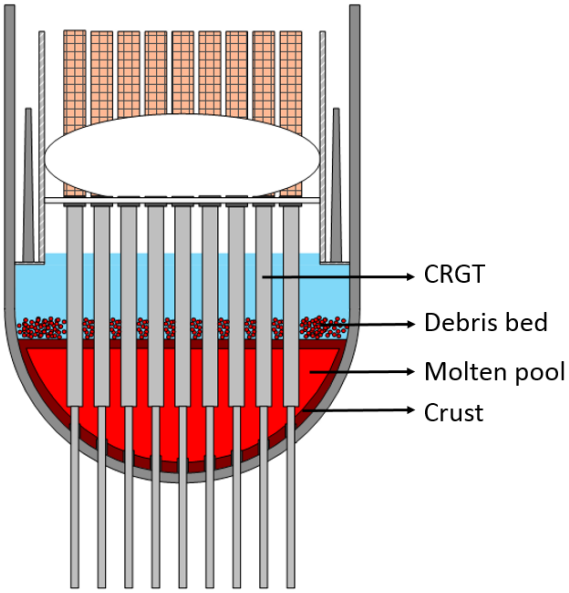

Figure 1-5 Molten pool behavior with debris bed in BWR lower plenum

1.2.4 BWR lower head failure mechanism

Through the loading from internal pressure, molten pool and debris bed, RPV wall may not keep its integrity and fail at last. During this progression, internal pressure and gravity load from materials in the lower plenum will cause primary stresses. The stresses would not decrease due to vessel wall deformation，but increase even wall thickness reduction. The temperature of the RPV would increases due to heat transfer from the corium pool to the vessel wall. And temperature gradients can lead to the second layer stresses. Thus, the main deformation mechanism of RPV wall is caused by creep and plasticity[17]. What's more, inside the METCOR experiment, corrosion process and eutectics formation could cause steel ablation at the interface between corium and vessel[18].

The pressure of BWR is usually lower than PWR. For BWR, wall is usually thinner than PWR. However, considering these two effects, BWR and PWR have similar behavior in creep rupture failure aspect. Due to thinner wall, the ablation of BWR vessel wall may be faster. In the other hand, penetration tube failure is more likely to happen than RPV wall melt-through failure, as shown in Figure 1-6. For BWR lower head, IGTs will be easier to fail because size of IGTs is smaller and there is no external support. Melt attack will cause damage of the weld between penetration housing and stub tube. Molten corium will enter interior space of penetration, and lead to further penetration damage[3] [19].

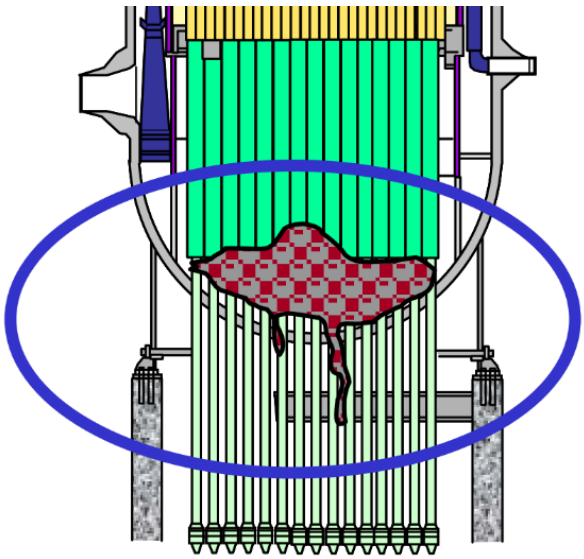

Figure 1-6 Failure of BWR lower plenum [6]

1.3 Past experimental study in lower plenum

1.3.1 Jet breakup experiments

A number of jet breakup experiments have been carried out to investigate jet fragmentation behavior in water pool. The purposes and objectives of jet breakup experiments are mainly 1) to identify physical processes in order to understand important phenomena during jet breakup process, such as breakup fraction, particle size, pressure increase and steam explosion possibility, 2) to provide quantitative and detailed experiment data to validate specific models and codes on simulation of jet breakup process. Some important jet breakup experiments, such as FARO [20], [21],

TROI [22], WFCI [23]and KROTOS [24], were conducted under the conditions close to the real case. A summary of some important jet breakup experiments is presented in Table 1-1.

Table 1-1Summary of important jet breakup (fuel coolant interaction) experiment

Program	Organization	Jet materials	Investigation emphasis
FARO	Ispra, Italy	UO_2+ZrO_2 (Zr)	Provide most prototypic data with corium melt being discharged into water close to its saturation temperature.
KROTOS	Ispra, Italy	Alumina, or Al_2O_3, or UO_2+ ZrO_2	A unique selection of experimental data for steam explosion and useful basic data for model development
WFCI	University of Wisconsin US	Tin	Detailed experimental data for propagation/escalation and expansion phases of vapor explosions.
TROI	KAERI Korea	UO_2/ZrO_2	Fundamental issue of explosively of reactor material contribute to development of severe accident management strategy for advanced Light Water Reactors (ALWRs).
MIXA[25]	AEA Technology	UO_2/Mo	Examination of mixing of pre-fragmented streams of UO_2/Mo at high temperatures (~3600 K) entering water in a jet-like configuration
QUEOS[26]	FzK, Karlshure, Germany	Molybdenum spheres or zirconia spheres	Study quenching of spheres 4-5 mm and 10 mm diameter with initial temperatures in range 1000 K- 2600 K
PREMIX[27]	Karlsruhe Germany	Alumina	Study mixing of high temperature melt streams with water at ambient and elevated pressures

1) FARO experiment

FARO experiments were performed at JRC Ispra[28]. FARO tests were designed to investigate corium/water interaction by using prototypical materials. These tests studied effects of system pressure, water depth, subcooling, and hydrogen generation on jet breakup process. The experiment provided behavior of water to quench core material before core material fell into pressure vessel bottom.

Figure 1-7 shows FARO equipment facility. Interaction vessel TERMOS and crucible were connected by release channel. The material was melted in FARO furnace, then delivered to release vessel, and then released into water. In initial condition, release vessel and furnace were under low pressure (0.2 MPa). When UO_2-ZrO_2 mixture was released to release vessel, protection valve SO1 and main isolation valve SO2 were shut down. Through use of argon, release vessel was pressured to pressure of THERMOS. When the pressure was equal, two melt catcher flaps open automatically. The lower flap allowed melt fall into water only by gravity. After mixed with water, debris on catcher was collected.

Following conclusions were obtained from this experiment. In FARO experiment, data on debris bed morphology was obtained after molten materials were quenched in water. Important data, such as melt jet breakup, energy release, debris morphology, bottom plate thermal shock, and zirconium oxidation were obtained from experiment. Compared with pure oxidic melt, in UO_2-ZrO_2 melt, additional metallic zirconium would improve early melt quenching and also lead to obvious production of steam and pressure increase in container.

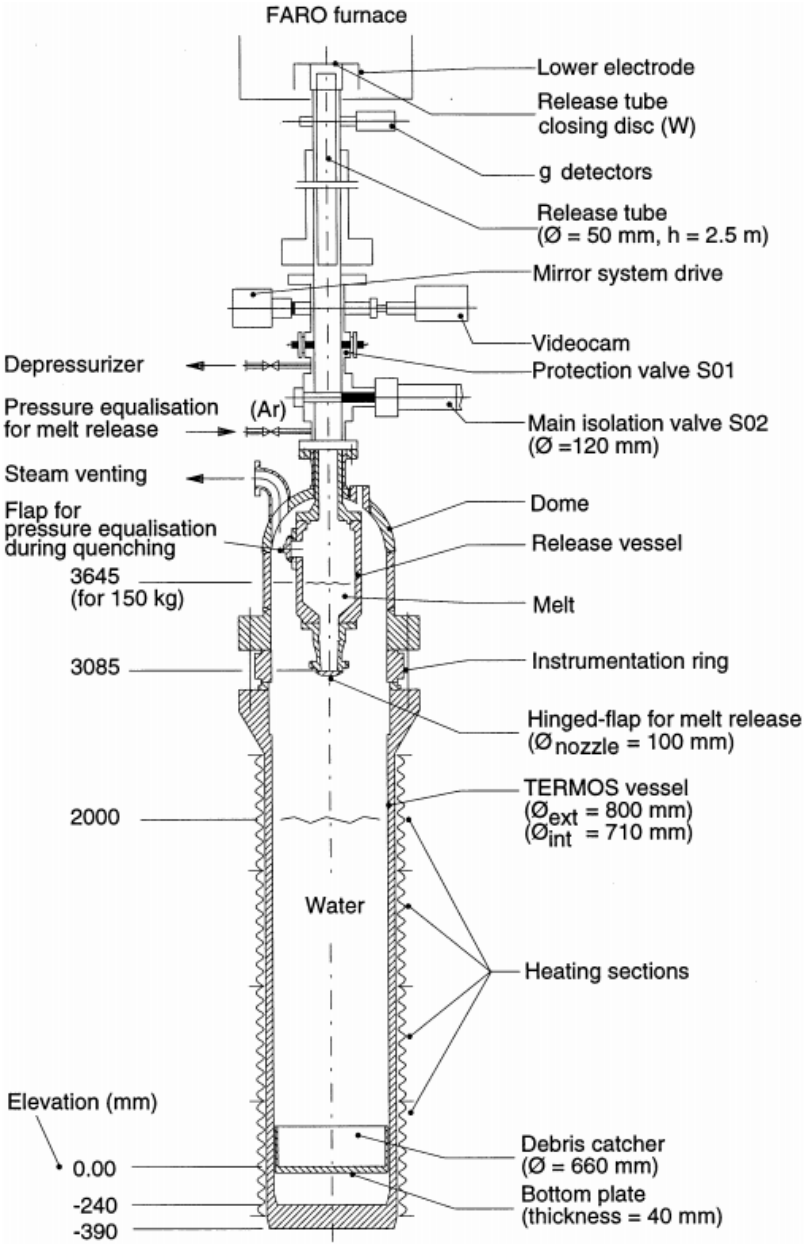

Figure 1-7 FARO test facility [28]

2) Jet breakup experiment for BWR lower plenum

A visualized jet breakup experiment was conducted by Saito et al. to simulate severe accident sequence in a BWR lower plenum [13]. Experimental equipment included a test section, a steady jet injection equipment and measurement equipment. The process of experiment was as follows. First, injection nozzle was adjusted to set position and height. After the set, water was injected into test section until water level reached set height. The simulant material was injected into tank by jet injection equipment. Jet behavior was captured by a high-speed camera.

Figure 1-8 shows jet injection behavior with and without tube structure. Through multi-channel experiment. From the experiment time series of jet velocity depended on complicated structures exists. The experimental results show that complicated structure could prevent jet expansion behavior in radial direction. Through experimental and theoretical results of contrast, the main fragmentation mechanism of jet breakup was shear stress. A correlation to calculate fragments' diameter inside BWR lower plenum was proposed by Saito et al. based on the experimental results [13].

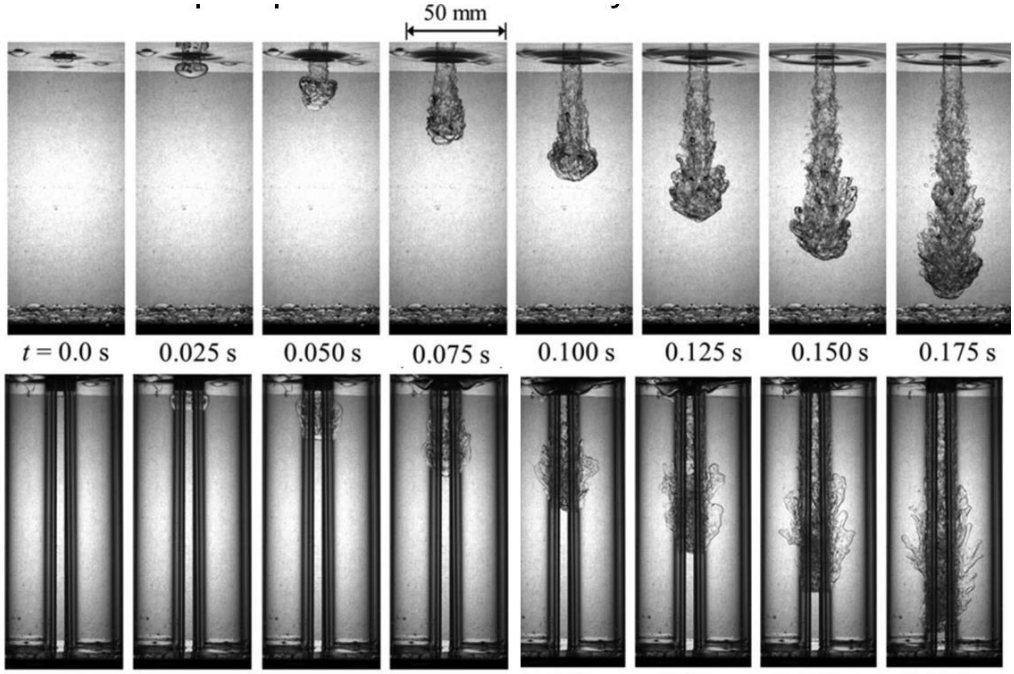

Figure 1-8 Saito et al. experiment images [13]

However, the jet breakup experiment related to BWR performed by Saito et al. had following limitations. Firstly, jet breakup experiments should indicate the amount of jet that becomes droplets (jet breakup fraction), but this experiment did not provide corresponding data. Secondly, surface tension of Fluorinert is similar to water, which may reduce droplet departure from surface of jet. Thirdly, particle diameter can be calculated from critical Weber number, yet surface tension also influences droplet diameter. Table 1 2 shows physical properties of corium and Fluorinert, from which it is clear that there is large difference on physical properties between corium and Fluorinert. A jet breakup experiment using the material whose physical properties are similar to the real corium needs to be conducted.

Table 1-2 Physical properties of corium and Fluorinert [13]

	Corium (80% UO_2, 20%ZrO_2)	Fluorinert
Density (kg/m^3)	7960	1830
Surface tension (N/m)	0.57	0.043

1.3.2 Scale experiments

A number of scaled experiments have been carried out to investigate molten materials behavior in lower plenum and lower head failure mechanism, such as COPO, ACOPO and LIVE[29]. The purpose and objectives of such experiments are mainly 1) to clarify thermal and chemical behavior of molten material in lower plenum and stratification behavior, 2) to get knowledge on failure time and events of lower head under different conditions, 3) to provide data for heat transfer correlations for severe accident analysis codes. A summary of some important experiments is presented in Table1-3[29].

Some of the important experiments can be concluded as the following aspects:

1) ACOPO experiment was used to study characteristics of natural convective heat transfer in a half-scale of RPV geometry volumetrically heated pool[30]. This experiment provided data on Rayleigh number up to 10^{16}. ACOPO test section was a 2 m diameter of hemispherical container, and was made of square tubing cooper. ACOPO results identified some important parameters for in-vessel retention (IVR) severe accident management strategy. The externally and internally driven natural convection problems were exactly analogous. The results from internally driven experiments could be used when there was exact geometric (including cooling walls) similarity. The heat transfer correlations in high Rayleigh number were obtained.

2) SIMECO was designed to study stratification effect on heat transfer characteristics of pool boundaries[31]. Effects of density difference between layers and miscibility or immiscibility of layers were studied. The experimental facility included a slice-type of vessel. The vessel included a semicircular section and a vertical section. The

following conclusions were obtained from this experiment. Interface between two layers could create additional upward thermal resistance. It would cause increase of downward heat transfer and maximum thermal loading on vessel just below interface. The maximum temperature and heat flux in heterogeneous pool were higher than that in homogeneous pool.

3) BALI experiment was used to provide heat transfer data base at corium pool boundaries for in-vessel and ex-vessel configuration[32]. Mechanistic research is related to volumetric heating of natural convection in high Rayleigh number (10^{15} to 10^{17}). 2-D full scale hemi-cylindrical was used in this experiment. Volumetric heating is obtained by direct current heating, of which water itself act as electrical resistance. Ice crust formation is obtained by heat exchanger, which is cooled by nitrogen. Through the experiment, heat transfer data of corium pool was obtained. The results from BALI and COPO Ⅱ experiment matched very well. Through experimental results and a simple transposition model, 3-D heat transfer correlations were obtained for reactor applications.

Table 1-3Summary of some important molten pool experiments[29]

Program	Organization	Simulant	Coolant	Investigation emphasis
UCLA	UCLA, USA	Freon-113	Water	Natural convection heat transfer in homogenously heated pools and effect of different boundary conditions
ACOPO	UCSB	Water	Water	Natural convection heat transfer in homogenously heated pools and confirmation and extension of mini-ACOPO results
SIMECO	KTH, Sweden	$NaNO_3$-KNO_3; Paraffin-water-chlorobenzene	Water	Natural convection heat transfer in homogenously heated pools and effect of two-layer and three-layer stratification
BALI	CEA, France	Salt water	Water	Natural convection heat transfer in homogenously heated pools, effect of viscosity and porosity and focusing effect of top met allayer
LIVE	KIT, Germany	$NaNO_3$-KNO_3	Water	Natural convection heat transfer in homogenously heated pools, crust growth characteristics and effect of initial relocation conditions
SIGMA -CP	Seoul National University, Republic of Korea	Water	Water	Natural convection heat transfer in homogenously heated pools and confirmation of custom designed heater
RASPLAV	GRS Germany	UO_2-ZrO_2- Zr, NaF-$NaBF_4$	$NaNO_2$-$NaNO_3$-KNO_3	Natural convection heat transfer in homogenously heated pools, prototypical material study and effect of layer stratification

1.4 Severe accident analysis codes

Most of severe accident experiments were used to point out significant events and clarify specific phenomena in detail. It is difficult to clarify different phenomena in full-range of a severe accident scenario by experiments. Integrated experiments used to simulate different severe accident conditions and using radioactive nuclides are difficulty and costly.Thus, it is necessary to have a code for whole-plant severe accident analysis. Currently, MELCOR and MAAP are widely used in severe accident analysis. These two codes use lumped parameter method. These two codes mainly use empirical correlations, many parameters from large-scale experiments and user tuning parameters. These two codes have the capability of evaluation of severe accident measurement and sensitivity analysis of PRA Level2 studies[33] [34] [35].

1.4.1 MELCOR

MELCOR was developed by Sandia National Labs (SNL) from 1982 and released in United States in 1986[3]. MELCOR is an engineering-level and fully integrated simulation code, which is used to calculate severe accident progression in a LWR. MELCOR could be used to simulate almost full range of phenomena in LWR, including thermal-hydraulic response of primary reactor coolant system under normal condition and severe accident sequences in LWR, core degradation, failure of lower head, core-concrete interaction, hydrogen production, fission product release, behavior of radioactive aerosols in reactor containment building. MELCOR has a number of different packages. Each package could be used to model a different portion of accident phenomenology or program control. For example, Control Volume Hydrodynamics (CVH) package simulate thermal-hydraulics of control volumes, and Core (COR) package investigate core and lower head behavior[36][37].

MELCOR COR package is used to investigate thermal response of core and lower plenum. This package can be used to simulate the progression from core relocation to debris injection into reactor cavity. As shown in Figure 1-9, core and lower plenum regions can be divided into concentric radial rings and axial levels. In individual cells, fuel pellets, cladding, grid spacers, canister walls, core baffles and formers, molten pool and particulate debris, were simulated respectively. In COR package, lower head

hemisphere and head penetrations (CRGTs and IGTs) were considered in lower plenum. Lower head can be divided into segments according to the user requirement. Vessel can be divided into several different temperature nodes. Heat transfer between penetration tubes and lower head nodal, debris and molten pool components is calculated. Heat transfer between particulate and debris, and convective heat transfer between debris and lower head surface are also simulated.

In MELCOR 1.8.6 and 2.1, in order to obtain a more detailed simulation of temperature profile in lower head, multiple segments are allowed to connect with a COR cell. The elevation of upper surface of a molten pool in lower plenum is simulated. Only heat transfer between molten pool and segments below upper surface is considered. In order to evaluate lower head failure mechanism, four damage criteria are used in COR package. The temperature of a penetration reaches the failure point set by user. A failure logical control function is found to be true. The lower head fails due to overpressure. Creep rupture failure of a lower head segment occurs. After lower head failure, two options are provide for user to simulate the mass of material that is available for ejection. One option is that the material is allowed to eject, no matter material is in melt or solid condition. Another option is that whether the material is allowed to eject and how much of the material is allowed to eject depend on the material conditions. For example, the masses of steel, zircaloy, and UO_2 available for ejection are only masses of these materials that are in molten condition.

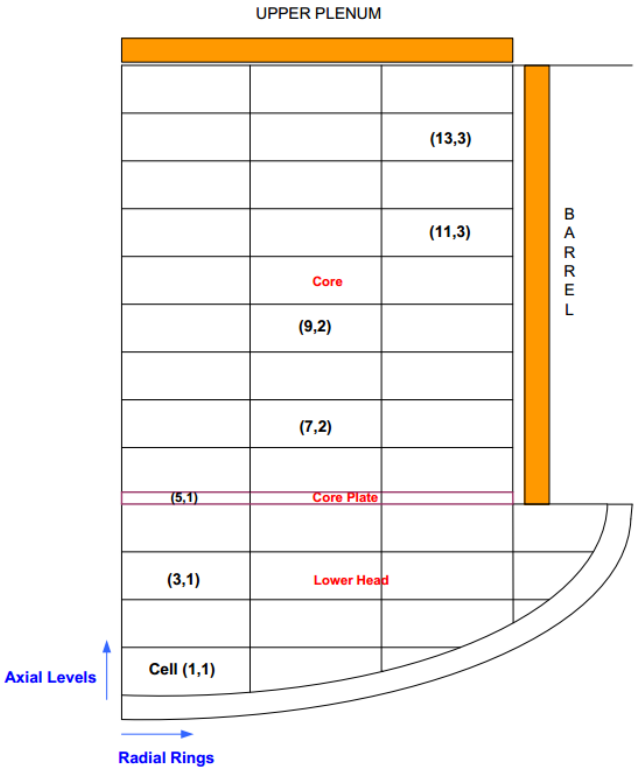

Figure 1-9 Illustration of lower head debris bed node in MELCOR [37]

1.4.2 MAAP code

The Modular Accident Analysis Program (MAAP) code was developed in early 1980s by Fauske and Associates [3]. MAAP can be used to analyze accident progression almost in all phases, including prediction of key events timing, evaluation of influence of mitigative systems, evaluation of effects of operator actions, and calculation of in-plant and ex-plant radiation doses. The phenomena that MAAP code could simulate include steam formation, core heat-up, cladding oxidation and hydrogen evolution, vessel failure, core debris-concrete interactions, ignition of combustible gases, and fission product release, transport, and deposition.

As regards to jet breakup behavior of corium, the falling jet is considered to be fully molten. The erosion of molten cylindrical jet model is used to simulate jet falling process. Particle size is determined by melt surface tension. Data from zirconium particle oxidation experimental is used to evaluate debris particulate oxidation behavior. Inside MAAP code, debris bed is divided into oxidic pool and overlying metallic layer. Crust could form at three positions: upper surface, RPV wall and

internal structures. The steady-state heat transfer relationships are used for heat transfer calculation. For crust, the temperature profile is 1-D, and internal decay heat is considered. Debris is mixed homogenously, and shares same thermo-physical properties. Debris crust and debris pool have same composition. Average debris temperature is used to evaluate debris is in solid or liquid condition. The metallic layer forms above pool at same time. For metallic layer, crust formation is not considered. The potential chemical attack from molten pool to RPV wall is not considered. The following phenomena are used to evaluate the failure of RPV. The attack from molten core debris will cause the damage of penetration. The heating from debris could weaken the weld of penetration support. Internal pressure, debris weight and high temperature together can lead to creep rupture of reactor vessel wall [38]–[40].

The following improvements were added in MAAP 5.0, in aspects of creep model, corium pool thermal–hydraulic model, and ex-vessel heat transfer model. The metal material properties were updated and expanded. The mechanistic heat transfer model used to simulate core debris in lower plenum was improved. A new insulation cooling channel between reactor vessel lower head and surrounding insulation was added. MAAP 5.0 could provide a more detailed calculation of heat flux in water flow channel. In BWR downcomers, volume versus height table is used to improve water level calculation. In lower plenum corium pool simulation, the model used to simulate the possibility of metallic crust formation above metal layer if water exists was added[41].

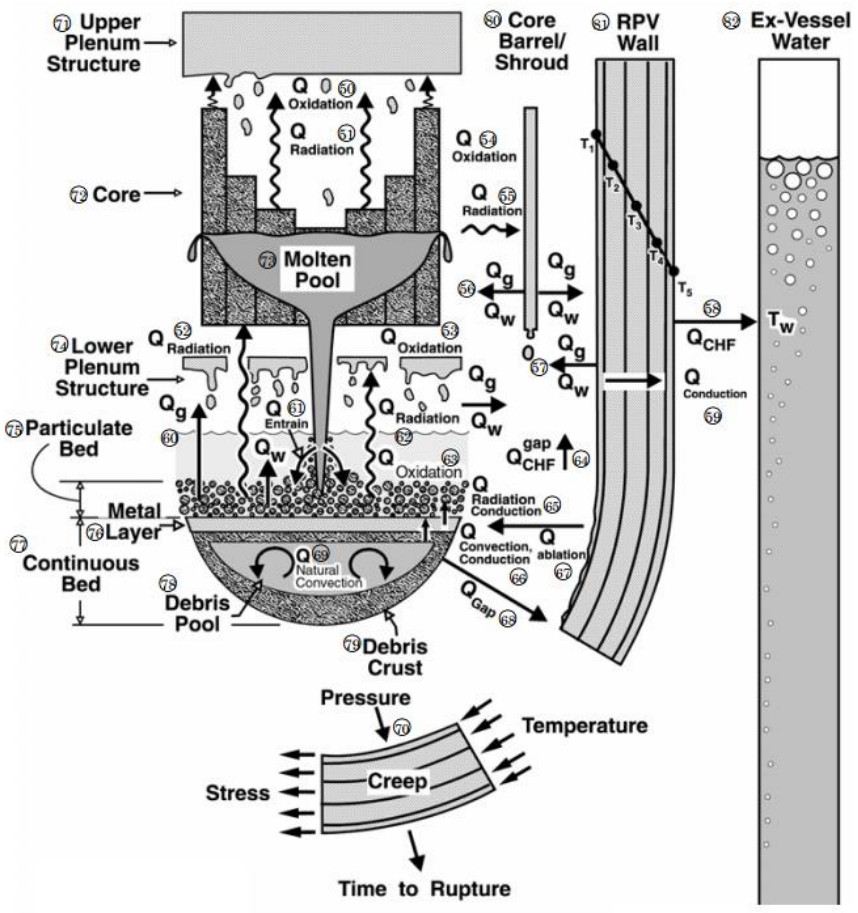

Figure 1-10 BWR lower plenum model in MAAP [42]

1.4.3 Limitations of MELCOR and MAAP

The limitations of MELCOR and MAAP are as follows:

1) These two codes lack of mechanistic models, for example, Navier-Stokes (N-S) equations are not solved in these codes. Molten pool could form in BWR lower plenum, with natural convection. Mechanistic models are needed to analyze such convection behavior and temperature distribution in molten pool.

2) These codes apply simplified models, which means that lumped parameter methods are used in MELCOR and MAAP. The complex thermal-hydraulic and severe accident phenomena must be considered in development and validation of severe accident management[43] [44]. Therefore, many of these complex interaction cannot be accurately predicted by these traditional codes. In mesh generation method, only several control volumes are used.

3) Many user tuning parameters and correlations are used in MELCOR and MAAP, which means that many parameters could be adjusted by users. Even for same conditions, different users could have different simulation results.

From the perspective of mechanistic modeling, the United States Nuclear Regulatory Commission (USNRC) has developed RELAP/SCDAP for the analysis of severe accident events in the reactor vessel and CONTAIN for the events inside the containment. Due to the complexity of severe accident phenomena, these mechanistic codes still could not obtain a sufficient understanding of these phenomena. They adopted simplified models. For example, SCDAP/RELAP5 could not simulate core materials spreading behavior in the vessel, and CONTAIN could not simulate the hydrogen combustion behavior. Moreover, the steam explosion was not simulated in these codes. In addition, they could not simulate the whole sequence from the RPV to the containment[35].

1.5 SAMPSON code for BWR lower plenum analysis

1.5.1 SAMPSON

Considering the importance and necessity mentioned above, SAMPSON (Severe Accident Analysis Code with Mechanistic, Parallelized Simulations Oriented towards Nuclear Field) has been developed based on fundamental physical principles, theoretical-based equations and mechanistic models. SAMPSON code was developed by Nuclear Power Engineering Corporation (NUPEC, Japan) in framework of IMPACT (Integrated Modular Plant Analysis and Computing Technology). SAMPSON code is the best-estimate code aiming at analyzing phenomena that happen in nuclear power plants as accurately as possible [43].

As results, the advantages of SAMPSON are very fewer user tuning parameters, high-speed simulation on the parallel processing of computers, multi-dimensional mechanistic models and consideration of various events in a hypothesized severe accident. Moreover, SAMPSON can be used to simulate a wide range of scenarios covering from the normal operation to the hypothetical severe accident events [44]. A summary of main difference between different severe accident codes is presented in Table 1-4.

As shown in Figure 1-11, SAMPSON has 11 severe accident modules, covering almost all of phenomena that may happen in LWRs. An analysis control module is used to manage analysis modules according to progression of severe accident events. THA is in-vessel thermal hydraulics analysis module. The RELAP section of RELAP/SCDAPSIM was introduced into THA module. FPTA is fission product transport analysis module. FRHA is fuel rod heat-up analysis module, which is used to simulate fuel behavior in severe accident, including fuel rod heat up, cladding oxidation , and melting caused fuel failure. FPRA is fission product release from fuel analysis module, which is used to assess fission product transfer with fuel pellet and fission product release from failure fuel, crust, debris and molten pool. This model is also used for decay heat calculation. MCRA is molten core relocation analysis module. DSA is debris spreading analysis module. DCRA is debris concrete reaction analysis module, which is used to analysis debris spreading behaviors after debris falling into containment vessel and concrete base. This module can be used to assess longer-term core-concrete response. CVPA is containment vessel thermal hydraulic analysis module. VESUVIUS is steam explosion analysis module, which is used to simulate steam explosion inside vessel or in containment by using mechanistic models.

Table 1-4 Comparison of severe accident analysis codes[44]

	MAAP	MELCOR	SCDAP/RELAP	SAMPSON
Developer	US EPRI	US NRC	US INEL→ Society	NUPEC(IAE)
Objective	In+Ex-Vessel	In+Ex-Vessel	In -Vessel	In+Ex-Vessel
Functions	No models on hydrogen explosion and steam explosion	No models on hydrogen explosion and steam explosion	No models on hydrogen explosion and steam explosion	Various areas in a hypothesized severe accident
User tuning parameters	Many	Many	Few	No
Simulation time	Very short	Several times of real time	1/2~1/4 of real time	About 20 times of real time
Characteristics	Many empirical correlations	Many empirical correlations	Similar to SAMPSON	Mechanistic models and fundamental physical principles
V&V of code modeling	Inside user group (part ISP)	Inside user group (part ISP)	Inside user group (part ISP)	ISP

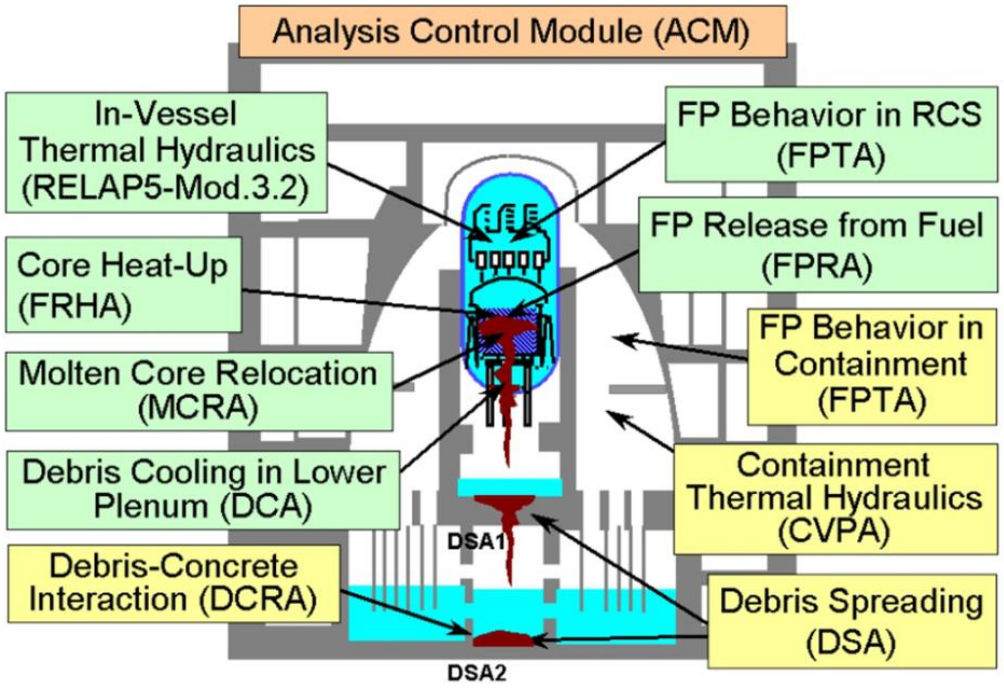

Figure 1-11 Modules of SAMPSON [45]

1.5.2 DCA module in SAMPSON

Figure 1-12 shows detailed information about DCA module, including the following models: the model representing continuation-phase debris spreading in the lower plenum (Debris Spreading), the model representing molten debris natural convection in the lower plenum (Molten Debris Cooling), core melt particle accumulation and cooling model (Debris Bed Cooling), pressure-vessel failure model (Reactor Vessel Failure), model representing gap water cooling between the continuation-phase debris and pressure-vessel wall (Gap CCFL)[46], [47].

1) Debris spreading model

After high temperature molten debris from core region falling into lower plenum, DCA module is used to analyze debris behavior in lower plenum, with the consideration of debris spreading, cooling, solidification and re-melt. Based on debris mass, momentum and energy conservation, three-dimensional (3-D) analysis is performed.

2) Molten debris cooling model

After molten pool is formed in the lower plenum, 3-D N-S equations are solved to simulate molten pool behavior with the consideration of buoyancy effect. Crust is assumed to be surrounding the molten pool. The radiative heat transfer from crust to the lower plenum structure, the convection heat transfer from crust to the water or steam inside the lower plenum, and heat conduction from the crust to RPV wall are considered.

3) Reactor pressure vessel model

After molten pool and debris bed form in the lower plenum, it could transfer heat to the RPV wall, causing the temperature of RPV wall to increase. The RPV model can be divided into 2 parts: reactor vessel heating part and reactor vessel failure part. In reactor vessel heating, 3-D heat conduction equations are solved to calculate the temperature distribution of RPV wall. The convection heat transfer is set as the RPV outside wall boundary condition if RPV outside surface connects with container atmosphere directly. The existence of RPV insulating material is considered as another option. In reactor vessel failure model, three failure mechanisms are considered: creep rupture from Larson-Miller parameter (LMP), melt from temperature increase, and the melt failure of the pipe penetration. The failure temperature and failure diameter are designated by user.

4) Debris bed cooling

The solid particles could form debris bed in lower plenum. Among many models that could be used for the simulation of cooling of debris bed, due to the good agreement with the experiment data, 1-D Lipinski model is used to evaluate the heat flux from the debris bed surface to ambient fluid. If the decay heat could not be removed by the coolant, the debris bed could melt again and mixt with molten pool.

5) Gap cooling model

Gap may exist between crust and RPV wall. DCA module tries to analyze the complex gap cooling phenomena mechanistically. If water does not enter into gap,

heat conduction through the steam layer is considered. If water could enter into the gap, boiling heat transfer at the gap between the crust and RPV wall is considered. Gap Counter-Current Flow Limitation (CCFL) model could be used to simulate the complex gap cooling phenomenon mechanistically. In multi-channel 1-D gap model, each channel can be calculated water ingression lengths. In DCA module, gap model provide boundary conditions for RPV wall and debris heat transfer calculation.

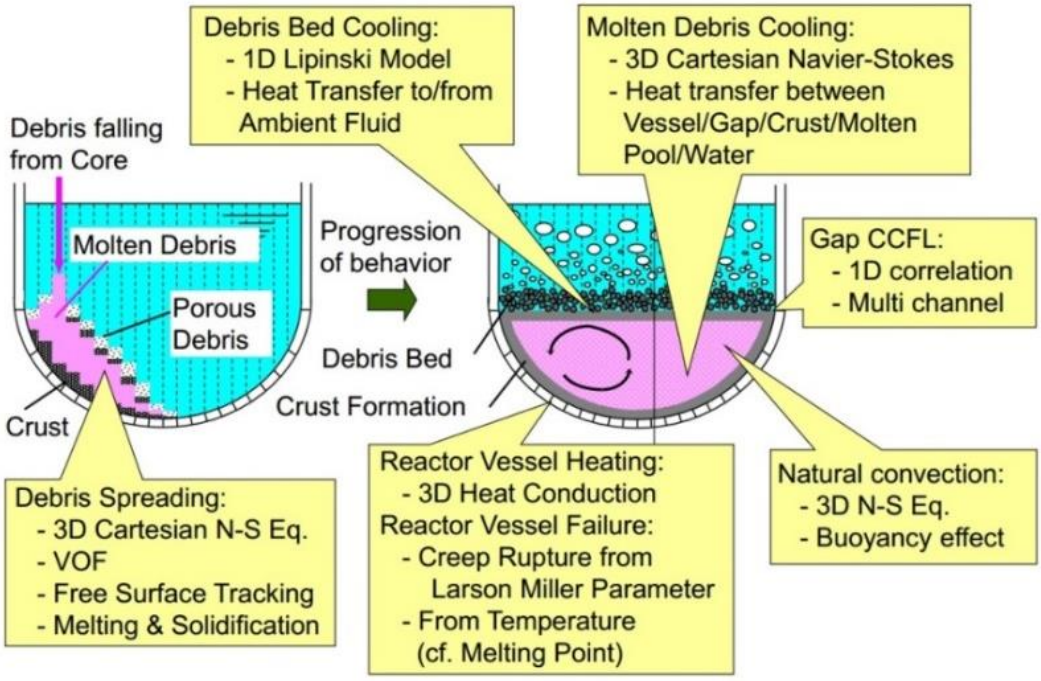

Figure 1-12 Original DCA module in SAMPSON [45]

As a result, the advantages of SAMPSON have been validated against phenomena in DCA module such as natural convection, fluid spreading and solidification[46] [47] [48].

1) For DCA module, in order to analyze the melting and solidification behavior accurately, to confirm DCA could simulate 3-D natural convection is one of the basic requirement. Toda et al. conducted a natural convection experiment under atmospheric pressure by using water as working fluid. By comparing temperature of calculated results and experimental data, the DCA module could reproduce the temperature distribution very well. This suggested that DCA module could predict 3-D natural convection temperature distribution accurately and used to simulate mass and heat transfer by using heat transfer correlations[46].

2) By simulating melt stainless steel spreading behavior in SPREAD experiment, the DCA module flow with consideration of energy transportation and solidification analysis ability was verified. SPREAD experiment was used to clarify melt spreading on the vessel behavior in the concrete floor in the containment. The SPREAD test section was a concrete floor with a cylindrical dam having a slit. By comparing flow spearhead and spreading area between simulation results and experimental data, the DCA module could reproduce the experiment process well. The difference of spreading area between the experimental and calculated results was in the range of - 8% and + 11%. This indicated that the debris spreading cooling model could be used for flow analysis. The DCA module could get reasonable spearhead location, and the simulation of melt pool and crust of spatial distribution, temperature distribution were physically reasonable[48].

3) An experiment on the spreading of water was used to validate the coupled DCA spreading and molten debris cooling models, as shown in Figure 1-13. Although unsymmetrical flow was obtained by the simulation result and the spreading shapes at each time were different from the experimental measurements. However, the average locations of spearhead obtained from the simulation agreed well with the experimental data, which indicated that the spreading model could be used for spreading analysis[47].

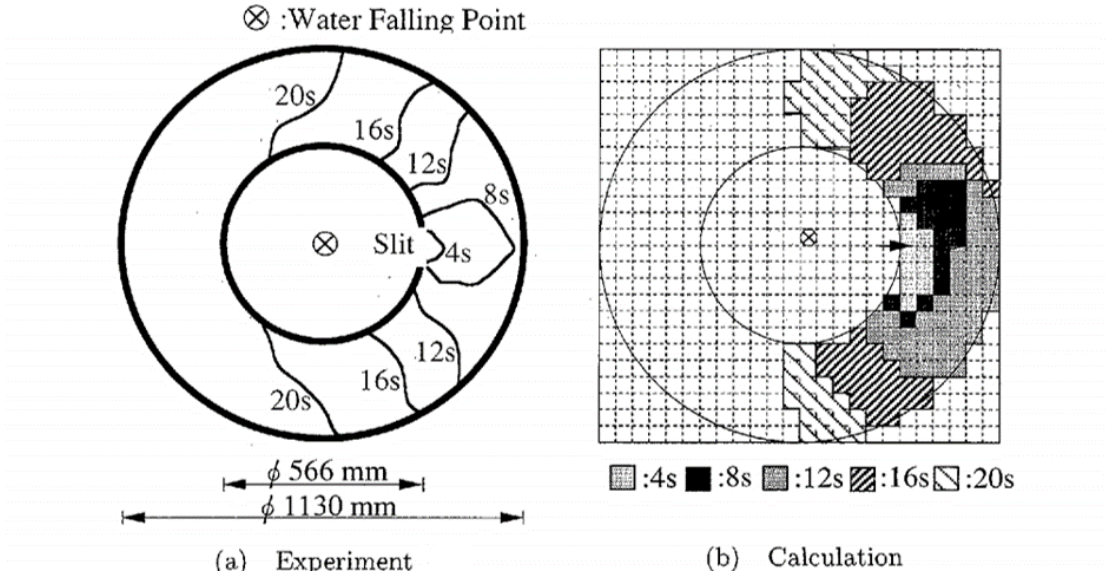

(a) Experiment (b) Calculation

Figure 1-13 Validation with water spreading experiment [47]

1.5.3 Limitations of DCA module for BWR lower plenum

The limitations of DCA module for BWR lower plenum are as follows:

1) Though the coupled DCA spreading and cooling models have been validated by the melting stainless steel spreading and solidification experiment. However, the coupled corium cooling and RPV models have not been validated yet. The large-scale experiment performed under more realistic conditions is needed for an adequate validation in order to confirm whether the DCA module could predict the main parameters of the corium and RPV well and calculate the heat transfer between the corium and RPV wall accurately.

2) Jet breakup process in BWR lower plenum has not been considered in the original DCA module. Jet breakup could happen during corium falling process. The pressure in the vessel could increase due to the violent heat transfer between corium and coolant. The jet breakup process also affect the following molten pool and debris bed formation, which is very important for the evaluation of RPV integrity.

3) In the original DCA module, the influence of penetration tube failure on corium behavior and lower plenum failure mechanism was not considered. In a hypothetical severe accident in BWR, after corium falls into the lower plenum, it could cause penetration tube failure and RPV failure. Which part fails first and how much time it takes for the failure event to happen are also very important for the later mitigation measures of severe accident management and require specific research and simulation work to understand the mechanism.

1.5.4 Developed DCA module for BWR lower plenum

Based on previous discussions, in this study, three additional models have been developed and incorporated into original DCA module for severe accident analysis in BWR lower plenum, namely heat transfer between molten pool and RPV wall model, jet breakup model, and penetration tube melt model, as shown in Figure 1-14.

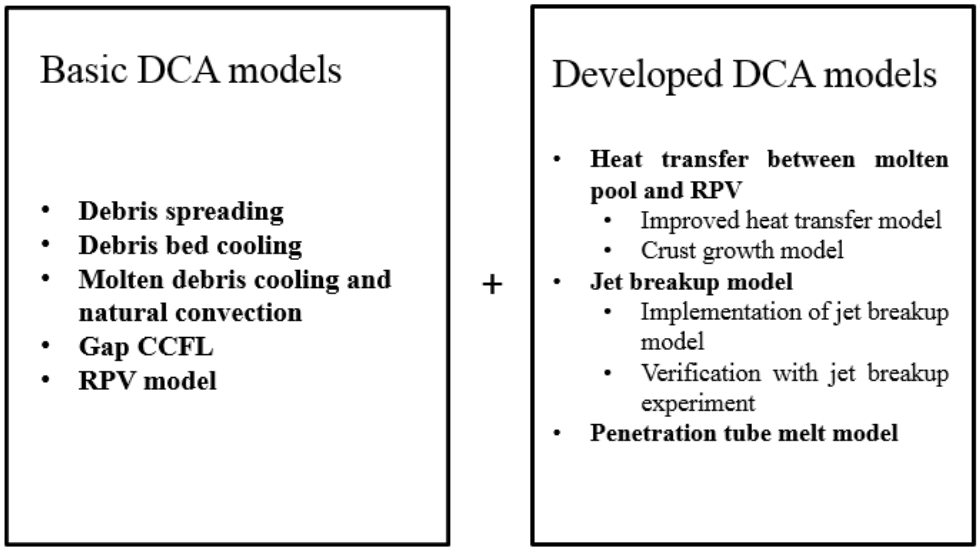

Figure 1-14 Developed DCA module for BWR case

1) Heat transfer between molten pool and RPV wall

The heat transfer between molten pool and RPV wall model has been developed to calculate the heat flux between molten pool and RPV wall based on 1-D convective heat transfer and crust growth models. 1-D transient crust growth model proposed by Zhang et al.[49] has been incorporated into DCA module to calculate the transient characteristics of crust, such as crust growth rate and crust thickness. The heat flux calculation method has also been improved. In the modified DCA module, liquidus temperature is used as boundary temperature instead of crust temperature to calculate the heat flux between molten pool and RPV wall accurately. Various heat transfer correlations have also been incorporated into DCA module to analyze the effects of different heat transfer correlations on the heat flux simulation.

2) Jet breakup model

Jet breakup model has been developed and incorporated into DCA module in order to analyze jet breakup process in BWR lower plenum. 1-D jet erosion model based on Kelvin-Helmholtz (K-H) instability has been incorporated into jet breakup model to simulate how much of jet could become particles. Molten droplet fragmentation model based on Rayleigh-Taylor (R-T) instability has been implemented into jet breakup model to analyze the molten droplets further breakup behavior. A vapor film model based on the quasi-steady state assumption

has also been incorporated into jet breakup model to calculate vapor film thickness and velocity along the jet.

3) Penetration tube melt model

   Penetration tube melt model has been implemented into DCA module to investigate how penetration tubes can affect corium behavior and the integrity of BWR lower head. By considering the heat sink capacity of penetration tubes for corium, 1-D penetration tube melt model has been incorporated into DCA module to calculate the temperature distribution of tubes and failure mechanism of BWR lower head during severe accident sequence.

Above all, the developed DCA module has covered most of the important phenomena that may happen in BWR lower plenum during severe accident.

1.6 Objective of current study

Hence, the main objectives of current study are as follows:

1) To improve DCA module in SAMPSON to simulate corium behavior in BWR lower plenum.
2) To further improve understanding of corium behavior in BWR lower plenum and clarify the tubes effect on the corium behavior.

In this study, DCA module has been improved to simulate corium behavior and clarify the effects of penetration tubes on corium behavior in BWR lower plenum. Firstly, important phenomena in BWR lower plenum during severe accident have been identified. Secondly, the heat transfer between molten pool and RPV wall model has been improved. The jet breakup model has been incorporated into DCA module and verified with a detailed jet breakup experiment. Penetration tube melt model has been implemented into DCA module. Last, after modification of DCA module, through LIVE-L4 test, FARO-L8 test, an original jet breakup experiment, and BWR molten pool simulation, validation and test simulation have been conducted to clarify how and penetration tubes (CRGTs and IGTs) could affect corium behavior in BWR lower plenum during falling process and after molten pool is formed in BWR lower plenum.

1.7 Originality of current study

The originality of current study is reflected on the following three aspects:

1) The past simulation work of traditional system codes, such as MELCOR and MAAP, was not capable to analyze the corium behavior accurately. Penetration tube effect on the jet breakup process was also not considered. The improved DCA module developed in current study is able to reveal effects of jet breakup process and penetration tube on corium behavior in BWR lower plenum.

2) An original jet breakup experiment has been conducted to clarify the effects of CRGTs on the jet breakup process. The simulant material, which has the similar physical properties with prototypic corium, has been used in the current experiment. The relative breakup fraction has been proposed to evaluate jet breakup phenomena in BWR lower plenum.

3) Penetration tube melt model has been incorporated into DCA module to investigate penetration tube effect on the integrity of BWR lower head. The failure mechanism of BWR lower plenum was analyzed by implementation of penetration tube melt model. The results give the knowledge that no matter in wet or dry condition, the penetration tubes could melt very quickly once molten pool formed, which is very important for the severe accident management and evaluation.

Chapter 2 Validation of heat transfer model in DCA module

This chapter focuses on the simulation of LIVE-L4 test by original and modified DCA modules. The simulation has been carried out after heat transfer between molten pool and RPV wall model has been improved and crust growth model has been incorporated into DCA module. The research focus is to investigate the heat transfer between molten pool and RPV wall, and also the crust growth behavior along the vessel. The influence of different heat transfer correlations on the heat transfer behavior has also been studied.

2.1 Original DCA module

In this study, SAMPSON 2013 version was used and DCA module in this version was referred as original DCA module.

2.1.1 Molten debris natural convection model

In molten debris natural convection model, 3-D N-S equations are solved to simulate molten debris convection and cooling behavior. The objective of molten debris cooling model is simulating molten debris pool natural circulation with the consideration of melting and solidification, as shown in Figure 2-1[50].

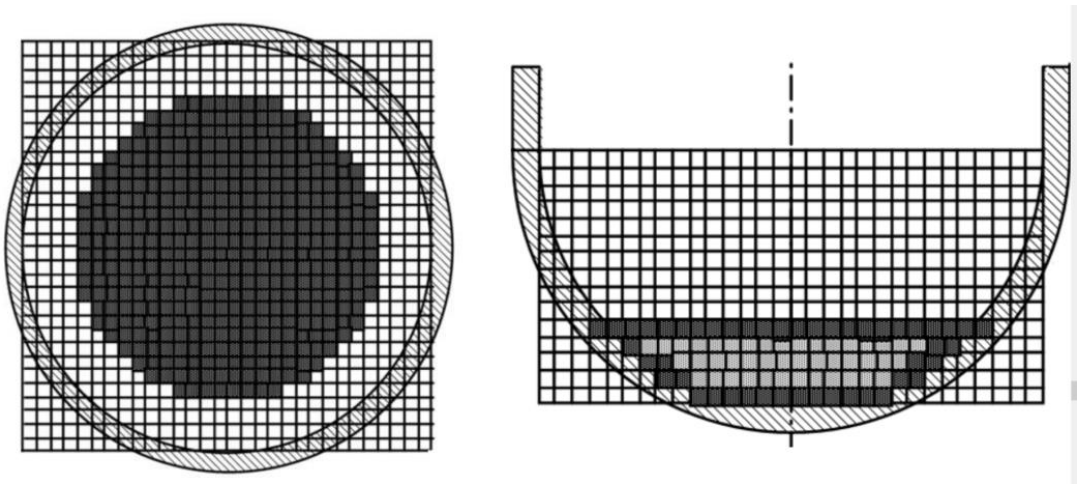

(a) Top view (b) Front view

Figure 2-1 Analytical coordinates in debris spreading-cooling model [50]

The mass, momentum, and energy equations of molten debris are given as:

Mass conversation:

$$\frac{\partial u}{\partial x}+\frac{\partial v}{\partial y}+\frac{\partial w}{\partial z}=0 \tag{2-1}$$

Momentum conversation:

$$\begin{aligned}&\frac{\partial u}{\partial t}+u\frac{\partial u}{\partial x}+v\frac{\partial u}{\partial y}+w\frac{\partial u}{\partial z}\\&\quad=-\frac{1}{\rho}\frac{\partial p}{\partial x}+\frac{1}{\rho}\frac{\partial}{\partial x}\left(\mu\frac{\partial u}{\partial x}\right)+\frac{1}{\rho}\frac{\partial}{\partial y}\left(\mu\frac{\partial u}{\partial y}\right)+\frac{1}{\rho}\frac{\partial}{\partial z}\left(\mu\frac{\partial u}{\partial z}\right)-g\frac{\partial H}{\partial x}\end{aligned} \tag{2-2}$$

$$\begin{aligned}&\frac{\partial v}{\partial t}+u\frac{\partial v}{\partial x}+v\frac{\partial v}{\partial y}+w\frac{\partial v}{\partial z}\\&\quad=-\frac{1}{\rho}\frac{\partial p}{\partial y}+\frac{1}{\rho}\frac{\partial}{\partial x}\left(\mu\frac{\partial v}{\partial x}\right)+\frac{1}{\rho}\frac{\partial}{\partial y}\left(\mu\frac{\partial v}{\partial y}\right)+\frac{1}{\rho}\frac{\partial}{\partial z}\left(\mu\frac{\partial v}{\partial z}\right)-g\frac{\partial H}{\partial y}\end{aligned} \tag{2-3}$$

$$\begin{aligned}&\frac{\partial w}{\partial t}+u\frac{\partial w}{\partial x}+v\frac{\partial w}{\partial y}+w\frac{\partial w}{\partial z}\\&\quad=-\frac{1}{\rho}\frac{\partial p}{\partial z}+\frac{1}{\rho}\frac{\partial}{\partial x}\left(\mu\frac{\partial w}{\partial x}\right)+\frac{1}{\rho}\frac{\partial}{\partial y}\left(\mu\frac{\partial w}{\partial y}\right)+\frac{1}{\rho}\frac{\partial}{\partial z}\left(\mu\frac{\partial w}{\partial z}\right)-g\frac{\partial H}{\partial z}+K\end{aligned} \tag{2-4}$$

Energy conversation:

$$\frac{\partial h}{\partial t}+u\frac{\partial h}{\partial x}+v\frac{\partial h}{\partial y}+w\frac{\partial h}{\partial z}=\frac{\partial}{\partial x}\left(\frac{\lambda}{\rho}\frac{\partial T}{\partial x}\right)+\frac{\partial}{\partial y}\left(\frac{\lambda}{\rho}\frac{\partial T}{\partial y}\right)+\frac{\partial}{\partial z}\left(\frac{\lambda}{\rho}\frac{\partial T}{\partial z}\right)+\frac{Q}{\rho} \tag{2-5}$$

where u, v, w are molten debris velocities, x, y, z are coordinate, p is pressure of molten debris, ρ is density of molten debris, μ is viscosity of molten debris, H is liquid head, g is gravity constant, h is specific enthalpy of molten debris, T is temperature of molten debris, λ is thermal conductivity of molten debris, Q is heat generation of molten debris. K is external force of Boussinesq approximation that can simulate the buoyancy and is given as:

$$K = -\frac{\Delta\rho}{\rho} g \qquad \textbf{(2-6)}$$

In the molten debris natural circulation model, solid-phase rate b is used to evaluate mesh solidification fraction.

$$\begin{aligned} b &= 0 && (h \geq h_l) \\ b &= \frac{(h - h_s)}{\Delta H} && (h_l > h > h_s) \\ b &= 1.0 && (h \leq h_s) \end{aligned} \qquad \textbf{(2-7)}$$

where b is solid-phase rate, h_l is molten debris specific enthalpy at melting point, h_s is debris specific enthalpy at solidification point, ΔH is latent heat.

When the debris mesh is in melting condition, solid-phase rate b is set as 0, and when the debris mesh is in solidification condition, solid-phase rate b is set as 1. If solid-phase rate b exceeds the flow limitation solid-phase rate, the molten debris is assumed as solidified and velocities of molten debris in this mesh were set as 0.0.

2.1.2 RPV model

In DCA module, a transient 3-D heat conduction model is used to evaluate RPV wall temperature distribution, and LMP is used to evaluate creep rupture failure behavior. If RPV wall temperature reaches the setting melting point or creep rupture occurs, RPV is assumed to fail and high temperature molten debris starts to discharge from the vessel.

The RPV wall temperature distribution is calculated by the following equation:

$$\rho \frac{\partial e}{\partial t} = \frac{\partial}{\partial x}\left(\lambda \frac{\partial T}{\partial x}\right) + \frac{\partial}{\partial y}\left(\lambda \frac{\partial T}{\partial y}\right) + \frac{\partial}{\partial z}\left(\lambda \frac{\partial T}{\partial z}\right) + Q \qquad \textbf{(2-8)}$$

where e is the enthalpy of RPV wall, ρ is density of RPV wall, λ is thermal conductivity of RPV wall, T is temperature of RPV wall. Here, Q represents the heat transfer between the RPV and its surroundings. Specifically, for the RPV inner wall, Q represents the heat transfer between the debris and RPV inner wall or between the water/steam still existing in the lower plenum and the RPV inner wall. For the RPV outer wall, Q represents the heat transfer between the RPV outer wall and flooded

water. The external cooling model could be used to evaluate the possibility of in-vessel debris retention.

LMP, which is widely used to evaluate creep failure behavior, is also incorporated into RPV model. LMP is given as:

$$LMP = T(C_1 + C_2 \log_{10} t_{rp}) \quad \textbf{(2-9)}$$

where T is temperature of RPV wall, C_1 and C_2 are experiment constants, t_{rp} is the time until the failure occur.

3-D N-S equations are solved to simulate the molten debris behavior. A transient 3-D heat conduction equation is used to simulate the RPV wall temperature. The heat transfer model used to calculate heat flux between the melt and RPV wall is described as follows.

2.1.3 Heat transfer model

Depending on the debris temperature, the debris in the mesh contacted with RPV wall can be in melt or solid condition. The heat transfer model for the debris and RPV wall can be divided into two aspects: the debris is in solid condition or melt condition.

1) Debris in solid condition

The debris will be in solid condition if the debris temperature is sufficiently low. The heat conduction model is used to simulate the heat transfer between RPV inner wall and solid debris. As shown in Figure 2-2, whether gap exists between the RPV wall and solid debris can be set by the user.

For the condition there is no gap between the solid debris and RPV inner wall, the heat conduction between the solid debris and RPV wall is calculated by the following equation,

$$q_{deb-rpv} = \frac{\lambda_{deb}\lambda_{rpv}\left(T_{deb} - T_{rpv}\right)}{x_{rpv}\lambda_{deb} + x_{deb}\lambda_{rpv}} \quad \textbf{(2-10)}$$

where q is heat flux, λ is thermal conductivity, T is temperature, x is distance, subscript deb is debris, subscript rpv is RPV wall.

For the condition there is a gap between the solid debris and RPV wall, the heat conduction between the solid debris and RPV wall is calculated by following equations,

$$q_{deb-in} = \lambda_{deb} \frac{T_{deb} - T_{deb-g}}{x_{deb}} \quad \textbf{(2-11)}$$

$$q_{rpv-in} = \lambda_{rpv} \frac{T_{g-rpv} - T_{rpv}}{x_{rpv}} \quad \textbf{(2-12)}$$

$$q_{gap-gas} = \frac{\lambda_g}{s}\left(T_{deb-g} - T_{g-rpv}\right) + \left(\frac{1}{1/\varepsilon_{deb} + 1/\varepsilon_{rpv} - 1}\right)\sigma\left(T_{deb-g}^4 - T_{g-rpv}^4\right) \quad \textbf{(2-13)}$$

where q is heat flux, λ is thermal conductivity, T is temperature, x is distance, ε is emissivity, σ is Stefan Boltzmann constant, subscript deb is debris, subscript rpv is RPV wall, subscript g is vapor.

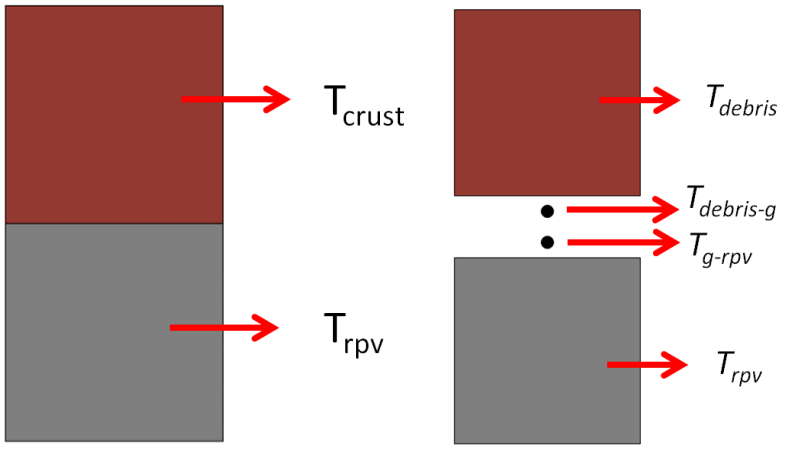

(a) Without gap (b) With gap

Figure 2-2 Heat conduction model between solid mesh and RPV wall used in original DCA module

2) Debris in melt condition

In the DCA module, if the debris in the mesh connected with RPV inner wall is in liquid state, a crust is assumed to form between the molten debris and RPV wall. The heat is first transferred from the molten debris to the crust by natural convection and from the crust to RPV wall by heat conduction. The bisection method is used to solve the heat transfer between RPV wall and molten debris, as shown in Figure 2-3. Because the mesh represents only the melt debris temperature, in the bisection method, the most important task is to determine a suitable crust temperature that can ensure that the heat convection through the melt and crust is the same as the heat conduction between the crust and RPV wall. The crust temperature is set as the average of the melt and RPV wall temperatures in the first stage, and then, interaction is allowed to occur until the difference between the heat convection through the melt and crust and the heat conduction between the crust and RPV wall is smaller than the set value. Whether this method can predict the heat flux for the molten pool should be validated.

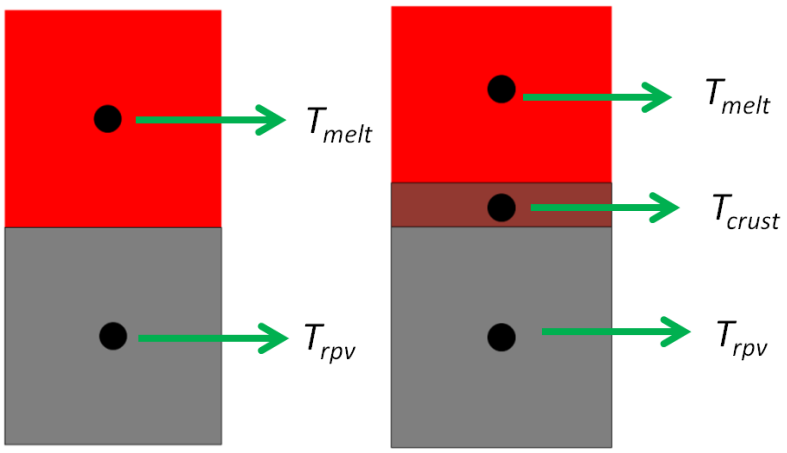

Figure 2-3 Model for heat transfer between molten debris and RPV wall used in original DCA module

The crust thickness is an important factor for determining the heat conduction between the crust and RPV wall. In the original DCA module, the following equation is used to calculate the thickness of crust:

$$x_{crust} = \begin{cases} b \bullet Mesh\ size\ (if\ \ b > 0) \\ user\ input\ (if\ \ b = 0) \end{cases} \quad \textbf{(2-14)}$$

If the solid-phase rate *b* is 0, a user-inputted crust thickness is used in the code, whereas if it is above 0, the crust thickness equals the mesh size multiplied by the solid-phase rate.

3) CCFL gap cooling model

In DCA module, gap cooling model can be divided into two kinds: water enters into the gap or not. In order to simulate the complex gap cooling phenomena, gap cooling model was used in the DCA module, as shown in Figure 2-4. Through multi-channel 1-D gap model, water ingression length is obtained. This model could provide boundary condition for debris and RPV wall heat transfer analysis. Wallis type CCFL correlation is used to calculate water penetration length[51].

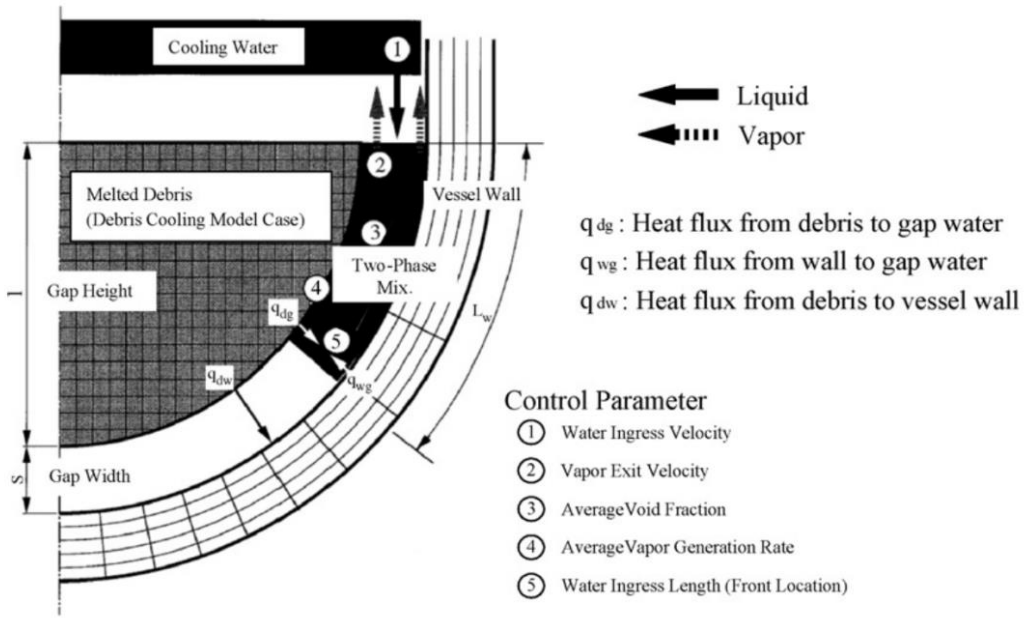

Figure 2-4 Physical model of water ingress into gap [51]

2.2 Validation of original DCA module against LIVE-L4 test

2.3 Development of heat transfer model in DCA module

2.4 Validation of developed DCA module against LIVE-L4 test

2.5 Conclusions

In this chapter, the modified DCA module was applied to LIVE-L4 test for validation of the improved heat transfer model and crust growth model. The following conclusions can be drawn from the present simulation.

1) DCA module was validated with LIVE-L4 test. The simulation results by the improved DCA module agreed well with experiential data by comparing the melt pool average temperature, which indicated that the heat transfer model in the improved DCA module could be used to evaluate the heat transfer more accurately for the real condition in BWR lower plenum.

2) The simulation results by the implemented crust growth module agreed well with the experimental data, by comparing the crust growth rate and crust thickness along the vessel wall in the steady sate. This indicated that the incorporated crust growth model has the capacity to predict the crust characteristic accurately.

3) The influence of various heat transfer correlations on the molten pool average temperature and heat flux was investigated. The simulation results indicated that the Asfia–Dhir and Jahn–Reineke heat transfer correlations could provide better simulation results.

**** The contents of Section 2.2, Section 2.3, Section 2.4 were submitted to Journal of "Annals of Nuclear Energy", as follows:***

Annals of Nuclear Energy, under review, "Improvement and evaluation of debris coolability analysis module in severe accident analysis code SAMPSON using LIVE experiment" (in collaboration with co-authors, Nejdet ERKAN, Koji OKAMOTO, Xiaoyang Gaus-Liu, Alexei Miassoedov)

Chapter 3 Implementation of jet breakup model

This chapter focuses on the simulation of jet breakup process by the developed jet breakup model. The simulations have been carried out on FARO-L8 test by developed 1-D jet breakup model and IAE jet breakup model. The research focus is whether the implemented jet breakup model is capable to simulate jet breakup process accurately and can be extrapolated to simulate jet breakup process in the real reactor. Different jet breakup simulation results by different jet breakup models have been compared. The importance of jet breakup fraction and average droplet diameter on the pressure increase process has also been investigated.

3.1 Jet breakup model

3.1.1 Kelvin-Helmholtz instability

After corium injects into water pool, jet breakup process could happen. In the jet breakup process, one important parameter is jet breakup fraction, which means, how much of the jet could become molten droplets. In this study, K-H instability was used to simulate how much jet could become molten droplets.

A linear K-H instability used to analyze the corium jet and coolant mixture behavior has been proposed by Epstein and Fauske [52]. This method was also developed by other research, such as Bang et al. [53] and Vierow et al. [54]. In this study, the above model was added into DCA module to analyze jet breakup process. Figure 3-1 shows the schematic of jet breakup model. Based on K-H instability, waves could generate on jet surface. These waves could grow up, causing breakup process to happen and molten droplets to depart from jet surface.

The jet breakup mass rate needs to be simulated, which means how much of the jet could become droplets. How much molten droplets could depart from the jet surface could be calculated by the following equation:

$$\Gamma = N\frac{4}{3}\pi\left(\frac{d_p}{2}\right)^3 \rho_j \frac{\Delta z}{\lambda} \qquad \textbf{(3-1)}$$

where Γ is breakup mass rate, N is droplets number than generate from one wave, d is droplet diameter, ρ is density, Δz is cell length, λ is wave length, subscript p means droplets, subscript j means jet.

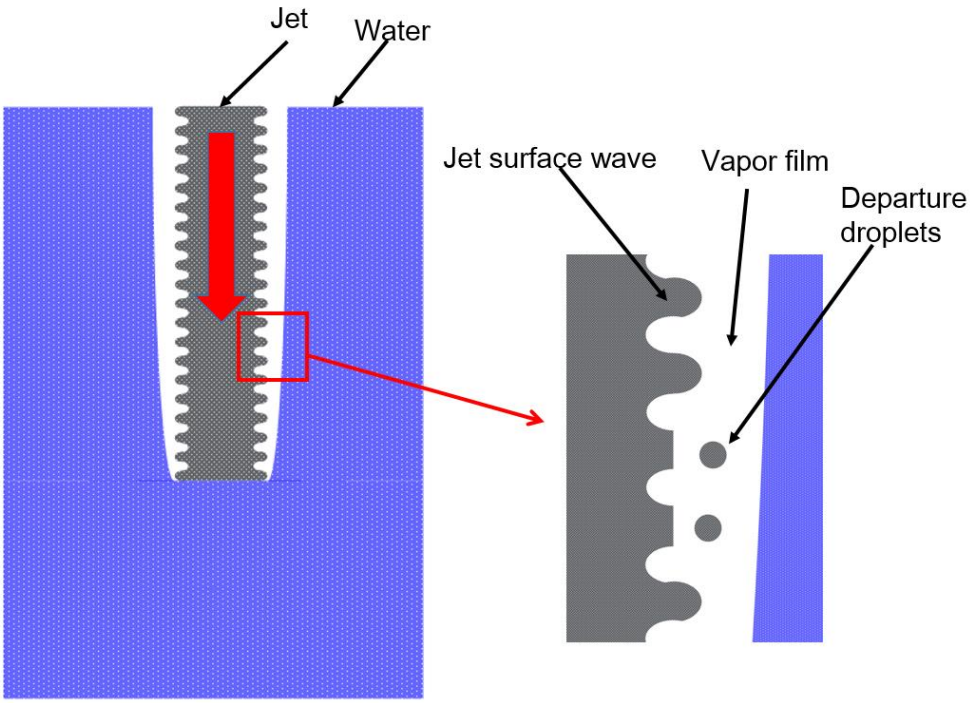

Figure 3-1 Schematic of jet breakup model

Vapor film could generate on jet surface due to corium temperature is very high. In the simplified jet breakup model, for the vapor film condition, in order to incorporate this into code to analyze the jet breakup behavior, two extreme limitations are assumed [53] [54]. In one condition, the vapor film is very thin and much smaller than the disturbance wavelength. In another condition, the vapor film is very thick and much thicker than the disturbance wavelength.

The following equations can be used to calculate the wavelength. In the condition when the vapor film is very thin, which means waves on the jet surface mainly contacts with water, the following equation is used to calculate wave number,

$$k = \frac{2\rho_j\rho_l\left(V_j - V_l\right)^2}{3\left(\rho_j + \rho_l\right)\left(\sigma_j + \sigma_l\right)} \quad \textbf{(3-2)}$$

where k is wave number, ρ is density, V is velocity, σ is surface tension, subscript j means jet, subscript l means liquid water.

Figure 3-1 shows wave number with relative velocity in thin vapor film condition based on Equation 3-2. Form this figure it is clearly that wave length largely depends on the relative velocity between the jet and surrounding coolant.

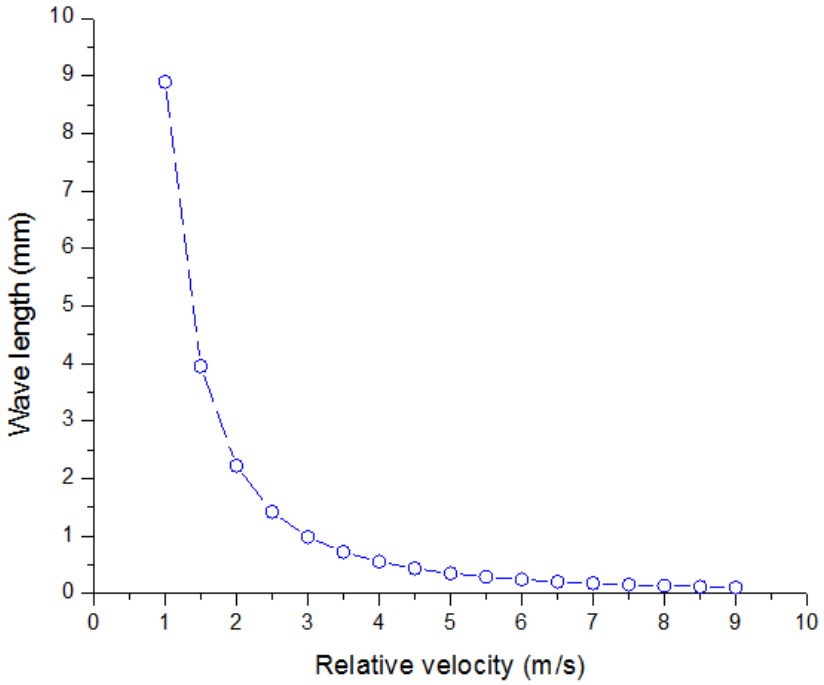

Figure 3-2 Wave number with relative velocity in vapor film thin condition

In another condition when the vapor film is very thick, which means that the waves mainly contact with vapor, the following equation is used to calculate wave number.

$$k = \frac{2\rho_j\rho_g\left(V_g - V_j\right)^2}{3\left(\rho_j + \rho_g\right)\sigma_j} \qquad \textbf{(3-3)}$$

where k is wave number, ρ is density, V is velocity, σ is surface tension, subscript j means jet, subscript g means vapor.

Figure 3-3 shows wave number with relative velocity in thick vapor film condition based on Equation 3-3. Form this figure it is clearly that wave length largely depends

on the relative velocity between the jet and surrounding coolant. Compared to the thin vapor film case, the wave length is much larger.

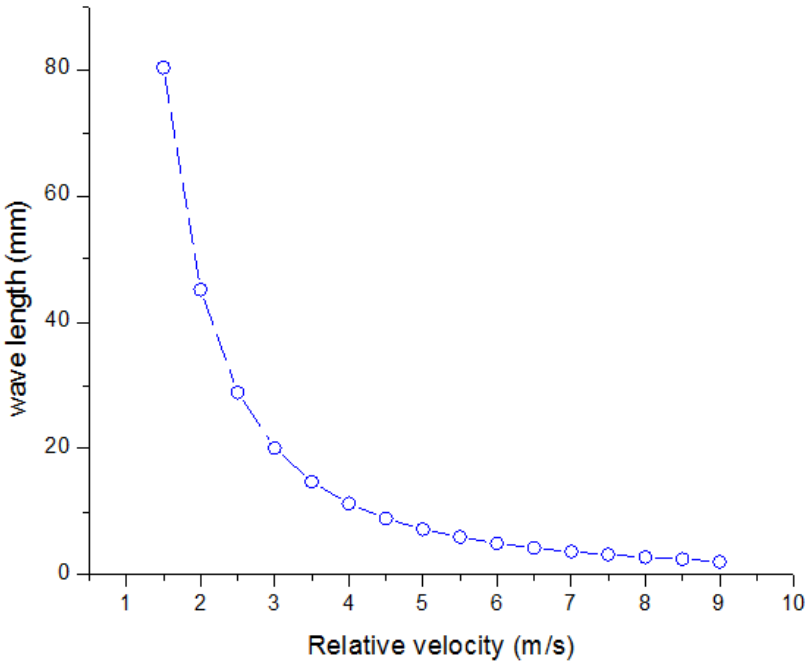

Figure 3-3 Wave number with relative velocity in vapor film thick condition

Base on the balance of shear stress and surface tension, the following equation is used to calculate the departure droplets diameter,

$$\frac{1}{2}C_{D,0}\rho_g V_{rel}^2 \pi d_{jet} d_{particle} = 2\pi d_{jet}\sigma_{jet} \quad \textbf{(3-4)}$$

Where $C_{D,0}$ is a empirical parameter, ρ_g is vapor density, d_{jet} is jet diameter, $d_{particle}$ is droplet diameter, σ_{jet} is jet surface tension, V_{rel} is relative velocity.

Figure 3-4 shows the droplets diameter with relative velocity based on Equation 3-4. Form this figure it is clearly that droplet diameter largely depends on the relative velocity between the jet and surrounding coolant.

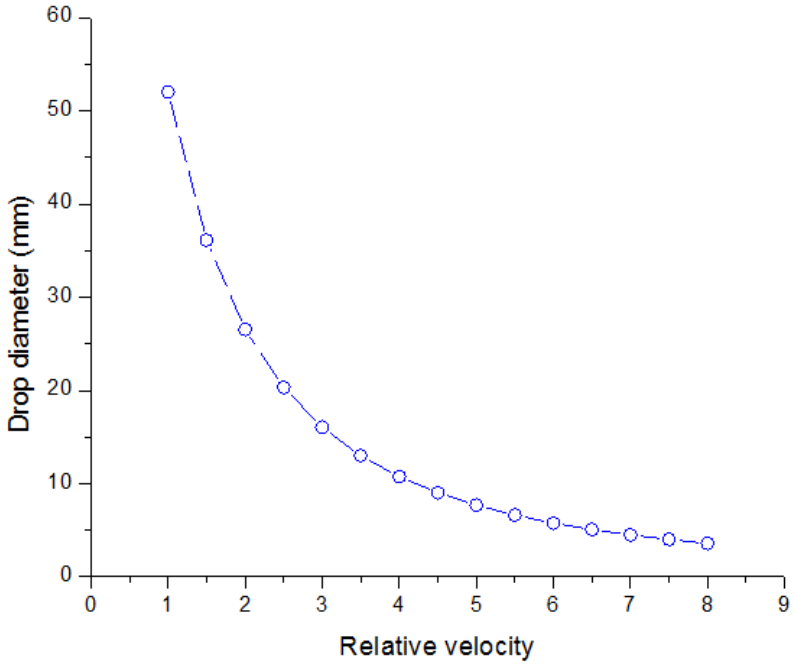

Figure 3-4 Droplets diameter with relative velocity

The vapor is in thin or thick condition has effect on the wave's generation and molten droplets departure process. Whether the vapor film is in thin or thick condition could be judged by the following equation.

$$\begin{aligned} \delta_{vapor} \geq \delta_t = \frac{2}{k} \quad & thick\ film \\ \delta_{vapor} < \delta_t = \frac{2}{k} \quad & thin\ film \end{aligned} \tag{3-5}$$

where k is wave number, δ_{vapor} is vapor thickness.

The vapor film velocity and thickness could has large effect on the growth of waves on the jet surface. A separate sub-model is used to analyze the vapor film behavior. The vapor film velocity and coolant evaporation rate determine the vapor thickness, as shown in Figure 3-5. The vapor film thickness and vapor velocity along the jet were calculated by quasi-steady state vapor film model. This method was proposed by Vierow [54] and was implemented into the current jet breakup model. The quasi-steady state mass, momentum and energy equations of the vapor film were solved to obtain the vapor film velocity and thickness along the jet.

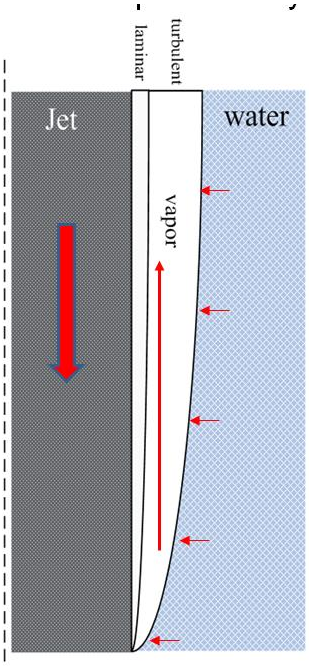

Figure 3-5 Vapor film model

Mass conservation equation for the vapor film is:

$$\Gamma_{k-1/2}\left(h_{sat,l}-h_{sat,g}\right)=F\varepsilon\sigma\left(T_{jet}^{4}-T_{s}^{4}\right)+\lambda_{g}\frac{T_{jet}-T_{s}}{\delta_{lam}}-\sqrt{\frac{\lambda_{l}\rho_{l}c_{p,l}}{\pi t}}\left(T_{s}-T_{l}\right) \quad \textbf{(3-6)}$$

Momentum conservation equation for the vapor film is:

$$\begin{aligned}&\pi d_{jet}\delta_{turb,k}\rho_{g,k}V_{turb,k}^{2}-\pi d_{jet}\delta_{turb,k-1}\rho_{g,k-1}V_{turb,k-1}^{2}\\&=-\pi d_{jet}\delta_{turb,k-1/2}\left(p_{k}-p_{k-1}\right)-F_{turb,lam,k-1/2}-\\&F_{l.turb.k-1/2}+\pi d_{jet}\Delta z_{k-1/2}\Gamma_{k-1/2}\left(V_{l,k-1/2}-V_{jet,k-1/2}\right)\end{aligned} \quad \textbf{(3-7)}$$

Energy conservation equation for the vapor film is:

$$\pi d_{jet}\delta_{turb,k}\rho_{g,k}V_{turb,k}-\pi d_{jet}\delta_{turb,k-1}\rho_{g,k-1}V_{turb,k-1}=\pi d_{jet}\Delta z_{k-1/2}\Gamma_{k-1/2} \quad \textbf{(3-8)}$$

where Γ is evaporation rate, h is enthalpy, F is view factor, ε is emissivity factor, σ is Stefan Boltzmann constant, T is temperature, λ is thermal conductivity, δ is thickness, ρ is density, c is specific heat at a constant pressure, d is diameter, subscript k is the node number, subscript g is vapor, subscript jet is jet, subscript lam is vapor film laminar layer, subscript l is liquid water.

3.1.2 Rayleigh-Taylor instability

The molten droplets could further break up into smaller droplets after departing from jet surface. The further fragmentation behavior of departure molten droplets can be simulated by R-T instability. A theoretical model for R-T instability was developed by Chu [55]. This theoretical model was simplified as a linear correlation in SCDAP/RELAP5-3D code [56]. In this study, the simplified linear correlation for R-T instability was implemented into jet breakup model.

The following equation can be used to calculate the diameter of droplets at a new timestep[56],

$$d_p^{n+1} = d_p^n \left(1 - C_1 \Delta t_b We^{0.25}\right) \quad \textbf{(3-9)}$$

where d is diameter, Δt_b is a non-dimensional time step, We is Weber number, subscript p means droplets, superscript n, n+1 is time step. C_1 is a constant determined empirically as:

$$C_1 = 0.1093 - 0.0785\left(\frac{\rho_l}{\rho_p}\right)^{0.5} \quad \textbf{(3-10)}$$

where ρ_l is the density of liquid, ρ_p is the density of droplet. C_1 is the value depend on the density of liquid and droplet and does not has significant effect on the simulation results.

In this model, the movement of departure droplets is determined by the gravity and drag force between droplets and coolant. The following equation can be used to simulate the rate of velocity change of a droplet [56]:

$$\frac{dV_p}{dt} = g - \frac{f_d}{1.333\pi r_p^3 \rho_p} \quad \textbf{(3-11)}$$

where V_p is the velocity of a droplet, t is time, g is acceleration of gravity, f_d is drag force r_p is the radius of a droplet ρ_p is the density of a droplet.

In the jet breakup process, energetic heat transfer exists between the molten droplets and surrounding coolant. In this study, the heat transfer correlations, which were summarized by SCDAP/RELAP5 manual [56], was also used here to calculate the heat transfer between the molten droplets and coolant.

3.2 Implementation of 1-D jet breakup model into DCA module

3.2.1 THA module in SAMPSON

The coolant condition in the lower plenum is not simulated by DCA module, but simulated by another module in SAMPSON, the THA module. In THA module, the thermal-hydraulics calculation is based on RELAP5/MOD3 extracted from SCDA/RELAP5/MOD3.1.

In RELAP5 thermal-hydraulic model, eight primary dependent variables are solved by eight field equations [57]. The nodalization schematic of two phase mass conservation equations, momentum equations and energy conservation equations used in the two-fluid nonequilibrium model is shown in Figure 3-6.

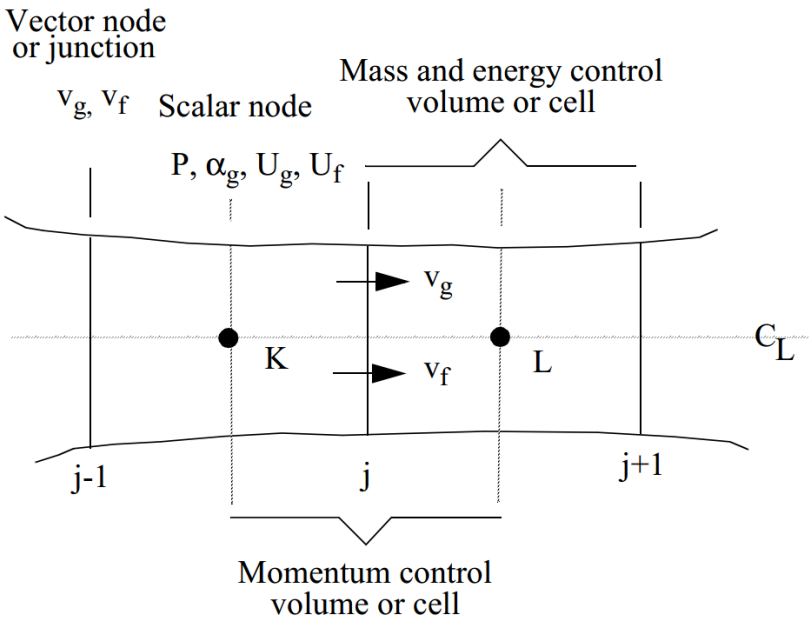

Figure 3-6 Difference equation nodalization schematic [57]

The continuity equation for the vapor phase is:

$$\frac{\partial}{\partial t}\left(\alpha_g \rho_g\right) + \frac{1}{A}\frac{\partial}{\partial x}\left(\alpha_g \rho_g v_g A\right) = \Gamma_g \tag{3-12}$$

The continuity equation for the liquid phase is:

$$\frac{\partial}{\partial t}\left(\alpha_f \rho_f\right) + \frac{1}{A}\frac{\partial}{\partial x}\left(\alpha_f \rho_f v_f A\right) = \Gamma_f \tag{3-13}$$

where α is void fraction, A is surface area, ρ is density, t is time, v is velocity, Γ is evaporation rate, x is spatial coordinate, subscript f means liquid water, subscript g means vapor.

The continuity equations do not include mass sources or sinks. As the requirement of continuity consideration, the vapor generation should be negative of liquid generation term, and this can be explained by:

$$\Gamma_g = -\Gamma_f \tag{3-14}$$

The momentum equation for the vapor phase is:

$$\begin{aligned}
&\alpha_g \rho_g A\frac{\partial v_g}{\partial t} + \frac{1}{2}\alpha_g \rho_g A\frac{\partial v_g^2}{\partial x} = \\
&-\alpha_g A\frac{\partial P}{\partial x} + \alpha_g \rho_g B_x A - \left(\alpha_g \rho_g A\right)\left(FWG\right)\left(v_g\right) \\
&+\Gamma_g A\left(v_{gI} - v_g\right) - \left(\alpha_g \rho_g A\right)\left(FIG\right)\left(v_g - v_f\right) - \\
&C\alpha_g \alpha_f \rho_m A\left[\frac{\partial\left(v_g - v_f\right)}{\partial t} + v_f\frac{\partial v_g}{\partial x} - v_g\frac{\partial v_f}{\partial x}\right]
\end{aligned} \tag{3-15}$$

The momentum equation for the liquid phase is:

$$\begin{aligned}
&\alpha_f \rho_f A\frac{\partial v_f}{\partial t} + \frac{1}{2}\alpha_f \rho_f A\frac{\partial v_f^2}{\partial x} = \\
&-\alpha_f A\frac{\partial P}{\partial x} + \alpha_f \rho_f B_x A - \left(\alpha_f \rho_f A\right)\left(FWG\right)\left(v_f\right) \\
&+\Gamma_g A\left(v_{fI} - v_f\right) - \left(\alpha_f \rho_f A\right)\left(FIG\right)\left(v_f - v_g\right) \\
&-C\alpha_f \alpha_g \rho_m A\left[\frac{\partial\left(v_f - v_g\right)}{\partial t} + v_g\frac{\partial v_f}{\partial x} - v_f\frac{\partial v_g}{\partial x}\right]
\end{aligned} \tag{3-16}$$

where α is void fraction, A is surface area, P is pressure, ρ is density, t is time, v is velocity, Γ is evaporation rate, x is spatial coordinate, Bx is body force, FWG and FWF are wall friction drags, FIG and FIF are interface friction drag, subscript f means liquid water, subscript g means vapor.

The thermal energy equation for the vapor phase is:

$$\begin{aligned}&\frac{\partial}{\partial t}\left(\alpha_g\rho_g U_g\right)+\frac{1}{A}\frac{\partial}{\partial x}\left(\alpha_g\rho_g U_g v_g A\right)=\\&-P\frac{\partial\alpha_g}{\partial t}-\frac{P}{A}\frac{\partial}{\partial x}\left(\alpha_g v_g A\right)+Q_{wg}+Q_{ig}+Q_{jetg}\\&+\Gamma_{ig}h_g^{*}+\Gamma_w h_g^{'}+DISS_g\end{aligned} \qquad \textbf{(3-17)}$$

The thermal energy equation for the liquid phase is:

$$\begin{aligned}&\frac{\partial}{\partial t}\left(\alpha_f\rho_f U_f\right)+\frac{1}{A}\frac{\partial}{\partial x}\left(\alpha_f\rho_f U_f v_f A\right)=-P\frac{\partial\alpha_f}{\partial t}-\frac{P}{A}\frac{\partial}{\partial x}\left(\alpha_f v_f A\right)\\&+Q_{wf}+Q_{if}+Q_{jetf}+\Gamma_{ig}h_f^{*}+\Gamma_w h_f^{'}+DISS_f\end{aligned} \qquad \textbf{(3-18)}$$

where α is void fraction, A is surface area, ρ is density, t is time, v is velocity, Γ is evaporation rate, x is spatial coordinate, subscript f means liquid water, subscript g means vapor, *DISSg* and $DISS_f$ are the sums of wall friction and pump effects, Q_{jetg} is heat flux between corium and vapor, Q_{jetf} is heat transfer between corium and liquid water, Q_{wg} and Q_{wf} are the wall heat transfer terms, Q_{ig} and Q_{if} are the interface heat transfer terms, h_f^{*} and h_g^{*} are phase enthalpies associated with bulk interface mass transfer, and $h_f^{'}$ and $h_g^{'}$ are phase enthalpies associated with wall (thermal boundary layer) interface mass transfer.

3.2.2 Implementation method

Figure 3-7 shows the code structure of SAMPSON. SAMPSON consists of a group of analysis modules applicable for severe accident analysis. The DCA module is used to analyze corium behavior in the lower head. The DCA module could not simulate the coolant condition by itself due to the specific code structure of SAMPSON. DCA module and THA module have been coupled together to simulate the jet breakup process and coolant condition.

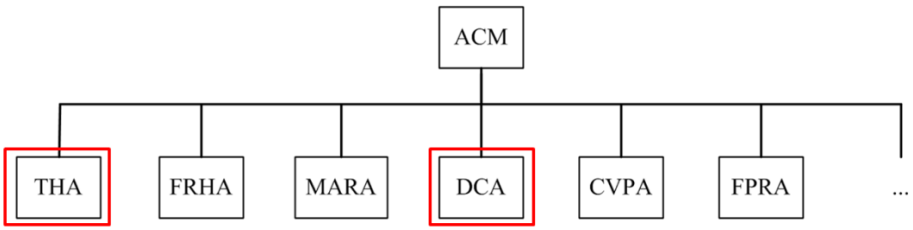

Figure 3-7 Structure of SAMPSON

In DCA module:

The jet breakup process is the complex mixture process of corium and coolant. The corium jet falling and fragmentation behavior was simulated in DCA module. In this model, the jet movement momentum equation was calculated. By solving the jet tip equation and jet velocity equation, the depth of the jet that merged into the water pool could be obtained. Since major jet breakup process happened after jet falling into the water pool, only the jet part that merged into water pool was simulated to calculate how much jet could become molten droplets that departure from jet surface. The departure molten droplets further breakup behavior was also simulated in DCA module. Both jet breakup and droplets breakup behavior were simulated in Lagrangian method. Specially, the vapor film model, which was used to calculate the vapor thickness and velocity along the jet, was simulated in the DCA module, not in the THA module.

In THA module:

The water and vapor behavior was calculated in the THA module in Euclerian fields. In the THA module, 1-D transient two-phase two phases mass, momentum and energy conservation equations were solved to simulate the coolant behavior.

Figure 3-8 shows data transfer between DCA module and THA module. THA module provided the water (vapor) pressure, temperature and void fraction information to the DCA module. The DCA module calculated the heat flux between molten material and coolant and provided heat flux information for the THA module.

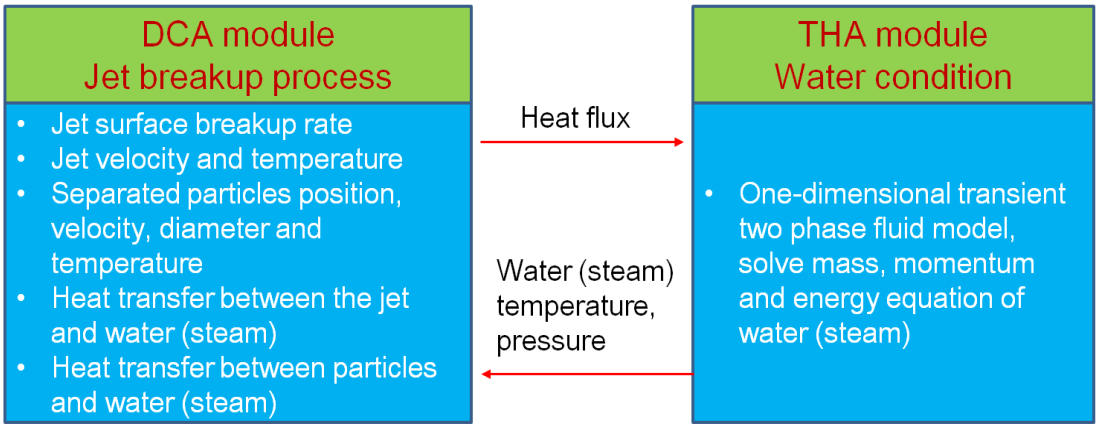

Figure 3-8 Data transfer between DCA module and THA module

Figure 3-9 shows the flow chart of implemented 1-D jet breakup model. The flow chart could be divided into two aspect: the simulation of jet breakup process in DCA module and the simulation of coolant condition in THA module.

In DCA module, 1-D control volumes were used to simulate the jet breakup process. After jet injected into water pool, K-H instability was used to calculate how much jet could become droplets. The temperature, velocity of jet were also simulated. After droplets departure from jet surface, the further breakup behavior was evaluated by R-T instability. The velocities and positions of droplets were updated after fragmentation calculation. The temperature of droplets was updated after calculation of heat transfer between molten droplets and coolant.

After the above process finished, the heat flux between molten material and coolant was transferred to THA module in SAMPSON. In THA module, after got the heat flux information, the continuity, momentum and energy equations for the liquid and vapor phase were solved to get the temperature, pressure information of coolant.

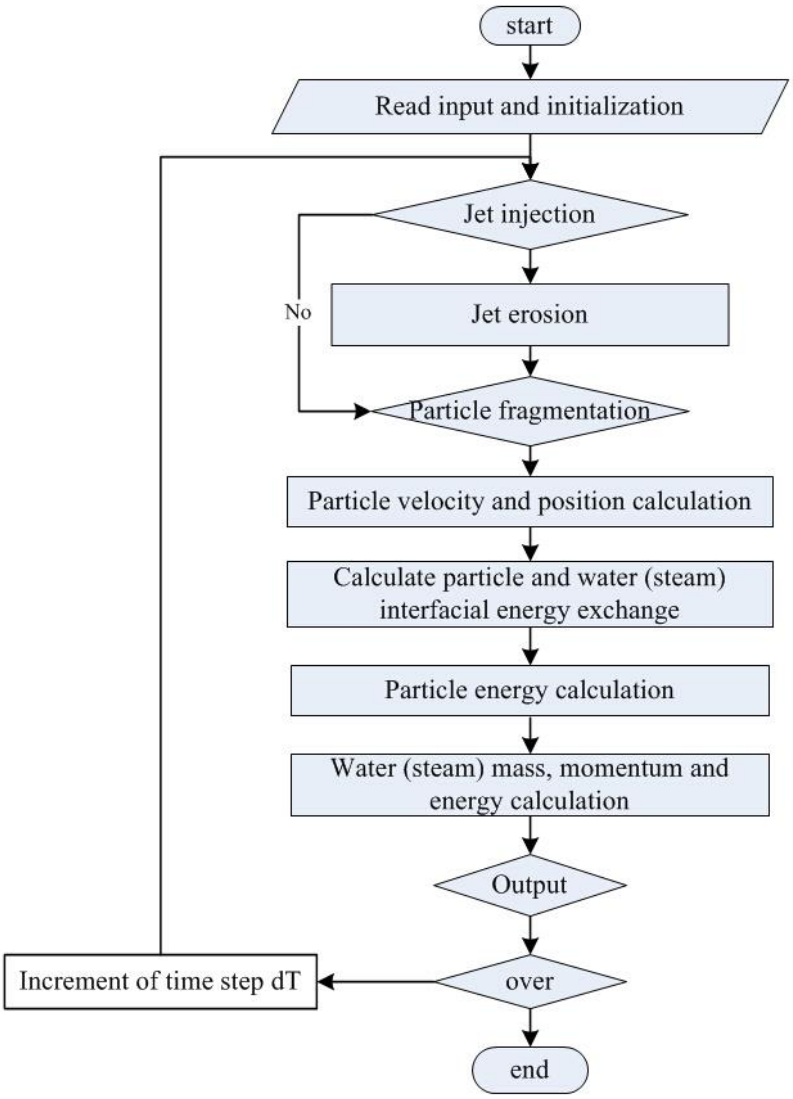

Figure 3-9 The flow chart of jet breakup model

3.3 IAE jet breakup model

IAE provided a lumped parameter method to evaluate jet breakup process in the latest SAMPSON. In the IAE jet breakup model, the diameter of molten jet is set as constant value and the jet is regarded as having cylindrical form. In heat transfer aspect, the convection heat transfer from molten jet to coolant is ignored and only radiation heat transfer is considered [58].

The calculation methods of jet breakup fraction and the molten droplet size are shown as follows:

1) Breakup fraction

The breakup rate from the jet is given as:

$$R = \min\left(1, \frac{H_l}{L}\right) \quad \textbf{(3-19)}$$

where R is breakup rate, H_l is jet length in the water pool.

L is breakup length and is given as:

$$L = 2.1 d_j \left(\frac{\rho_f}{\rho_l}\right)^{1/2} Fr^{1/2} \quad \textbf{(3-20)}$$

where d_j is jet diameter, ρ_f is molten material density, ρ_l is liquid density Fr is Frouder Number.

2) Breakup droplet diameter

The molten droplets are assumed to breakup and reach the hydro-dynamically stable size immediately after reaching water surface. The further breakup of molten droplets is not considered during molten droplets falling process. The diameter of molten droplets is set as a constant value and molten droplets fall through water with constant velocity.

The diameter of molten droplets is given as:

$$d = \min\left(d_{\max}, \max\left(d_{\min}, d_B\right)\right) \quad \textbf{(3-21)}$$

where d is droplet diameter, $d_{\max}$ is maximum droplet diameter set by user, $d_{\min}$ is minimum droplet diameter set by user, d_B is droplet diameter calculated by critical Weber number and is given as:

$$d_B = \frac{We\sigma}{\rho_l v_r^2} \quad \textbf{(3-22)}$$

where We is Weber number, σ is surface tension of molten droplet, ρ_l is the density of liquid, v_r is the relative velocity between molten droplets and coolant.

3.4 Validation of 1-D jet breakup model

3.4.1 Test Description of FARO-L8 test

The FARO-L8 test was conducted to study the fuel-coolant interaction by using prototypical corium melt [32] [59]. The FARO-L8 test was conducted under the conditions related to light water condition. In this study, FARO-L8 test was adopted to validate the implemented 1-D jet breakup model.

Table 3-1 shows main parameters of FARO-L8 test. In the FARO-L8 test, prototypic material was used (80% UO_2, 20% ZrO_2) and this material was heated up to around 3000K, which was close to the real situation. 44 kg molten material (80 wt% UO_2, 20 wt% ZrO_2) were heated up and then poured into the water pool through the 0.1 m diameter nozzle.

The initial pressure was 5.8 MPa and initial water temperature was 536 K, very close to the real condition. The inner diameter of the pressure vessel was 0.71 m and the height of the water pool in the vessel was about 1m. The scale of the test facility could match with the real size of the reactor lower plenum, for example, the jet falling height.

Table 3-1 Main parameters of FARO-L8 test

Parameters	FARO-L8 test
Diameter of test vessel (m)	0.71
Initial height of water pool (m)	1.0
Composition of material	80% UO_2, 20% ZrO_2
Jet initial temperature (K)	3023
Jet mass (kg)	44
Initial pressure in vessel (MPa)	5.8
Initial water temperature (K)	536

3.4.2 Simulation conditions of FARO-L8 test

In this study, the implemented 1-D jet breakup model and IAE jet breakup model performed the simulation of FARO-L8 test. In 1-D jet breakup model, according to the FARO-L8 test geometrical and heat transfer conditions, the mesh was divided as one dimension as shown in Figure 3-10. In IAE jet breakup model, since lumped parameter method was used for jet breakup analysis, one control volume was used.

The boundary and initial conditions were set as follows. The jet was assumed to keep the cylindrical form in every calculation cell. Only the jet part that merged in the water pool was simulated. Based on the position and departure time from the jet surface, the molten droplets were divided into different groups. When the jet or droplets reached the bottom of the vessel, the jet and the droplets with temperature higher than the melt solidus point would form the molten pool. The droplets with temperature lower than the melt solidus temperature would remain solid condition and form debris bed. For the initial conditions, the water was set as 536 K at the pressure of 5.8 MPa while the vapor was also set as 536 K at the pressure of 5.8 MPa. The physical properties functions in DCA module had the capacity to calculate the corium physical properties.

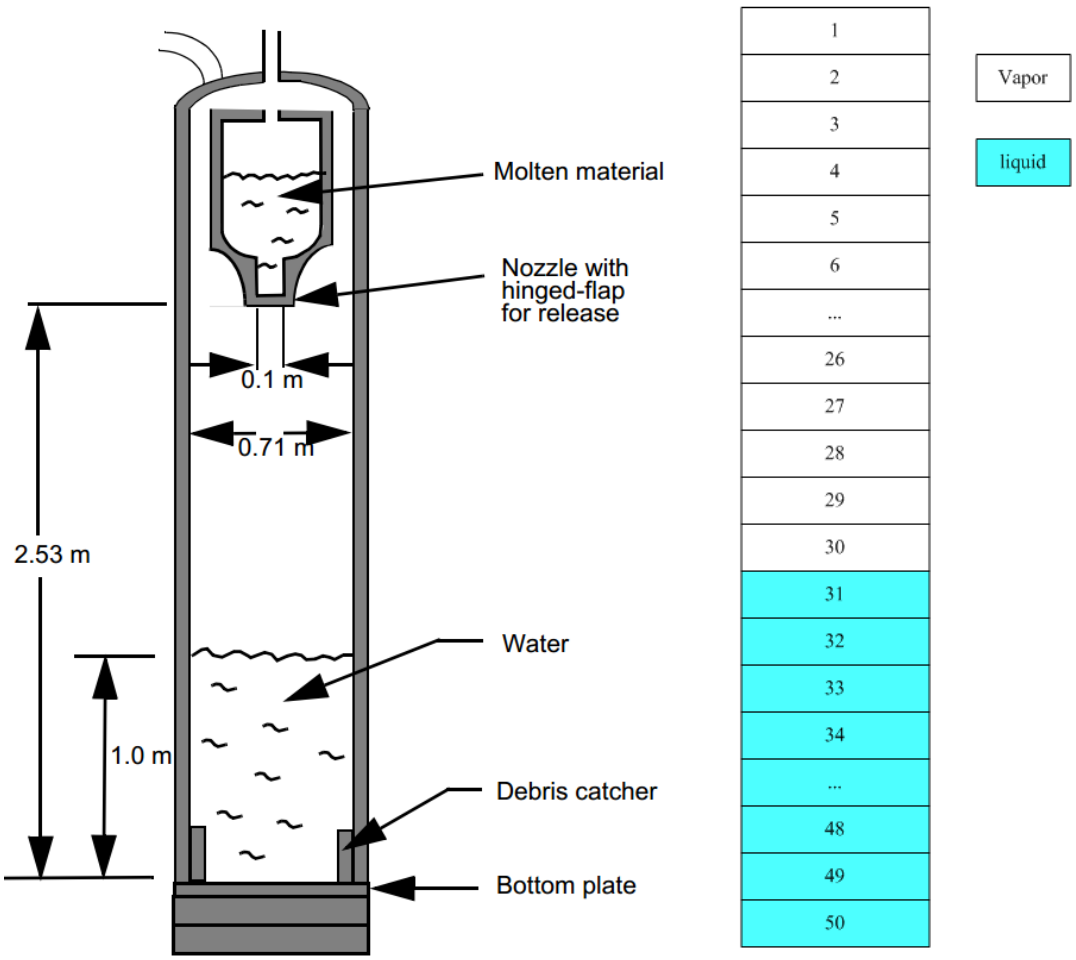

(a) FARO-L8 test vessel [60] (b) Nodalization in 1-D jet breakup model

Figure 3-10 Nodalization of FARO-L8 test

3.4.3 Results and discussion

Both 1-D jet breakup model and IAE jet breakup model were used to simulate FARO-L8 test. Table 3-2 shows the jet fragmented mass, droplets mean diameter, maximum pressure increase in the vessel and maximum water swell predicted by simulation codes and obtained from the experiment. Around 30 kg particles formed after experiment, this value was 36 by 1-D jet breakup model and 7.5 by IAE jet breakup model. Correspondingly, breakup fraction in experiment was 0.68 while this value was 0.82 by 1-D jet breakup model and only 0.16 by IAE model. The breakup fraction was overestimated by 1-D jet breakup model.

Similar agreement by 1-D jet breakup model could also be seen in parameters, such as droplets mean diameter, maximum pressure increase in vessel and maximum level swell of water. For the FARO-L8 test, the average diameter was 3.8 mm; the data predicted by 1-D jet breakup model was 3.9 mm, which was slightly higher than the predicted data. The predicted droplet diameter by 1-D jet breakup model was within the range of most probable sizes obtained in the experiment. After the jet injection into water pool, large amount of steam generated due to the strong heat transfer between the molten material and coolant. This also caused the water level swell in the vessel. Due to the overestimation of jet breakup fraction predicted by the 1-D jet breakup model, much more heat was transferred from the melt to the coolant, which caused higher pressure increase and water swell predicted by 1-D jet breakup model.

Table 3-2 Comparison of simulation results with FARO-L8 test

Parameters	FARO-L8 test	1-D model	IAE model
Fragmented mass (kg)	30	36	7.5
Breakup fraction	0.68	0.82	0.16
Droplets mean diameter (mm)	3.8	3.9	1.0
Maximum pressure increase in vessel (MPa)	1.7	1.9	0.45
Maximum level swell of water pool (m)	0.15	0.2	0.05

Figure 3-11 shows comparison of pressure history between experimental data and simulation results by 1-D jet breakup model and IAE jet breakup model. The pressure history simulated by 1-D jet breakup model matched well with the experimental data. After the fuel jet began to inject into the water pool, due to the instability, the droplets generate on the surface and deapart from jet surface. The liquid water that surrouding the jet and droplets evaporated very quickly. The pressure in the vessel increased sharply due to such violent heat transfer. About 1.0 s after the jet injection into water, the vessle pressure was about 7.6 MPa and then decreased slowly in the simulation by 1-D jet breakup model, which had the similar trend as the FARO-L8 test. Due to the overestimation of the fragmentation by K-H

instability used in the 1-D jet brekaup model, the pressure predicted by 1-D jet breakup model was higher than the experimental data in the initial stage. In other hand, the pressure in the vessel increased slowly by IAE jet breakup model and there was large difference between FARO-L8 test and simulation result by IAE jet breakup model. Therefore, the pressure in the vessel was depened on departure moletn droplets mass and droplets mean diameter. The larger the departure molten droplets mass was, the higher pressure increase was. The smaller the droplets mean diameter was, the higher the pressure increse was.

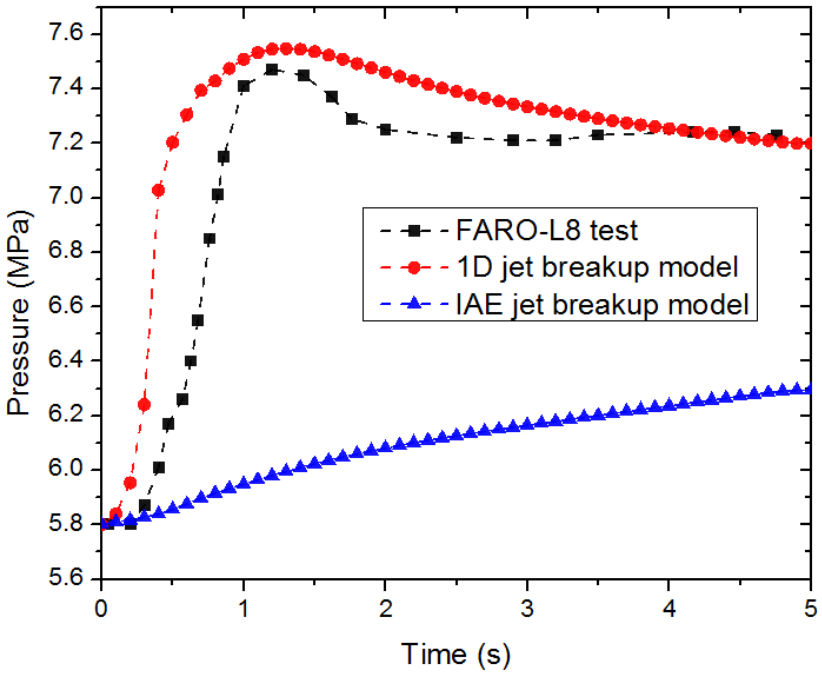

Figure 3-11 Compared of simulated cover gas pressure with FARO-L8 test

Figure 3-12 shows the vapor velocity along the jet by 1-D jet breakup model. Figure 3-13 shows the vapor film thickness along the jet by 1-D jet breakup model. Due to the high jet temperature, vapor film could generate on jet surface. The vapor gatherd together and went up along the jet. Both the vapor velocity and vapor film thickness increased along the jet. The vapor film thickness was strongly related to the vapor generation rate and vapor velocity. The lower was the vapor velocity was, the thickner the vapor film was.

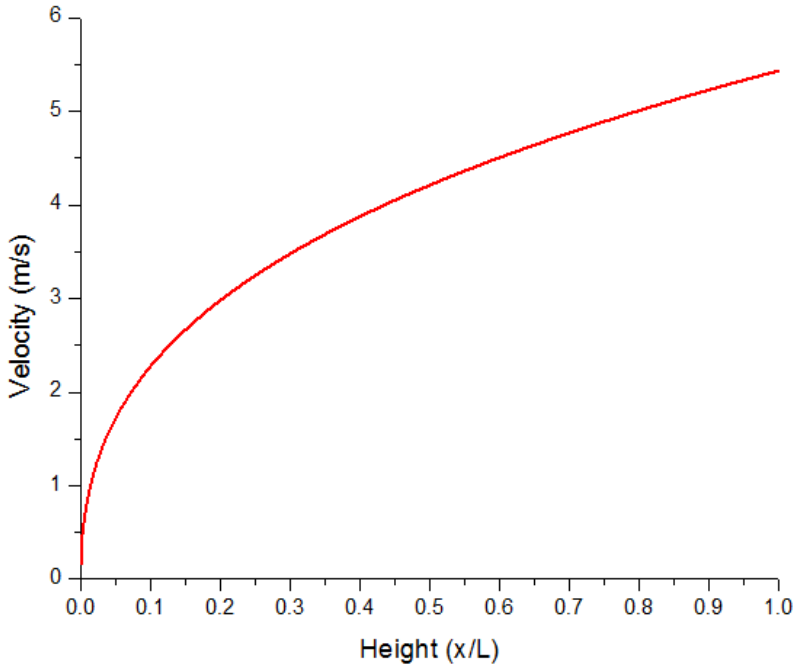

Figure 3-12 Vapor velocity along the jet by 1-D jet breakup model

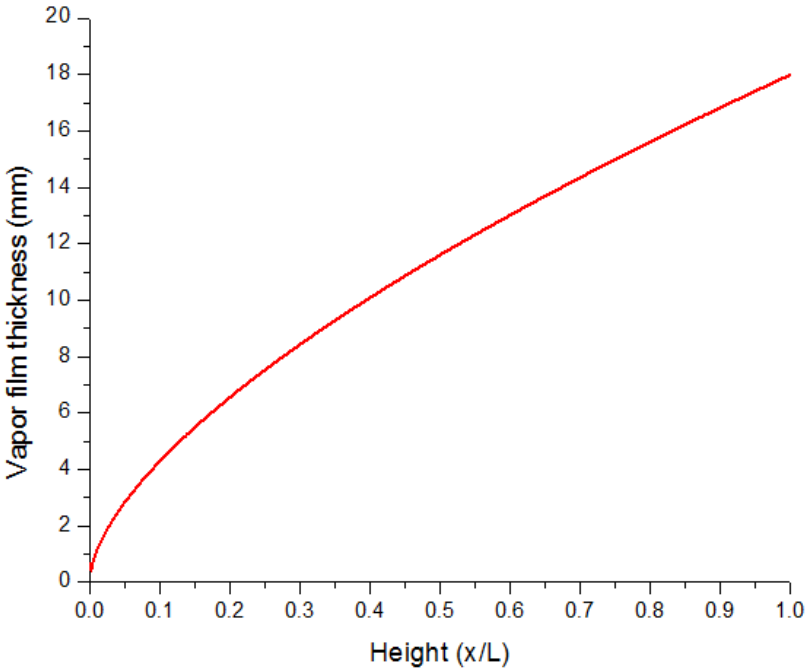

Figure 3-13 Vapor film thickness along the jet by 1-D jet breakup model

Figure 3-14 shows the total droplets' average diameter predicted by by 1-D jet breakup model. The droplets' average diameter predicted by 1-D jet breakup model was slightly higher than the experimenatl data. The droplets' average diameter was

very small and the totally molten droplets had large connecting surface with coolant. During the experiment, the jet falling time was very short and the jet had fewer connecting surface with coolant compared to molten droplets. Compared to the heat transfer between the jet and coolant, the heat transfer between molten droplets and coolant was much higher. Longer falling time and larger connecting surface area enhanced the heat transfer between molten droplets and coolant.

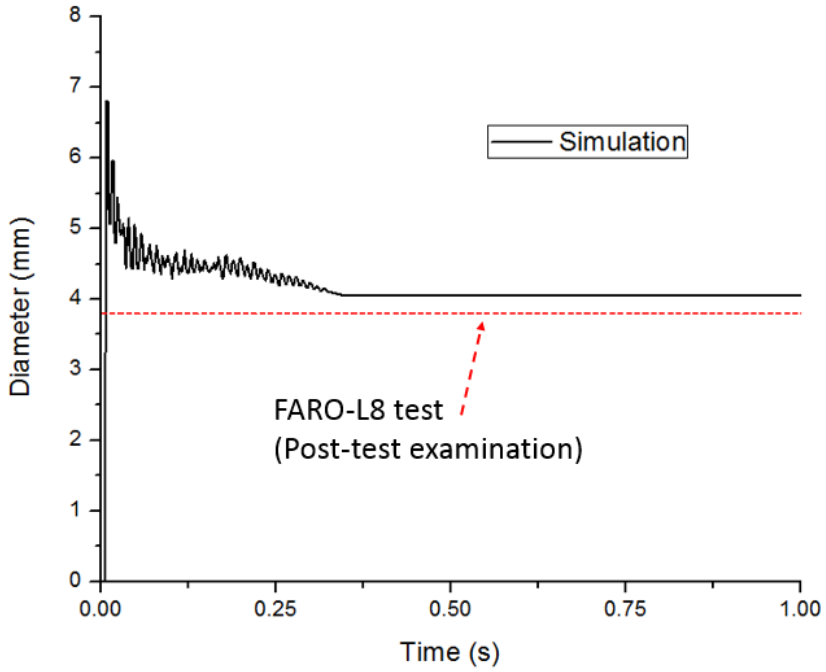

Figure 3-14 Calculated total droplets diameter by 1-D jet breakup model

3.5 Conclusions

In this chapter, the developed 1-D jet breakup model and IAE jet breakup model were used to simulate FARO-L8 test for validation of the implemented 1-D jet breakup model. The following conclusions can be drawn.

1) The developed 1-D jet breakup model was validated with FARO-L8 test. Compared to the experimental data, the predicted breakup fraction, droplet mean diameter and pressure history by the implemented 1-D jet breakup model generally agreed well with FARO-L8 test data. This indicated that the developed 1-D jet breakup model was capable to simulate jet breakup process accurately and can be extrapolated to simulate jet breakup process in reactor case.

2) The simulation results indicated that jet breakup fraction and average droplets diameter are dominant parameters on the pressure increase. The higher jet breakup fraction was, the higher pressure increased in the vessel. The smaller the droplet diameter was, the higher the pressure increased in the vessel.

Chapter 4 Verification with jet breakup experiment

This chapter focuses on designing and conducting an original jet breakup experiment with consideration of CRGTs. The detailed small-scale jet breakup experiment has been conducted to confirm whether the implemented 1-D jet breakup model is suitable for BWR case. The research focus is the effect of CRGTs on jet breakup process. Through comparison between the cases with and without CRGTs, the CRGTs effect on jet breakup process has been clarified. Important parameters, such as breakup fraction and particle diameter have been obtained from the current experiment.

4.1 Experimental method

4.2 Experiment results and discussion

4.3 Modification of jet breakup model based on experimental results

The current experiment was conducted under isothermal condition. During jet breakup process that happen in BWR lower plenum, vapor film could generate on jet side surface. However, when applying it to the real condition, the effect of vapor has to be considered.

Figure 4-1 shows the jet breakup mass for different conditions based on Equation 3-1. The breakup mass in the water condition was about 4 times of the case in vapor condition, there was no order difference. Compared to the real condition, the jet breakup mass was overestimated by the present jet breakup experiment. For the conditions without or with vapor, the jet breakup mass trend was similar, and this indicated that the current experiment could be used to estimate the real case.

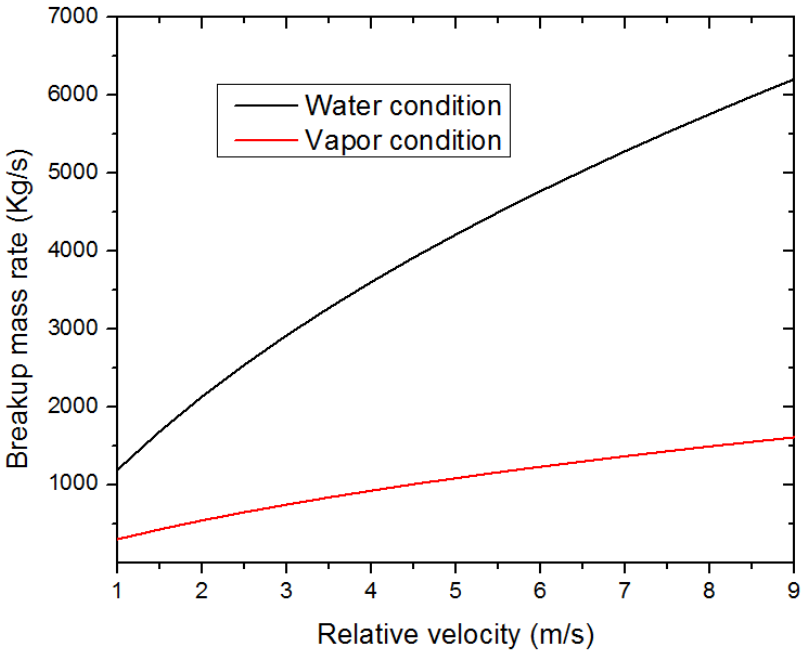

Figure 4-1 Breakup mass rate for different conditions

After molten droplets departure from jet surface, it is possible that these departure droplets will solidify during falling process. After these solidified droplets form debris bed, it is likely that they will re-melt. However, this solidying re-melting process does not influence the jet breakup process.

The relative breakup fraction is proposed to evaluate jet breakup process for BWR case. The breakup rate is modified as follows:

$$f_{CRGT} = Cf \qquad \textbf{(4-1)}$$

Where f_{CRGT} is breakup rate with CRGTs, f is breakup rate without CRGTs, C is relative breakup fraction.

4.4 Conclusions

In this chapter, to understand the influence of CRGTs on jet breakup behavior, a dedicated small-scale jet breakup experiment was performed to observe the phenomena via high-speed photography. Based on the jet breakup experiments, the following conclusions could be drawn:

1) CRGTs could limit jet breakup process and their influence mainly depended on the P/D ratio of CRGTs. During the jet breakup process, waves could generate on the jet surface. These waves could grow up and cause further breakup, and then droplets could depart from jet surface. While for the case without CRGTs, such departure phenomenon could be observed obviously. While for the case with CRGTs, the CRGTs could prevent the waves from growing up and droplets departing from jet surface.

2) Relative breakup fraction was proposed to evaluate jet breakup process when CRGTs exist. The relative breakup fraction was 0.2 in the case of CRGTs at a P/D of 1.37, whereas the relative breakup fraction was 0.8 in the case of CRGTs at a P/D of 2.47. The P/D ratio had huge effect on jet breakup fraction.

3) CRGTs almost had no effect on droplet size. The Sauter mean diameters of droplets were located between the values predicted by K-H instability and critical Weber number theory. Also, the present jet breakup experiment validated that the physical mechanism of jet breakup process could be well clarified by K-H instability and critical weber number theory.

4) From the PIV method, the surrounding water velocity profiles in the cases with CRGTs were larger than the case without CRGTs. In all cases, the water velocity increased with the jet depth in the axial direction.

5) Although the current experiment was conducted under isothermal condition, it is still possible to use the current experiment to evaluate the real case. One of the differences between the real case and the current experiment is vapor could generate on the jet surface in the real case, but there is no order difference in breakup mass rate with or without vapor film. The solidification process of droplets also does not affect the jet breakup process significantly.

**** The contents of Section 4.1 and Section 4.2 were submitted to Journal of Visualization, as follows:***

Journal of Visualization, under review, "Experimental investigation of the effect of control rod guide tubes on the breakup of a molten metal jet in the lower plenum of a boiling water reactor under isothermal conditions" (in collaboration with Nejdet ERKAN, Koji OKAMOTO)

Chapter 5 Development of new penetration tube melt model

This chapter focuses on the simulation of molten pool behavior in BWR lower plenum by the implementation of penetration tube melt model. Molten pool simulation with different penetration tube melt models under dry and wet condition were conducted. The research focus is how penetration tubes affect molten pool behavior and BWR lower plenum failure mechanism. Important parameters such as failure time events, RPV wall temperature distribution and penetration tubes temperature distribution have been studied. The penetration tube effects on BWR failure mechanism have also been investigated.

5.1 IAE penetration tube melt model

5.1.1 Method

In the latest version of SAMPSON DCA module, IAE provides the option of the penetration tube melt model. In DCA module, the Cartesian mesh is used to simulate the spreading and cooling behavior of corium. The meshes used for the molten pool in the X, Y, and Z directions were 22, 22, and 12 separately. In the penetration tube melt model, the above meshes are divided into two kinds: corium meshes and penetration tube meshes, as shown in Figure 5-1[61].

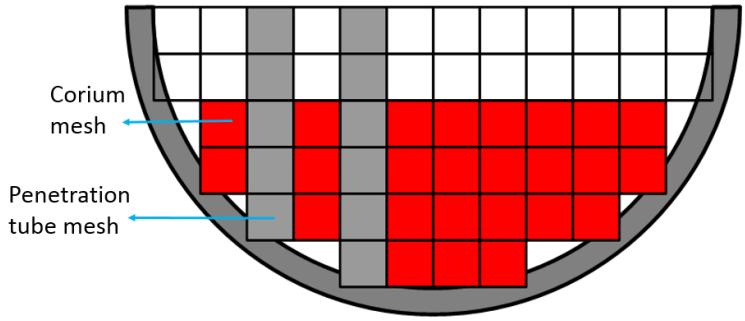

Figure 5-1 Penetration tube melt model proposed by IAE

The penetration tube melt model is combined with corium cooling and RPV failure model. In IAE penetration model, several penetration tubes gather together and are represented by one penetration tube mesh. The penetration tubes provide the wall

boundary condition for the molten pool, and also act as obstacles for the molten pool natural convection. The penetration tube meshes also connect with RPV wall meshes.

The energy conservation of each penetration tube mesh could be calculated by the following equation[46]:

$$\rho \frac{\partial h}{\partial t} = \frac{\partial}{\partial x}\left(\lambda \frac{\partial T}{\partial x} \right) + \frac{\partial}{\partial y}\left(\lambda \frac{\partial T}{\partial y} \right) + \frac{\partial}{\partial x}\left(\lambda \frac{\partial T}{\partial z} \right) + Q_{db} + Q_{fl} + Q_{rpv} \qquad \textbf{(5-1)}$$

where ρ is density, h is specific enthalpy, λ is thermal conductivity, T is temperature, Q_{db} is heat transfer between penetration tubes and debris, Q_{fl} is heat transfer between debris and coolant, Q_{rpv} is heat transfer between penetration tube and RPV wall, t is time, and x, y, z, are coordinates.

After the penetration tube temperature reaches the melting point, the penetration tube will be melt by the corium. The penetration tube meshes will be changed to corium meshes at the same time automatically.

5.1.2 Limitations

The penetration tube melt model proposed by IAE has the following limitations:

1) Due to the unsophisticated penetration tube and corium mesh configuration method in the IAE penetration tube melt model, one penetration tube mesh could be used to represent several penetration tubes. The mesh is distributed uniformly in the model, and one mesh could only be used to represent one material, namely either the penetration tubes or corium. Several penetration tubes gather together and cause one penetration tube mesh to have higher thermal capacity compared to one real penetration tube.

2) In the real condition, not only inside the vessel, the penetration tubes also have extension parts outside the vessel and pass through the RPV wall. For simplification purpose, only the parts of penetration tubes inside RPV are simulated and the left parts are ignored. Namely, the other effects of the ignored parts of penetration tubes on the severe accident progression, such as cooling

outside the vessel, corium flows inside the tubes, could not be simulated by this penetration tube melt model.

5.2 Implementation of new penetration tube melt model into DCA module

5.2.1 Mesh method

The new penetration tube melt model which considered about the real structure of the BWR lower plenum was proposed, as shown in Figure 5-2. The penetration and corium mesh systems were coupled with the heat transfer between corium and penetration tubes.

In the new penetration melt model, every penetration tube was simulated and 1-D heat condition model was used to calculate the temperature distribution of penetration tubes. The heat transfer between penetration tubes and corium, RPV wall and coolant was also considered. Different from IAE penetration tube melt model, a new mesh generation method was used to represent the penetration tubes. In the center of every corium mesh, a hollow cylinder was used to represent the penetration tube as shown in Figure 5-2. Besides the penetration tube part inside the RPV, the penetration part that connected to the RPV wall was also considered. For the extension part of penetration tubes outside the RPV, heat transfer with the coolant was also considered.

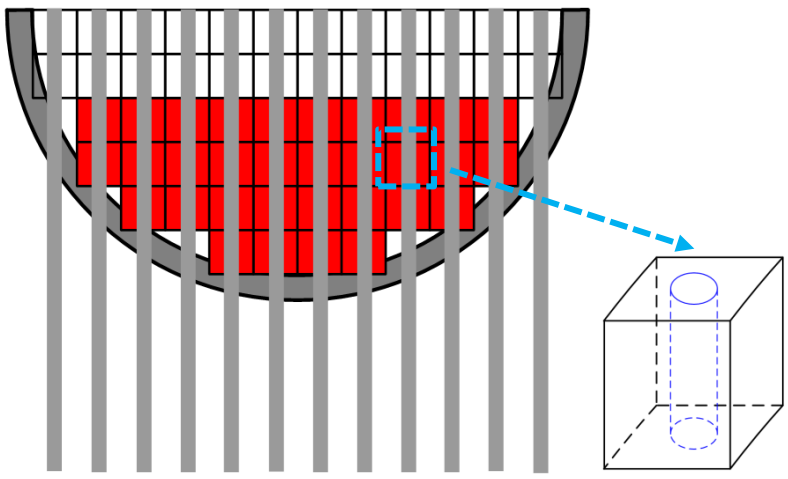

Figure 5-2 The new penetration tube melt model

Both CRGTs and IGTs were considered in the current study. In detail, the number of CRGTs and IGTs varies with different types of BWRs. For simplification purpose, the arrangement of CRGTs and IGTs in the simulation is shown in the Figure 5-3. In new penetration tube melt model, the meshes used for the molten pool in the X, Y, and Z directions were 22, 22, and 12. Totally 316 CRGTs and IGTs were simulated in this study, of which the number of CRGTs was 240 and the number of IGTs was 76. The number of CRGTs varies from 150 to 200 in different BWR design[3]. Compared to the real case, the current simulation overestimated the number and weight of CRGTs and IGTs. If the number of penetration tubes increase, the heat sink capacity for molten pool will also increase. The molten pool temperature would decrease more quickly in this case, and this could cause the penetration tubes to fail at a later time. However, the purpose of this study was to investigate the failure mechanism in BWR lower plenum, and did not focus on any special BWR reactor.

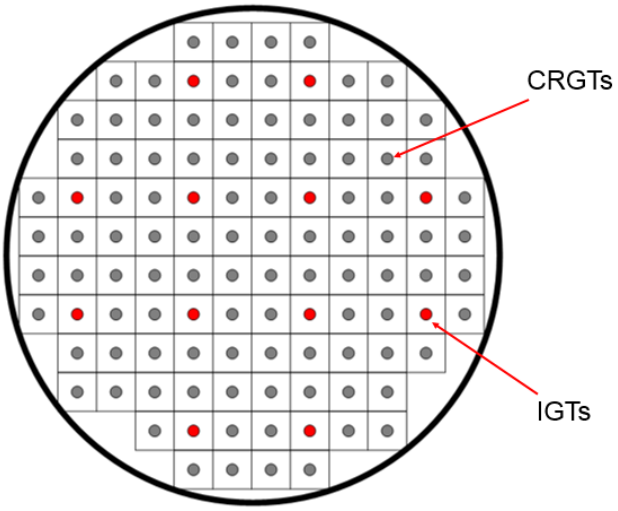

Figure 5-3 Top view of the arrangement of CRGTs and IGTs

5.2.2 Energy conservation equation

Up to now, there is no experiment about how these penetration tubes could affect molten pool flow. In this study, the effect of penetration tubes on molten pool flow behavior was not considered. Basically, the heat sink effect of penetration tubes on the molten pool behavior and RPV wall has been considered.

Figure 5-4 shows the details of the new penetration tube melt model. Penetration tube melt model is based on energy conservation equation. The energy equation model was mainly used to simulate the temperature change of the penetration tubes and its melting behavior.

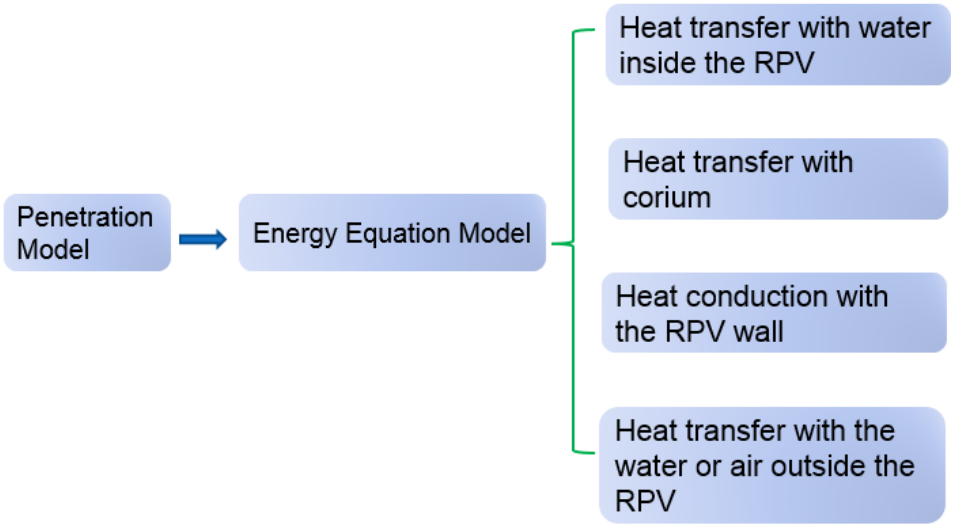

Figure 5-4 The functions of the penetration tube melt model

The penetration tube specific enthalpy can be calculated by the following equation:

$$\rho \frac{\partial e}{\partial t} = \frac{\partial}{\partial z}\left(k \frac{\partial T}{\partial z} \right) + \mathrm{Q} \qquad \textbf{(5-2)}$$

where e is specific enthalpy, ρ is density, t is time, k is thermal conductivity, T is temperature, and Q is heat source. Q in this equation was calculated by the following four heat transfer models.

1) Heat transfer between corium and penetration tubes

It was assumed that crust exist between corium and penetration tubes. Based on the specific heat transfer between corium and penetration tube, 1-D crust growth model, which was proposed by Zhang et al.[49], was used to calculate the transient characteristic of the crust, as shown in Figure 5-5.

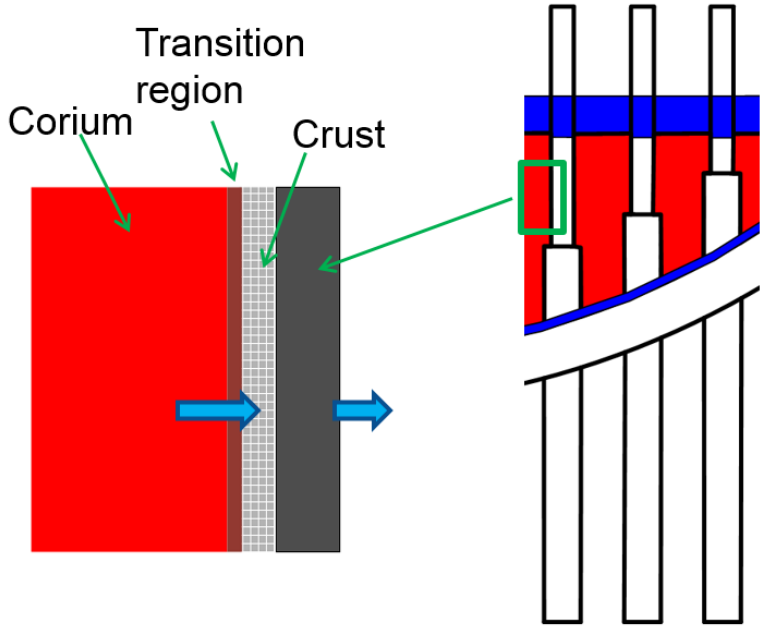

Figure 5-5 Heat transfer between corium and penetration tubes

2) Heat transfer with coolant inside RPV

The correlations used to calculate heat transfer between penetration tubes and coolant are shown as follows:

The nucleate boiling heat flux is obtained through the Rehsenow relation [37]:

$$\left[\frac{c_{pl}\left(T_{surf}-T_{sat}\right)}{h_{fg}}\right]=C_{sf}\left[\frac{q''_{nb}}{\mu h_{fg}}\left(\frac{\sigma}{g\left(\rho_l-\rho_v\right)}\right)^{1/2}\right]^{n}\mathrm{Pr}^{m} \qquad \textbf{(5-3)}$$

where q''_{nb} is nucleate boiling heat flux, , c_{pl} is heat capacity of liquid at T_{sat}, T_{surf} is temperature of penetration tube, T_{sat} is saturation temperature, C_{sf} is a constant determined empirically for different surfaces and fluids (default = 0.013), μ is dynamic viscosity of liquid at T_{avg}, h_{fg} is latent heat, σ is surface tension at T_{avg}, g is acceleration of gravity, ρ_l is density of liquid at T_{sat}, ρ_v is density of vapor at T_{sat}, n is constant (default = 0.33) Pr is Prandtl number, and m is constant (default = 1.0).

The critical heat flux is given by [37]:

$$q''_{chf} = 0.18\rho_v h_{fg}\left[\sigma(\rho_l-\rho_v)g/\rho_v^2\right]^{1/4}\left[\rho_l/(\rho_l+\rho_v)\right]^{1/2} \quad \textbf{(5-4)}$$

where q''_{chf} is critical heat flux, ρ_v is density of vapor at T_{sat}, ρ_l is density of liquid at T_{sat}, h_{fg} is latent heat, g is acceleration of gravity, σ is surface tension at T_{avg}, T_{sat} is saturation temperature, T_{surf} is temperature of penetration tube.

The minimum film boiling heat flux is given by [37]:

$$q''_{mfilm} = 0.09\rho_v h_{fg}\left[\sigma(\rho_l-\rho_v)g/\rho_v^2\right]^{1/4}\left[\rho_l/(\rho_l+\rho_v)\right]^{1/2} \quad \textbf{(5-5)}$$

where q''_{mfilm} is the minimum film boiling heat flux

The film boiling heat flux is given by [37]:

$$q''_{film} = 0.943\left[\rho_v(\rho_l-\rho_v)gk_v^3\left(h_{fg}+0.5c_{pv}\Delta T\right)/\mu_v L_c\right]^{1/4}\Delta T^{0.75} \quad \textbf{(5-6)}$$

where q''_{film} is film boiling heat flux, L_c is characteristic length of the surface, T_{surf} is temperature of this penetration tube, T_{sat} is saturation temperature, g is acceleration due to gravity, h_{fg} is latent heat, ρ_l is density of liquid at T_{sat}, ρ_v is density of vapor at T_{sat}, c_{pv} is heat capacity of vapor at T_{sat}, μ_v is dynamic viscosity of vapor at T_{avg}, and k_v is thermal conductivity of vapor at T_{avg}.

3) Heat conduction with the RPV

Through a stub tube and control rod drive housing, a CRGT is welded on the BWR lower head, and IGTs are also weld at the bottom lower head. 1-D heat conduction model was used to calculate the heat transfer between RPV wall and penetration tubes.

4) Heat transfer between air and penetration tube outside the RPV.

In the cavity, the penetration outside the RPV will transfer its heat to the air. The following equations were used to calculate the heat transfer between penetration tubes and air [62].

$$Nu = C\left(Gr \cdot \Pr\right)^n$$

$$C = \begin{cases} 0.59 & 1.43\times10^4 \le Gr < 3\times10^9 \\ 0.0292 & 3\times10^9 \le Gr < 2\times10^{10} \\ 0.11 & 2\times10^{10} \le Gr \end{cases} \qquad \textbf{(5-7)}$$

$$n = \begin{cases} 0.25 & 1.43\times10^4 \le Gr < 3\times10^9 \\ 0.39 & 3\times10^9 \le Gr < 2\times10^{10} \\ 0.33 & 2\times10^{10} \le Gr \end{cases}$$

where Nu is Nusselt number, Gr is Grashof number, and $\Pr$ is Prandtl number.

5.2.3 Flow chart

Figure 5-6 shows the calculation process of modified DCA module, with new penetration tube melt model. Gap cooling model, molten pool model, RPV model and debris bed model were already existed in the DCA module, while penetration model is newly incorporated and coupled with other models in DCA module. At first, initial and boundary conditions were set and input in the code. Then the following process was conducted to simulate molten pool behavior and thermal response of RPV wall and penetration tubes. The gap cooling model was used to calculate heat flux between molten pool and RPV wall. Then molten debris cooling model was conducted and the temperature and velocity distribution of molten pool inside RPV were obtained. Penetration tube melt model was carried out followed by the molten debris cooling model. After penetration tube melt model, RPV failure model was used to calculate RPV wall temperature distribution, and to evaluate whether RPV reached the failure point by melt or creep rupture.

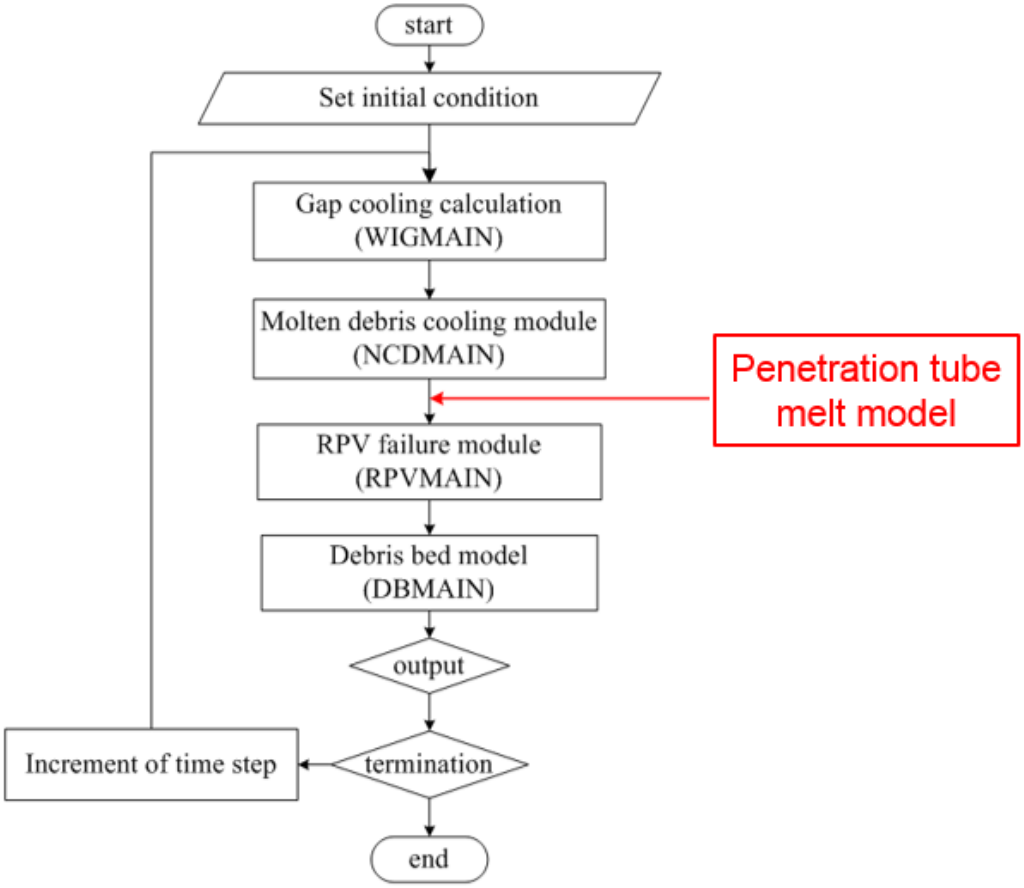

Figure 5-6 Flow chart of the new DCA module

5.3 Molten pool simulation

After the penetration tube melt model was implemented into DCA module, different simulation cases were conducted to study penetration tube effects on the integrity of RPV and molten pool behavior.

5.3.1 Simulation conditions of different cases

Table 5-1 shows simulation conditions of different cases. Figure 5-7 shows the simulation cases with different models under dry and wet conditions. Both in IAE penetration tube melt model and new penetration tube melt model, the penetration tubes could act as the heat sink for the molten pool. The failure mechanism and failure time may be different for the cases with or without penetration tube melt model. Different penetration tube model may also cause different results such as RPV or penetration tube failure time.

Table 5-1 Simulation cases

	Penetration model	Dry or wet condition
Case 1	-	Dry
Case 2	-	Wet
Case 3	New penetration tube melt model	Dry
Case 4	New penetration tube melt model	Wet
Case 5	IAE penetration tube melt model	Dry
Case 6	IAE penetration tube melt model	Wet

In the severe accident management aspect, to make sure that water could inject into RPV is very important to ensure the integrity of RPV. In this study, the water was assumed to keep to inject into lower plenum. This was used to investigate whether it could cool the corium down. In these simulation cases, whether penetration tubes could act as the heat sink for corium cooling was also studied.

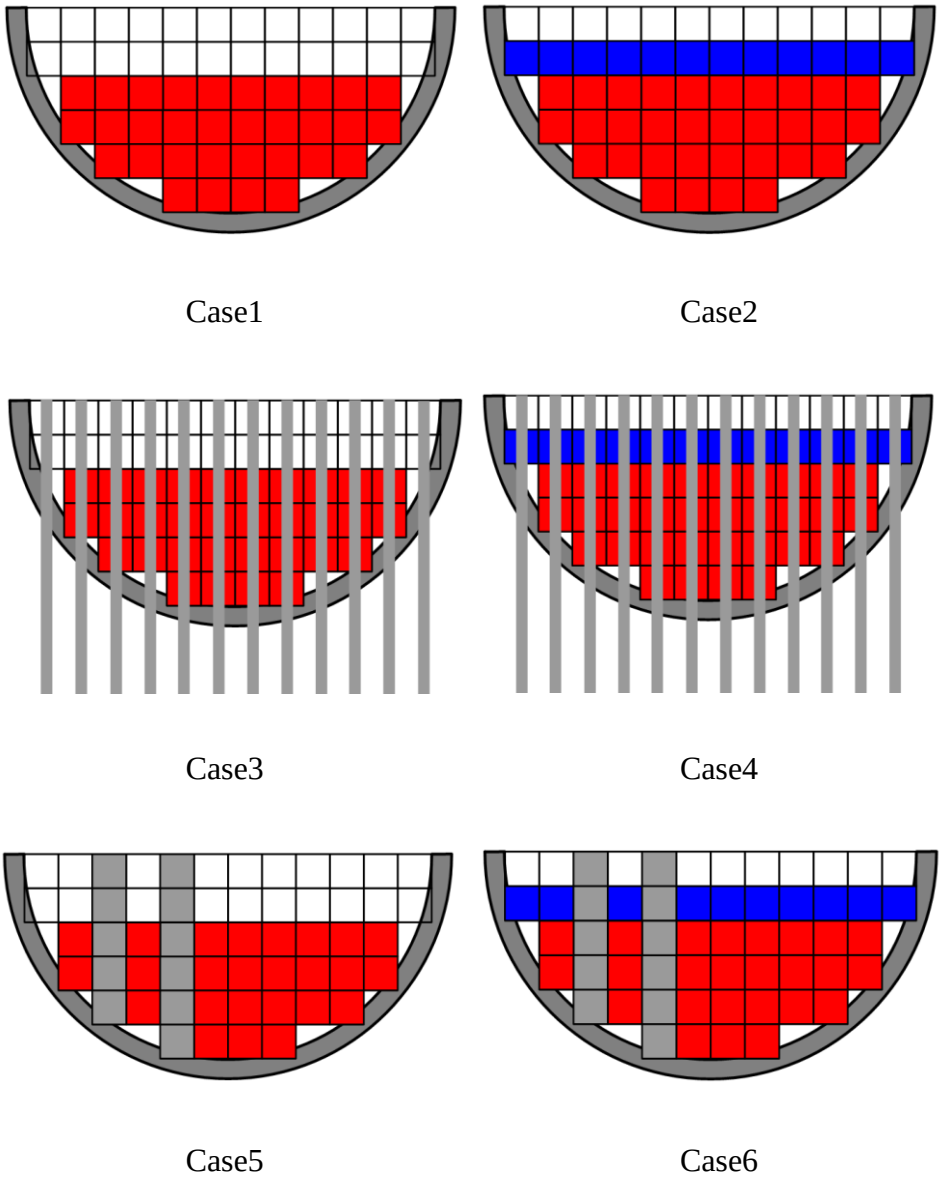

Figure 5-7 Simulation conditions

Table 5-2 shows the initial conditions for molten pool simulation. In the simulation, there was gap existing between crust and RPV wall, and outside the RPV, there was no water cooling and only air was outside. During the simulation process, even the penetration tubes reached the melting point, it was still assumed that there was no leakage from the failure penetration tubes. In a hypothetical severe accident, if the welds of IGTs fail, IGTs could fall down and leave holes in the lower plenum, causing corium to discharge into the containment. If CRGTs fail, corium could flow into the CRGTs. This assumption could lead to overestimation of total mass and temperature of corium in the molten pool.

In the wet condition, water was kept to inject into lower plenum and could guarantee that molten pool was covered by water. In the wet condition, it was also assumed that gap existed between crust and molten pool, and CCFL gap cooling model was used to simulate the gap cooling behavior. In this study, the mass of penetration tubes in new penetration tube model and in IAE model were set as the same value. In this study, it was assumed that there was a large amount of corium (200 000 kg) discharging into BWR lower plenum. In a hypothetical severe accident, if molten pool form in the core region, the further core plate or shroud failure could cause large amount of corium to fall into lower plenum. During the simulation, both the RPV wall and penetration tube melt temperature were set as 1700 K. The simulation lasted for 10000s.

Table 5-2 Initial conditions for molten pool simulation

Parameters	Dry condition	Wet condition
Corium initial temperature (K)	2800	2800
Corium falling mass rate (kg/s)	400	400
Corium falling time (s)	500	500
RPV wall initial temperature (K)	420	420
Penetration tube temperature (K)	420	420
Injection water temperature (K)	-	400
Pressure in lower plenum (MPa)	1.5	1.5

5.3.2 Results and discussion

1) BWR lower plenum failure time events

Table 5-3 shows the RPV creep rupture time, penetration tube melt time and RPV wall melt time for different simulation cases under dry and wet condition. Firstly, under dry condition, for the RPV creep rupture behavior, the failure time was 864 s if penetrations effect was not considered, while the failure time was 1337 s if penetration tube effect was considered by the new penetration tube melt model. Under wet condition, for the RPV creep rupture behavior, the failure time was 1128 s if penetrations effect was not considered, while the failure time was 1753 s if

penetrations effect is considered by the new penetration tube melt model. For RPV creep rupture time, without penetration tube melt model and IAE penetration tube melt model had similar time both under dry and wet conditions. For new penetration model, no matter under wet or dry condition the RPV creep rupture time was longer. Secondly, for RPV wall melt, under wet condition, due to CCFL gap cooling, RPV wall melt did not occur for all cases. Under dry condition, new penetration model had longer failure time than the other two models. The lastly was penetration tube melt time. For new penetration model, no matter under dry or wet condition, it did not affect melt time. For IAE penetration model, wet condition could prolong penetration melt time. In a short, penetration tubes failed earlier than RPV. RPV failure time delayed with penetration tube.

The BWR lower plenum failure mechanism is very important for the nuclear safety analysis and severe accident management. Different failure mechanism could cause different phenomenon, which could cause different later development of severe accident. If RPV wall reaches melt point or creep rupture happens first, there is high possibility that large amount of corium could discharge into the containment. If penetration tubes reach failure point first, the later severe accident scene may be quite different.

Table 5-3 BWR lower plenum failure time

Penetration tube melt model	Conditions	Without	New	IAE
RPV creep rupture time (s)	Dry	864	1337	1062
	Wet	1128	1753	1376
Tubes melt time (s)	Dry	-	420	956
	Wet	-	427	1294
RPV wall melt time (s)	Dry	1051	2683	1686
	Wet	Not happen	Not happen	Not happen

2) RPV wall temperature distribution

Figure 5-8 shows RPV wall temperature distribution along the vessel wall for different cases. Obviously, RPV wall temperature for the case without penetration model increased faster than the other two cases. The RPV wall temperature difference at the bottom and on the side wall by the new penetration model was smaller, while the difference in the result by IAE penetration model was higher. Different models could cause quiet different RPV wall temperature distribution.

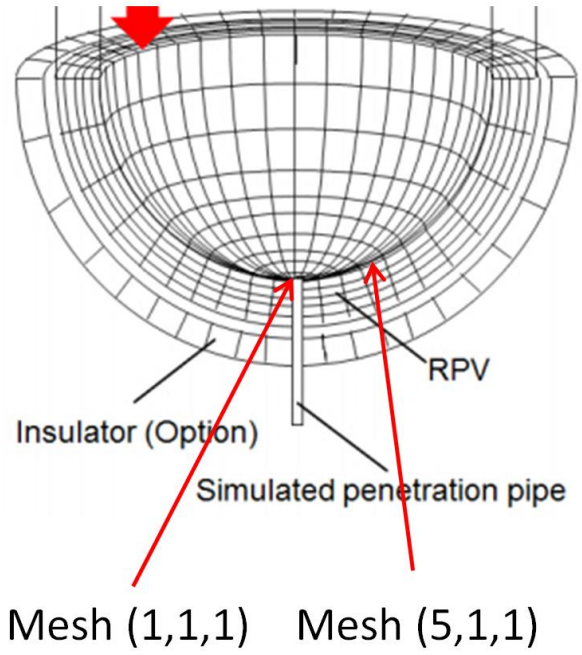

(a) Mesh number in the RPV

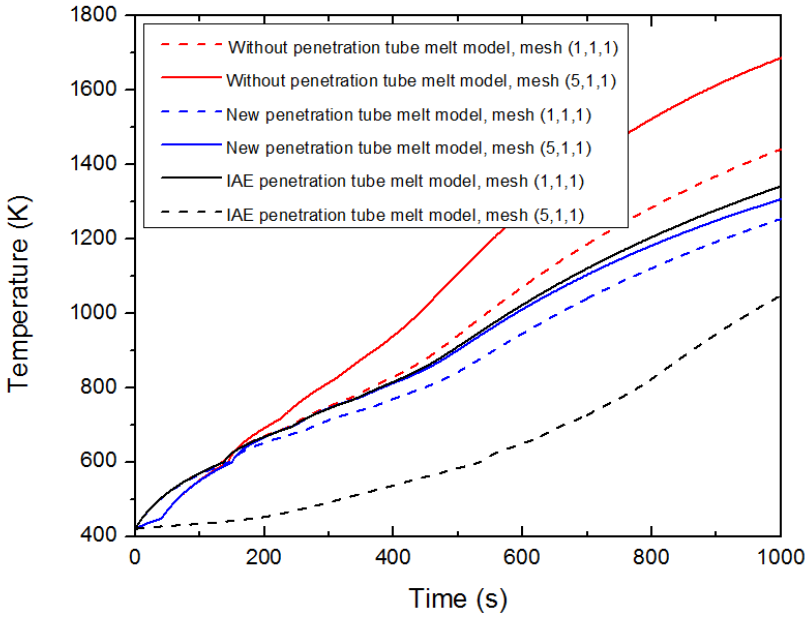

(b) Corresponding RPV wall mesh temperature distribution

Figure 5-8 RPV wall temperature distribution by different models

Figure 5-9 shows the RPV wall temperature distribution for the case with new penetration tube melt model, the results indicated that RPV inner wall highest temperature was not in the bottom, but in the edge position. For the new penetration tube melt model, the RPV wall temperature for these locations was quite similar.

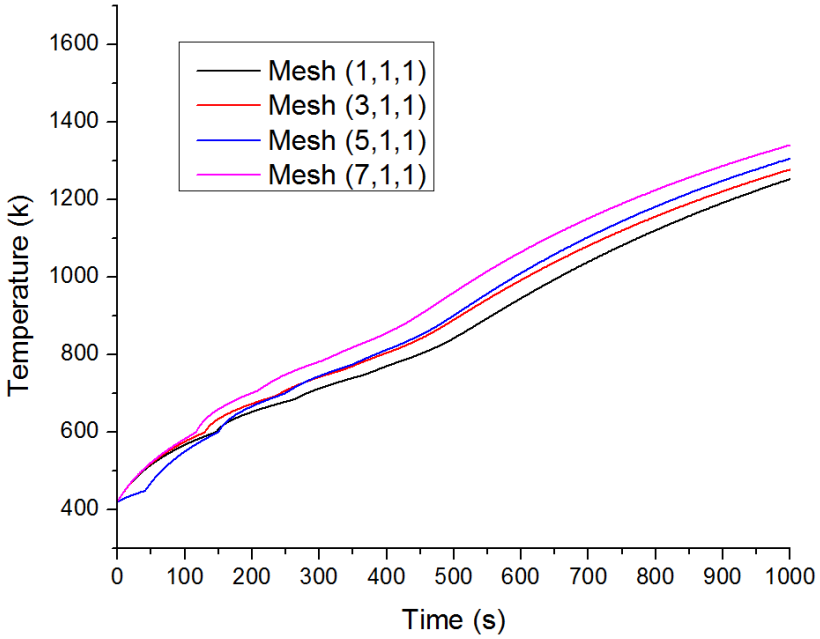

Figure 5-9 RPV wall temperature distribution by new penetration tube melt model

Figure 5-10 shows RPV inner wall temperature along the vessel for the case with IAE penetration tube melt model. While in the IAE penetration model there were huge differences between different locations. This was due to different cells. If the cell was penetration tube, the RPV vessel temperature increased slowly. If the cell was corium, RPV wall temperature was higher.

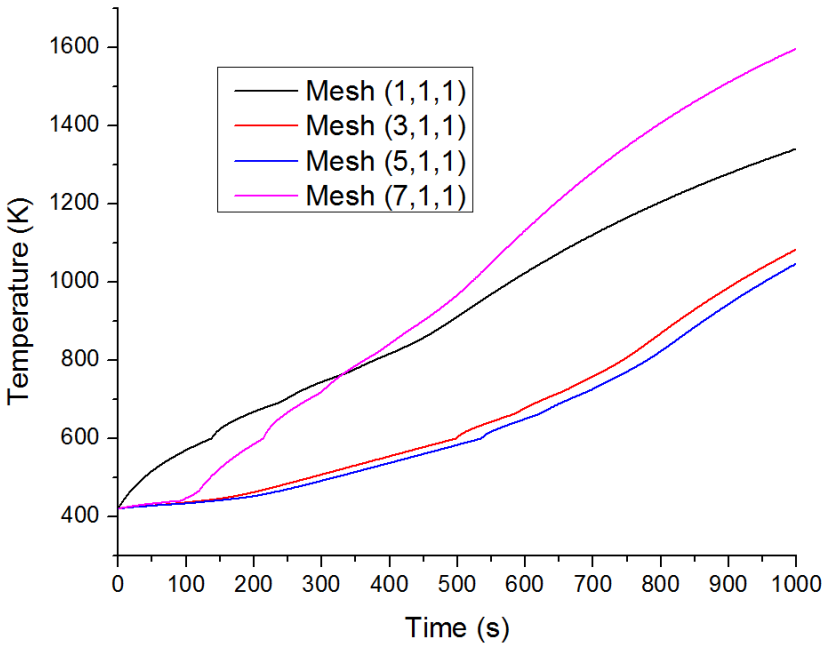

Figure 5-10 RPV wall temperature distribution by IAE penetration tube melt model

During the severe accident, the RPV wall temperature distribution is also very important for the severe accident management, especially for the water cooling outside the vessel. Different penetration tube melt models could cause different RPV wall temperature distribution. In the new penetration tube model, the RPV wall temperature distribution tended to be more unique, while in the IAE penetration tube model, large difference existed for different locations in the BWR lower plenum.

3) Penetration tubes temperature distribution

Figure 5-11 shows penetration tube position chosen for analysis with different models. Figure 5-12 shows penetration tubes inside RPV temperature distribution at 200 s, 500 s and 1000 s. In the beginning, the penetration tubes temperature was low. At about 500 s, for new penetration model, the penetration tubes started to melt, while in IAE penetration model, the penetration tubes were still under melt point. At about 1000 s, almost all of the penetration tube parts that merged into molten pool melt.

The penetration tube temperature increase in new penetration model was faster than IAE model. This was because in the IAE penetration model, one cell can represent several penetration tubes, and this assumption could cause penetration tubes to have higher thermal capacity compared to new penetration tube melt model.

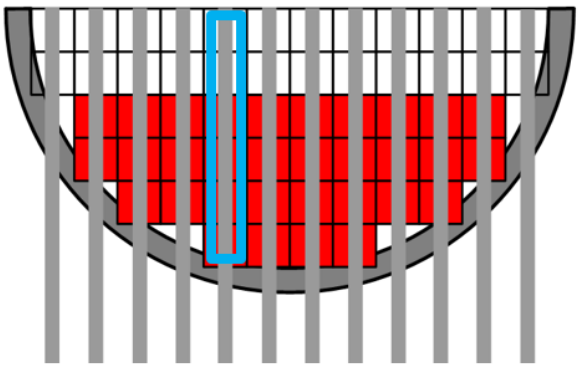

(a)New penetration tube melt model

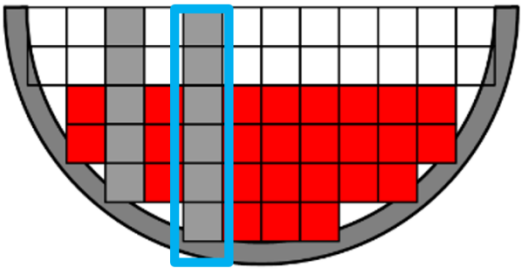

(b)IAE penetration tube melt model

Figure 5-11 Penetration tube position chosen for analysis

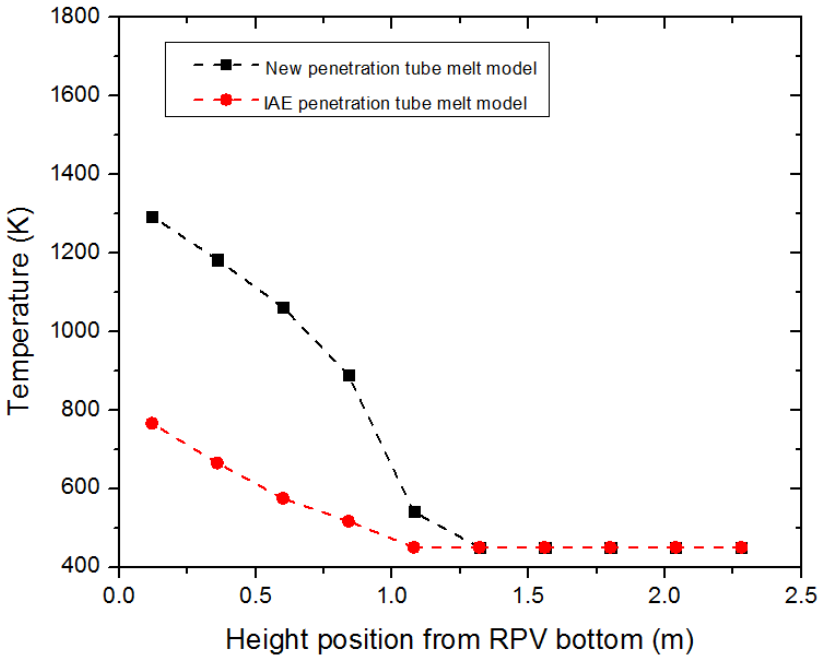

(a) 200s

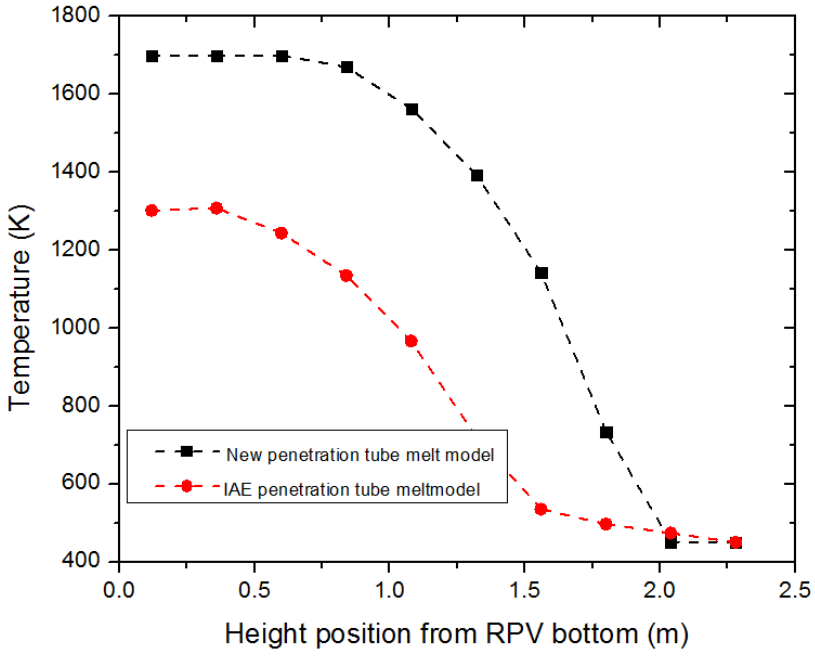

(b) 500s

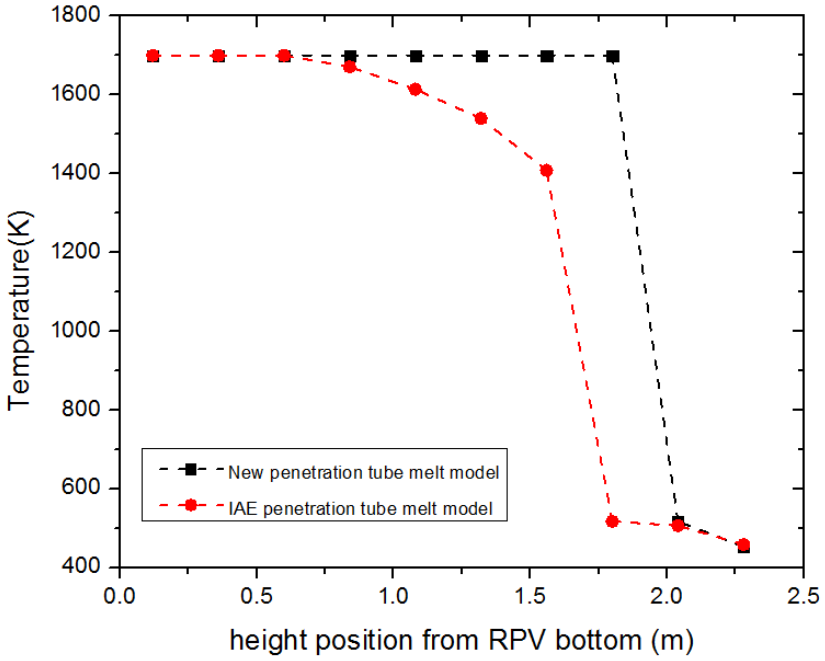

(c) 1000s

Figure 5-12 Penetration tubes inside RPV temperature distribution at 200s, 500s and 1000s

Figure 5-13 shows the penetration tube temperature distribution under dry and wet condition by new penetration tube melt model. In this case whether the penetration tubes could be the heat conduction pipe for molten pool was studied. Penetration

tubes could absorb heat from molten pool and the heat transfer between the penetration tubes and water was also very strong. Though cooled by water from the upper part, the penetration tube temperature in the corium part was also increase very quickly and reach melting point easily. The predication of penetration tube melt time under dry and wet conditions were consistent. This indicated that water cooling did not have significant influence on the delay of the failure time of penetration tubes. In this simulation, even assuming water could inject into the lower plenum, it was still impossible to keep the integrity of penetration tubes, and also did not delay the penetration tube failure time significantly.

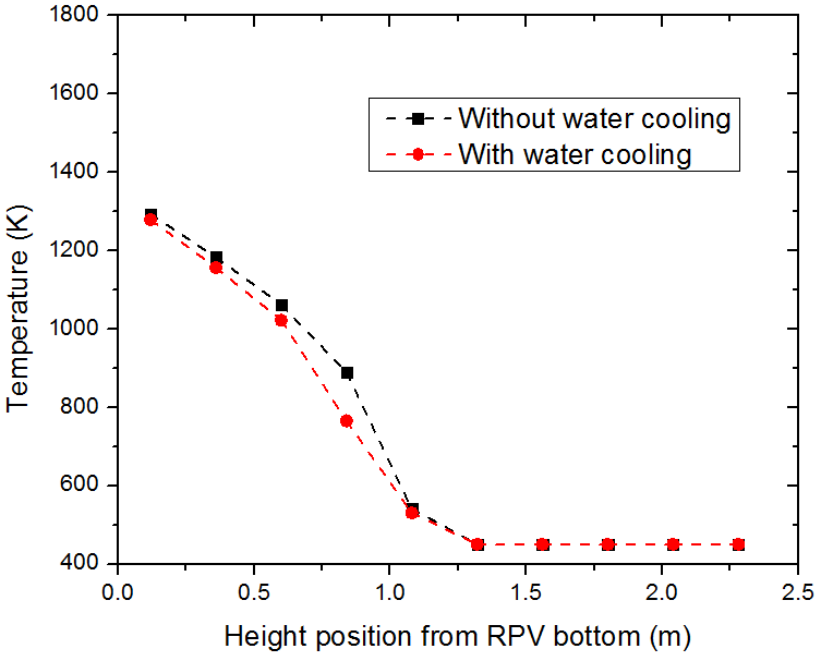

(a) 200 s

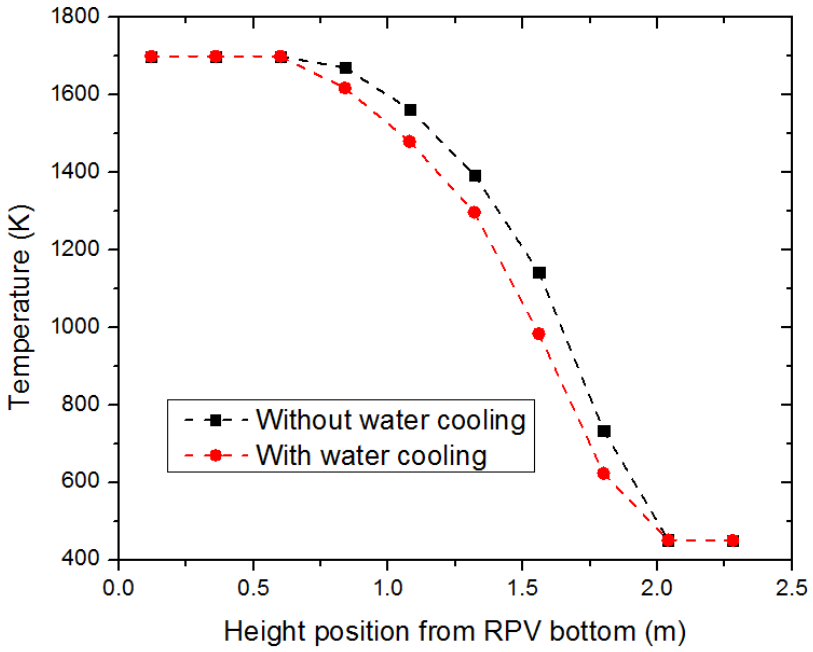

(b) 500 s

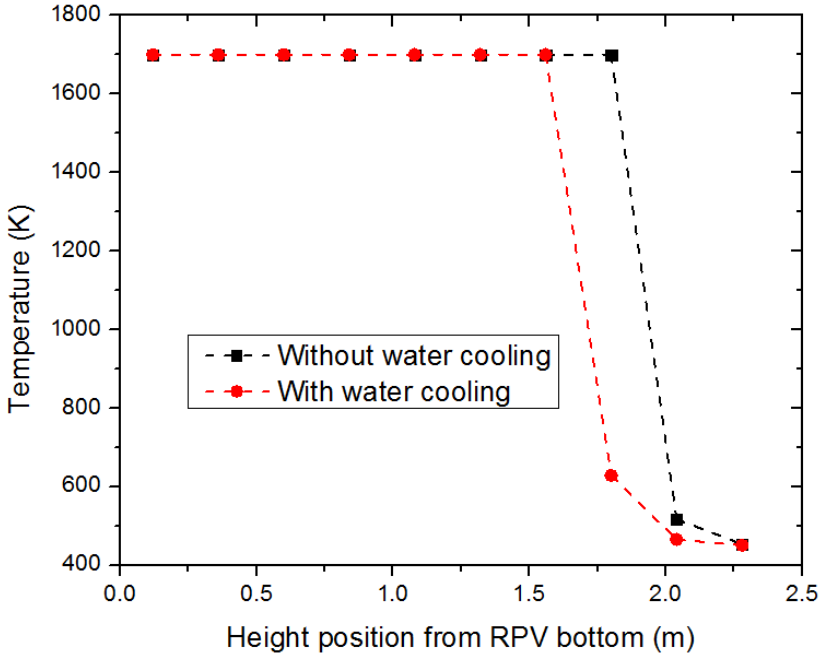

(c) 1000 s

Figure 5-13 Penetration tubes temperature distribution under dry and wet conditions

Figure 5-14 shows the maximum corium temperature changed with time. The corium temperature in the case without penetration tube melt model was higher than other two cases. Without penetration tube melt model, the corium only transferred its heat to the RPV and the heat sink was just the RPV and the air outside the RPV. In the

new penetration tube melt model, the corium transferred its heat to the penetration tubes and RPV. The temperature of corium in the case with new penetration model was lower than other two cases. For the case with new penetration tube melt model, the extra heat sink was the penetration heat capacity and the heat transfer between the penetration extension part and the air outside the RPV. For the case with IAE penetration tube model, the temperature of corium was lower than the case without penetration tube model, but was higher than the case with new penetration tube model. This was because compared to the new penetration tube model, IAE penetration tube melt model had less connecting surface with corium, so the heat transfer between corium and penetration tubes was lower than the case with new penetration tube melt model.

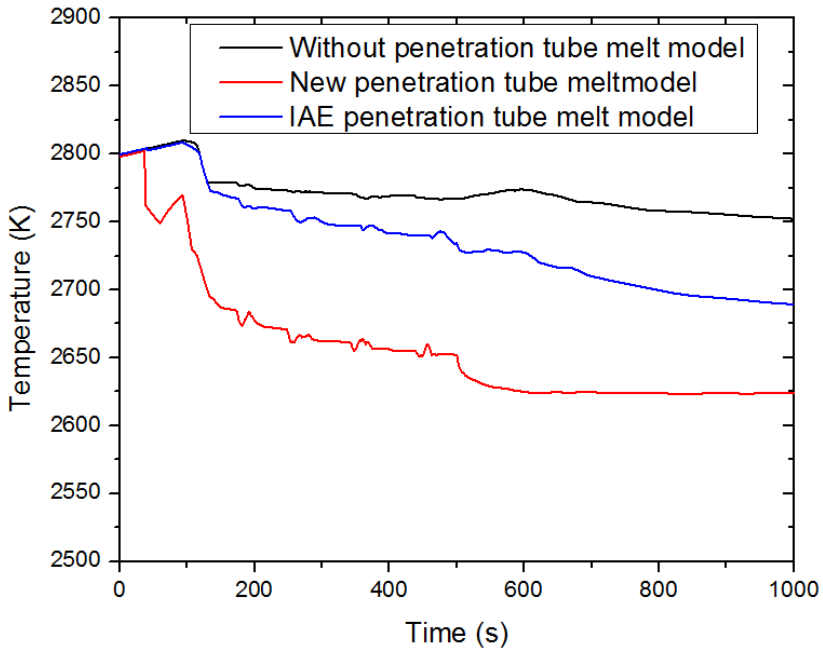

Figure 5-14 Corium max temperature with and without penetration tube melt model

Figure 5-15 shows the RPV wall temperature along the vessel wall with time by new penetration tube melt model under dry and wet conditions. In the initial time, since the temperature difference between crust and RPV wall was large, the heat flux between RPV wall and molten pool was also very large, which caused the RPV wall temperature to increase very quickly during this period. The RPV wall temperature in the water cooling condition was lower than the case without water cooling. During the simulation period, the RPV wall temperature in the water existing condition was

below the melting point. Whether water could penetrate into the gap had significant effect on the RPV wall temperature. Through cooling by water and vapor existing between crust and RPV wall, the RPV wall temperature was still below the melting point, though it was also very high.

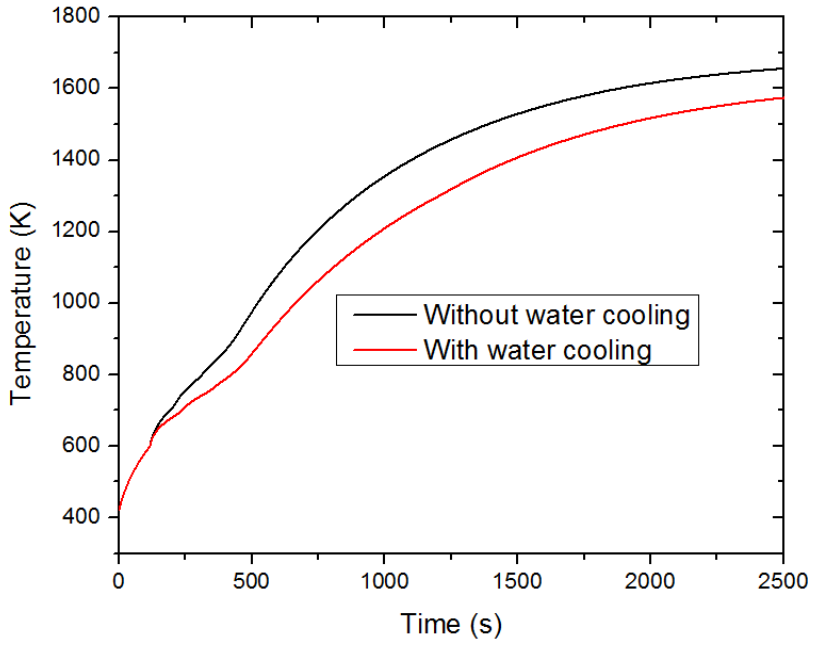

Figure 5-15 RPV max temperature

5.4 Conclusions

In this chapter, new penetration tube melt model was implemented into DCA module. The thermal response of corium, RPV and penetration tubes in BWR lower plenum were studied. Both dry and wet conditions were analyzed. Lower head failure time events were investigated by implementation of new penetration tube melt model. The following conclusions can be drawn from present simulation:

1) By comparison of different models and under different conditions, the simulation results indicated that penetration tubes failed earlier than RPV wall. The failure time events is very important for the evaluation of severe accident management.

2) The predictions of penetration tube melt time under dry and wet conditions were consistent. By comparison of simulation results under dry and wet conditions, whether penetration tubes could act as heat sink for molten pool was clarified. The

results indicated that no matter under dry or wet condition, the penetration tube failure time was similar and water cooling was not effective in preventing penetration tubes failure.

3) RPV failure time delayed with penetration model. By comparing the simulation results with and without penetration tubes in dry condition and wet conditions it is clear that the RPV failure time delayed while considering penetration tubes as the heat sink. The simulation results indicated that for BWR lower plenum, more attention should be paid to the failure of penetration tubes in severe accident management aspect.

Chapter 6 Conclusion and future work

6.1 Conclusion

In this thesis, DCA module in severe accident analysis code SAMPSON has been developed for corium behavior analysis in BWR lower plenum. The improved DCA module has been validated against LIVE-L4 test and FARO-L8 test. Penetration tube effects on the jet breakup process have been clarified by a detailed original jet breakup experiment. BWR lower plenum failure mechanism and time events have been investigated with the improved DCA module. Especially, this study has succeeded in attaining the following achievements:

- A multidimensional and phenomenological study on corium behavior in BWR lower plenum has been carried out with improved DCA module, of which 3-D N-S equations are solved for molten pool behavior and 3-D heat conduction equations are solved for RPV wall thermal response. The DCA module is based on mechanistic models, rather than traditional system codes using simplified models with many user-tuning parameters.

- A detailed penetration tube melt model based on the real geometry structure of CRGTs and IGTs in BWR lower plenum has been incorporated into DCA module. The simulation results obtained by the improved DCA module could provide important guidance on the evaluation of severe accident management in BWR case.

Additionally, the following important conclusions can be drawn from the current study:

1) The DCA module has been improved and validated with LIVE-L4 test and FARO-L8 test. The crust growth model has been implemented into DCA module. Heat transfer between molten pool and RPV wall model has been improved. Compared to the results of original DCA module, the validation results of modified DCA module could predict the LIVE-L4 test process reasonably by comparing molten pool average temperature, crust growth rate and heat flux along the vessel wall. The developed 1-D jet breakup model was also validated

with FARO-L8 test. The predicted breakup fraction, particle mean diameter and pressure history by the implemented 1-D jet breakup model generally agreed well with FARO-L8 test data. This indicated that the developed 1-D jet breakup model is capable to simulate jet breakup process accurately and can be extrapolated to simulate jet breakup process in reactor case. After improvement and validation, the modified DCA module could be used to investigate corium behavior in lower plenum accurately.

2) To understand the effects of CRGTs on jet breakup phenomenon for BWR case, dedicated original small-scale jet breakup experiments have been performed to observe the jet breakup phenomenon via high-speed photography. CRGTs could restrain the jet breakup process and their influence mainly depended on P/D ratio of the CRGTs. The relative breakup fraction has been proposed to evaluate the jet breakup fraction in the presence of CRGTs. The relative breakup fraction was 0.2 in the case of CRGTs at a P/D of 1.37, whereas the relative breakup fraction was 0.8 in the case of CRGTs at a P/D of 2.47. The experiment data also suggested that the departure droplet diameter was almost not affected by CRGTs. Based on the experimental results, the implemented jet breakup model has been modified for BWR case.

3) The penetration tube melt model has been implemented into DCA module and coupled with corium cooling model and RPV failure model. By assuming no corium leakage from failure penetration tubes, the improved DCA module has been used to evaluate thermal behavior of corium, RPV wall and penetration tubes during severe accident. Regarding the failure modes of BWR lower plenum, the simulation results indicated that penetration tubes fail earlier than RPV wall. The penetration tube failure time was consistent no matter under dry or wet condition. It is suggested that penetration tube failure effect and mechanism have to be considered for the evaluation of BWR severe accident management.

6.2 Future work

Despite the study on corium behavior in BWR lower plenum presented in this thesis, there are still some improvements and issues that should be addressed in future work on corium behavior in BWR lower plenum.

1) The study in this thesis mainly investigates tubes heat sink effect on corium behavior and BWR lower plenum failure mechanism. However, a more detailed model related to penetration tube effects on molten pool convection should be considered to carry out later. Metallic and ceramic materials may separate and form different layers due to density difference. Phenomena, such as focusing effect, thermal stratification and heat transfer with debris bed, also need to be considered.

2) For BWR, it is very likely that penetration tubes fail first and corium flows into the penetration tubes. After corium discharge into tubes, there are uncertainties regarding whether corium can be cooled down or would melt the tube again. Therefore, a more detailed model about corium behavior inside the penetration tubes needs to be considered.

Reference

[1] IAEA (International Atomic Energy Agency), Defence in depth in nuclear safety, INSAG-10/a report by the International Nuclear Safety Advisory Group. ISBN 92-0-103295-1.Vienna: International Atomic Energy Agency, 1996.

[2] Bhabha atomic research centre, Safety of Nuclear Reactors : Design level Safety, http://www.barc.gov.in/pubaware/snr_dls.html.

[3] B. R. Sehgal, Nuclear safety in light water reactors: Severe accident phenomenology. Academic Press, U.K. 2012.

[4] JAEA, シビアアクシデント進展解析コード MELCORについて、 http://www.aesj.or.jp/~fuel/Pdf/WG_Meltdown/WG_Doc/20120220_WG-3_Maruyama.pdf, 2012.

[5] Y. Amano, The Fukushima Daiichi Accident Report by the Director General,ISBN 978-92-0-107015-9 (set).Vienna: International Atomic Energy Agency, 2015.

[6] Tokyo Electric Power Company, MAAP analysis and Core concrete reaction, http://www.tepco.co.jp/en/nu/fukushima-np/images/handouts_111130_08-e.pdf, 2011.

[7] S. A. Hodge and L. J. Ott, BWRSAR calculation of reactor vesseldebris porous for peach bottom short-term station blackout, Nucl. Eng. Des., vol. 121, pp. 327–339, 1990.

[8] S. A. Hodge and M. Petek, Assessment of two BWR accident management strategies, Nucl. Eng. Des., vol. 148, pp. 185–203, 1994.

[9] P. Hofmann et al., Reactor core materials interactions at very high temperatures, Nucl. Technol, vol. 87, 1989.

[10] P. Hofmann, Current knowledge on core degradation phenomena, a review, J. Nucl. Mater., vol. 270, pp. 194–211, 1999.

[11] G. Bandini et al. Molten Material Relocation into the Lower Plenum: a status report, NEA/CSNI/R(97)34,1998.

[12] R. Meignen, S. Picchi, J. Lamome, B. Raverdy, S. C. Escobar, and G. Nicaise, The challenge of modeling fuel-coolant interaction: Part i - Premixing, Nucl. Eng. Des., vol. 280, pp. 511–527, 2014.

[13] R. Saito, Y. Abe, and H. Yoshida, Experimental study on breakup and fragmentation behavior of molten material jet in complicated structure of BWR lower plenum, J. Nucl. Sci. Technol., vol. 51, no. 1, pp. 64–76, 2014.

[14] R. Saito, Y. Abe, and H. Yoshida, Breakup and fragmentation behavior of molten material jet in multi-channel of BWR lower plenum, J. Nucl. Sci. Technol., vol. 53, pp. 147–160, 2016.

[15] B. R. Sehgal, A. Jasiulevicius, and M. Konovalikhin, Investigation of the Potential for In-Vessel Melt Retention in the Lower Head of a BWR by Cooling through the Control Rod Guide Tubes, SKI Report 2004 : 51,2004.

[16] C. T. Tran, P. Kudinov and T. N. Dinh, An approach to numerical simulation and analysis of molten corium coolability in a boiling water reactor lower head, Nucl. Eng. Technol., vol. 240, pp. 2148–2159, 2010.

[17] H. G. Willschütz, E. Altstadt, B. R. Sehgal, and F. P. Weiss, Coupled thermal structural analysis of LWR vessel creep failure experiments, Nucl. Eng. Des., vol. 208, no. 3, pp. 265–282, 2001.

[18] S. V. Bechta, V. B. Khabensky, V. S. Granovsky, E. V. Krushinov, and S. A. Vitol, Experimental Study of Interactions Between Suboxidized Corium and Reactor Vessel Steel, Proceedings of ICAPP'06, Reno, NV USA, June 4-8, 2006.

[19] S. A. Hodge, BWR reactor vessel bottom head failure modes, CONF-890546-3, DE89 009623.

[20] D. Magallon and I. Huhtiniemi, Corium melt quenching tests at low pressure and subcooled water in FARO, Nucl. Eng. Des., vol. 204, no. 1–3, pp. 369–376, 2001.

[21] D. Magallon and H. Hohmann, High pressure corium melt quenching tests in FARO, Nucl. Eng. Des., vol. 155, no. 1–2, pp. 253–270, 1995.

[22] J. H. Song, I. K. Park, Y. S. Shin, J. H. Kim, S. W. Hong, B. T. Min, and H. D. Kim, Fuel coolant interaction experiments in TROI using a UO2/ZrO2 mixture, Nucl. Eng. Des., vol. 222, no. 1, pp. 1–15, 2003.

[23] H. S. Park, R. Chapman, and M. Corradini, Vapor explosions in a one-dimensional large scale geometry with stimulant melts, NUREG/CR-6623, 1999.

[24] I. Huhtiniemi, D. Magallon, and H. Hohmann, Results of recent KROTOS FCI tests: alumina versus corium melts, Nucl. Eng. Des., vol. 189, no. 1, pp. 379–389, 1999.

[25] B. J. Broadhouse and P. J. Gale, Analysis of the MFCI Mixing Experiments MIXA01 and M1XA06, AEA Technology report AEA-RS-4525 (Revision 1), 1995.

[26] B. D. Turland and G. P. Dobson, Molten fuel coolant interactions: a state of the art report, EUR 16874, 1996.

[27] A. Kaiser, W. Schutz, and H. Will, PREMIX experiments PM12-PM18 to investigate the mixing of a hot melt with water, FZKA-6380, 2001.

[28] D. Magallon, I. Huhtiniemi, and H. Hohmann, Lessons learnt from FARO/TERMOS corium melt quenching experiments, Nucl. Eng. Des., vol. 189, no. 1, pp. 223–238, 1999.

[29] L. Zhang, Y. Zhou, Y. Zhang, W. Tian, S. Qiu, and G. Su, Natural convection heat transfer in corium pools: A review work of experimental studies, Prog. Nucl. Energy, vol. 79, pp. 167–181, 2015.

[30] T. G. Theofanous, M. Maguire, S. Angelini, and T. Salmassi, The first results from the ACOPO experiment, Nucl. Eng. Des., vol. 169, pp. 49–57, 1997.

[31] B. R. Sehgal, V. A. Bui, T. N. Dinh, J. A. Green, and G. Kolb, SIMECO Experiments on In-Vessel Melt Pool Formation and Heat Transfer with and without a Metallic Layer, Proc. OECD/CSNI Workshop, Garching, Germany, 1998.

[32] J. M. Bonnet and J. M. Seiler, Thermal hydraulic phenomena in corium pools: the BALI experiment, 7th International Conference on Nuclear Engineering, Tokyo, Japan, April 19-23, 1999.

[33] H. Ujita, N. Satoh, and M. Naitoh, Development of Severe Accident Analysis Code SAMPSON for IMPACT Project, 7th International Conference on Nuclear Engineering, Tokyo, Japan, April 19-23,1999.

[34] K. I. Ahn and D. H. Kim, A state-of-the-art review of the reactor lower head models employed in three representative U.S. severe accident codes, Prog. Nucl. Energy, vol. 42, no. 3, pp. 361–382, 2003.

[35] 日本原子力学会,シビアアクシデント評価に関する 調査研究報告書, http://www.aesj.or.jp/special/report/2013/r_SAhyoka20131100.pdf, 2013.

[36] Gauntt, R.O., Cash, J.E., Cole, R.K. et al., MELCOR Computer Code Manuals, Sandia National Laboratories. NUREG/CR 6119, SAND2005-5713, 2005.

[37] L.L. Humphries, R.K. Cole, D.L. Louie, V.G. Figueroa, M. F. Young, MELCOR Computer Code Manuals, Sandia National Laboratories, SAND2015-6692 R, 2015.

[38] K. Y. Suh and R. E. Henry, Debris interactions in reactor vessel lower plena during a severe accident II. Integral analysis, Nucl. Eng. Des., vol. 166, no. 2, pp. 165–178, 1996.

[39] K. Y. Suh and R. E. Henry, Integral analysis of debris material and heat transport in reactor vessel lower plenum, Nucl. Eng. Des., vol. 151, no. 1, pp. 203–221, 1994.

[40] K. Y. Suh and R. E. Henry, Nuclear Engineering and Design accident I . Predictive model, Nucl. Eng. Des., vol. 166, pp. 147–163, 1996.

[41] EPRI, Modular Accident Analysis Program 5 (MAAP5) Applications Guidance, 2015.

[42] Tokyo Electric Power Company, Research plan regarding improvement of simulation code for understanding the status of fuel debris in the reactor, 2012.

[43] H. Ujita, Y. Nakadai, T. Ikeda, and M. Naitoh, PWR and BWR plant analyses by Severe Accident Analysis Code SAMPSON for IMPACT Project, GENES4/ANP2003, Sep. 15-19, 2003, Kyoto, JAPAN.

[44] 内藤正則, 我が国における軽水炉シビアアクシデント評価技術の今後, 日本原子力学会2012春の年会, 熱流動部会・計算科学技術部会合同企画セッション, 2012.

[45] M. Naitoh, T. IKEDA, and H. UJITA, Overview of the IMPACT Severe Accident Analysis Code SAMPSON- On Core Degradation and Lower Plenum Debris Behavior in the Main, CARE/CATHARE SEMINAR, 2001.

[46] H. Ujita and M. Hidaka, Model Verification of the Debris Coolability Analysis Module in the Severe Accident Analysis Code ‘SAMPSON, J. Nucl. Sci. Technol., vol. 38, no. 4, pp. 229–241, 2001.

[47] H. Ujita, M. Hidaka, A. Susuki, and N. Ishida, Development of Debris Coolability Analysis Module in Severe Accident Analysis Code SAMPSON for IMPACT Project, J. Nucl. Sci. Technol., vol. 36, no. 10, pp. 940–951, 1999.

[48] M. Hidaka, N. Sato, and H. Ujita, Verification for Flow Analysis Capability in the Model of Three-Dimensional Natural Convection with Simultaneous Spreading, Melting and Solidification for the Debris Coolability Analysis Module in the Severe Accident Analysis Code 'SAMPSON' (II), J. Nucl. Sci. Technol., vol. 39, no. 5, pp. 520–530, 2002.

[49] Y. P. Zhang, G. H. Su, S. Z. Qiu, W. X. Tian, X. Gaus-Liu, F. Kretzschmar, and A. Miassoedov, A simple novel and fast computational model for the LIVE-L4, Prog. Nucl. Energy, vol. 68, pp. 20–30, 2013.

[50] M. Hidaka and H. Ujita, Verification for Flow Analysis Capability in the Model of Three-Dimensional Natural Convection with Simultaneous Spreading, Melting and Solidification for the Debris Coolability Analysis Module in the Severe Accident Analysis Code 'SAMPSON', (I), J. Nucl. Sci. Technol., vol. 38, no. 9, pp. 745–756, 2001.

[51] E. Baglietto, H. Ninokata, and M. Naitoh, Investigation of ALPHA experiment by severe accident analysis code SAMPSON, Nucl. Eng. Des., vol. 238, no. 7, pp. 1561–1568, 2008.

[52] M. Epstein and H. Fauske, Steam film instability and the mixing of core-melt jets and water, ANS Proc, 1985.

[53] K. H. Bang, R. Kumar, and H. T. Kim, Modeling corium jet breakup in water pool and application to ex-vessel fuel-coolant interaction analyses, Nucl. Eng. Des., vol. 276, pp. 153–161, 2014.

[54] K. Vierow, M. Naitoh, K. Nagano, and K. Araki, Development of the VESUVIUS Code for Steam Explosion Analysis Part 1: Molten Jet Breakup Modeling, J. Japanese of. Multiph. Flow, vol. 12, no. 3, pp. 242–248, 1998.

[55] C. C. Chu and M. L. Corradini, One-Dimensional Transient Fluid Model for Fuel/Coolant Interaction Analysis, Nucl. Sci. Eng., vol. 101, no. 1, pp. 48–71, 1989.

[56] Idaho National Engineering and Environmental Laboratory, Scdap/relap5-3D code manual volume 2: modeling of reactor core and vessel behavior during severe accidents, INEEL/EXT-02-00589, Rev. 2.2, 2003.

[57] Nuclear Safety Analysis Division, RELAP5/MOD3 Code Manual, Volume 1:Code Structure, System, Models, and Solution Methods., NUREG/CR-5535/Rev 1-Vol I, 2001.

[58] IAE, IMPACT/SAMPSON, 2015.

[59] D. Magallon and H. Hohmann, Experimental investigation of 150-kg-scale corium melt jet quenching in water, Nucl. Eng. Des., vol. 177, no. 1–3, pp. 321–337, 1997.

[60] Idaho National Engineering and Environmental Laboratory, SCDAP/RELAP5-3D code manual volume 5: assessment of modeling of reactor core behavior during severe accidents, INEEL/EXT-02-00589, Rev. 2.2, 2003.

[61] P. Marco and M. Naitoh, Methods for investigation of severe accidents as support to Fukushima Daiichi NPP decommissioning, NUSSA 2014, Kashiwa, Chiba, Japan, September 3-5, 2014.

[62] Yang Shiming and Tao Wenquan. Heat Transfer. Beijing: Higher Education Press, 2006.